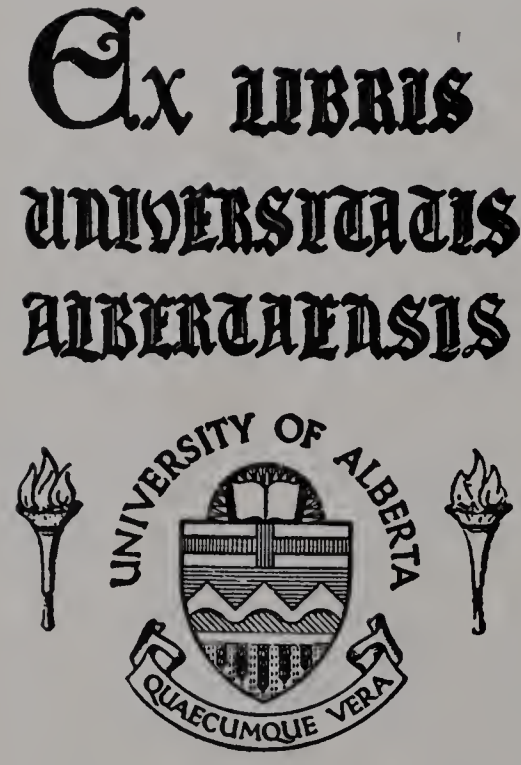

THE UNIVERSITY OF ALBERTA

FABRICATION OF LITHIUM ION DRIFTED GERMANIUM DETECTORS AND THEIR APPLICATION IN THE GAMMA RAY SPECTROMETRY OF NUCLEAR REACTIONS

by

Bijan Miremadi-K.

A THESIS

SUBMITTED TO THE FACULTY OF GRADUATE STUDIES

IN PARTIAL FULFILMENT OF THE REQUIREMENTS FOR THE DEGREE

OF MASTER OF SCIENCE

DEPARTMENT OF PHYSICS

EDMONTON, ALBERTA

April, 1966

UNIVERSITY OF ALBERTA

FACULTY OF GRADUATE STUDIES

The undersigned certify that they have read, and recommend to the Faculty of Graduate Studies for acceptance, a thesis entitled FABRICATION OF LITHIUM ION DRIFTED GERMANIUM DETECTOR AND ITS APPLICATION IN GAMMA RAY SPECTROMETRY OF NUCLEAR REACTIONS, submitted by Bijan Miremadi-K. in partial fulfilment of the requirements for the degree of Master of Science

ABSTRACT

In this thesis the method of fabrication of lithium-ion-drifted detectors and their application to gamma-ray spectrometry of $Si^{30}(d,n\gamma)P^{31}$ and $Be^{9}(\alpha,n\gamma)C^{12}$ reactions are described.

The planar-type detectors up to 5 cm^3 sensitive volume and a coaxial type detector of 10 cm^3 sensitive volume have been fabricated. But due to the high leakage current caused by surface contamination, only a few planar-type detectors have been successfully tested.

The intrinsic resolution of these detectors for 661 KeV gamma-ray of Cs^{137} vary between 3.4 KeV to 16.7 KeV. The energy resolution of the best detector obtained was 3.4 KeV and 7.7 KeV for gamma-rays of energies 0.122 and 2.62 MeV respectively. This detector exhibited an absolute efficiency of 70% for 122 KeV, decreasing to 0.8% near the 2 MeV region.

A detector with sensitive volume of 3 cm^3 has been used to study the gamma-rays produced in the $Si^{30}(d,n\gamma)P^{31}$ reaction with the hope of determining the branching ratios of P^{31} gamma-ray transitions. But the low efficiency of the detector above 4 MeV did not allow such measurements to be made. In addition, the 4.43 MeV gamma-ray for C^{12} produced by the $Be^{9}(\alpha,n\gamma)C^{12}$ reaction was studied. This gamma-ray exhibited a Doppler shift and broadening which is discussed as a means of obtaining the lifetimes of nuclear excited states.

ACKNOWLEDGMENTS

I take this opportunity to express my sincere thanks to my supervisor, Dr. W. C. Olsen, and for his encouragement during the entire course of this project, particularly for his patient work in checking the drafts of this thesis.

Thanks are also due to Dr. J. T. Sample for suggesting this subject, to Dr. G. C. Neilson whose interest and cooperation in this project were of considerable importance, and to Dr. W. K. Dawson for programming the computer.

Many thanks to C. W. H. Vermette, D.B., for his valuable assistance during the entire work and to A. A. Fife for programming and operation of the computer.

The technical assistance of J. B. Elliott, C. F. Green, R. Gordon, L. Holm, R. Popik and P. Karvonen is greatly appreciated.

I should also like to thank Dr. H. Baadsgaard of the Geology Department for supplying us with deionized distilled water prior to the installation of a distillation system.

Many thanks as well to Mrs. P. Babet for typing the manuscript.

TABLE OF CONTENTS

LIST OF ILLUSTRATIONS

LIST OF TABLES

Fabrication of Lithium Ion Drifted Germanium Detector and its Application in Gamma Ray Spectrometry of Nuclear Reactions

INTRODUCTION

Because the detection of nuclear radiation is of great importance in all experimental work in the field of nuclear physics, there has been considerable research effort devoted to the development of detection devices. During the past few years, most encouraging results have been obtained with an entirely new technique using semiconductors. The application of these detectors is most valuable in charged particle spectrometry. These detectors provide pulses whose amplitudes are proportional to the energy of the ionizing particle, and whose rise times are of the order of a few nanoseconds, thus permitting their use in timing experiments in a moderate background of gamma, beta and neutron radiations. The combination of good resolution with fast rise time opens up new fields in particle detection and their small size and good linearity help to achieve more accurate results in scattering experiments and in the measurement of reaction cross sections. Their disadvantages lie in the fact that they give a very small signal so that considerable amplification is needed. Furthermore, the small sensitive volume of conventional semiconductor detector makes them extremely low efficiency detectors for gamma and beta rays.

Historically the application of germanium semiconductor detectors to radiation detection was first made by McKay (1) in 1950 who utilized germanium crystal for the detection of alpha particles. In 1955, Orman et al (2) reported results similar to that of McKay. Simon (3) reported the use of gold-germanium barriers as alpha counters and then Mayer and Gossick (4) found the pulse-height for such counters to be proportional to the energy of incoming alpha particles. By 1959 several groups were actively engaged in developing these detectors at Oak Ridge National Laboratory and Chalk River Nuclear Laboratories. These groups demonstrated that solid state (or semiconductor) detectors can be operated at room temperature if they are constructed from silicon. Other centers of early development were Brookhaven National Laboratory and Bell Telephone Laboratories whose efforts produced significant advances within a short period of time.

Recently a lithium-drifting technique for producing semiconductor detectors with larger sensitive volumes has been developed by Pell (5), which have been used for the detection of gamma rays. Since this early period, a large number of groups have continued to make important contributions to the improvement of semiconductor detectors and there seems to be no doubt that the speed of development will be sustained in the future, and that these devices will make a contribution to experimental nuclear physics even more important than that already made by scintillation counters.

The contents of this thesis are divided into four chapters. Chapter one begins with a simple and brief explanation of the theory of semiconductors, more specifically, the theory of P-N junction detectors with special reference to results and terminology which are applied in the later chapters and ends with a summary of the different types of semiconductor detectors. Chapter two describes the method of preparation of lithium ion drifted germanium detectors and illustrates their performance characteristics. In chapter three the experimental arrangement and the electronics is discussed. Chapter four deals with the use of these detectors in investigating the gamma ray spectrum in the nuclear reactions $Si^{30}(d, n\gamma)P^{31}$ and $Be^{9}(\alpha,n\gamma)C^{12}$.

CHAPTER 1

THE THEORY OF P-N JUNCTION DETECTORS

1.1 Properties of semiconductors:

Prior to the theoretical description of P-N junction detectors it will be necessary to outline the principles of the semiconductor detectors as a whole, and give a brief explanation of their properties. Considering an atom in a solid, the outer orbit electrons are more weakly bound to their parent atoms than the inner orbit electrons. For this reason they are called valence electrons and the orbit in which these exist is called valence band. If the electrons from the valence band acquire enough thermal energy they can cross a small forbidden region into the outer atomic space and reach an empty band called the conduction band. The region between the two bands is termed the energy gap, or the forbidden gap, i.e., the minimum energy required for an electron to enter the conduction band from the valence band. Once a valence band has lost an electron in this way, it can acquire another electron from neighboring atoms and the neighboring atoms themselves might also acquire an electron from the other neighbors. It is evident that each free electron which results from breaking of a covalent bond will produce an electron deficiency which moves through the crystal. This deficiency can be considered as a positively charged particle called a hole. It is possible for an electron to reach the conduction band without originating in the valence band. This can occur by an impurity in the

crystal releasing electrons into the conduction band without leaving corresponding holes in the valence band. As an example consider a semiconductor material such as germanium or silicon which are both in Group IV of the periodic table to be doped with an element of group V such as phosphorous. This impurity atom contains five electrons in its valence band. Four of these will be used to form covalent bonds with the group IV elements but the fifth one is free to leave its parent atom and occupy a state just below the conduction band. The energy level of this state is termed an impurity level and it lies near the top of the energy gap. As the temperature rises, electrons from the impurity atoms acquire enough energy to enter the conduction band. This type of impurity level is called a "Donor-Level" and the resulting material is termed an N-type semiconductor.

It is also possible that impurity levels create holes in the valence band without releasing an electron into the conduction band. This happens when semiconductors are doped with an element of group III such as gallium. All three valence electrons of gallium are used in the covalent bond with the group IV element but a lack or deficiency of one electron provides an empty space resulting in an incomplete bond. This empty space or "hole" is able to accept an electron. The level corresponding to this type of impurity is termed an Acceptor-Level and it lies near the bottom of the energy gap. Such

materials are called P-type. It should be noticed that crystals always have both donor and acceptor impurities and their behavior as an N-type or P-type depends on the net concentration of donors and acceptors.

a. Trapping: At equilibrium, the carriers are being exchanged between their bands and the localized impurity energy levels within the forbidden gap. The removal of a carrier from its condition of mobility to a localized level is termed trapping. These carriers will be released after a time which depends on the energy depth of the trapping centers below the conduction band.

b. Recombination: It happens often before a carrier can be released from trapping centers, that another carrier of opposite charge enters and these two carriers cease to exist as a free charged carrier, in other words, they recombine. This process, which is a form of trapping, is known as recombination. On this basis, even a pure and perfect crystal would have a finite trapping rate and the presence of impurities or defects in the crystal will increase this rate.

c. Life Time: The time interval spent by a carrier before being trapped or the average time that a carrier exists as a free carrier is known as its life time. This time depends on concentration of trapping centers and therefore on purity and perfection of the crystal.

d. Carrier Concentration: In any classical semiconductor where Maxwell-Boltzmann statistics apply, the concentration of electrons is $n = C_n \exp [-E_n/kT]$ and that of holes is $p = C_p \exp [-E_p/kT]$, where C_n and C_p are constant and n and p are electron and hole concentration respectively. E_n is the energy difference between the fermi level and the bottom of the conduction band. E_p is the energy difference between the fermi level and the top of the valence band. The fermi level, is a level below which the occupation probability of charge carrier is equal to one and above which this probability is zero at the temperature of absolute zero. (k) is the Boltzmann constant and (T) the absolute temperature. The product of the two concentrations is therefore constant regardless of the position of fermi level.

$$np = C_n C_p \exp [-(E_n + E_p)/kT] \quad ,$$

but $E_n + E_p = E_g$, the energy gap. Thus,

$$np = C_n C_p \exp (-E_g/kT). \qquad (1.1)$$

e. Mobility: The conductivity of any solid is largely determined by the carrier concentration but a factor of almost equal importance is the speed with which carriers move under the influence of an applied field. At normal temperatures the electrons in the conduction band interact with the crystal lattice

(which is undergoing thermal vibrations) and are in a state of random motion. Application of an electric field provides a net velocity (drift velocity, v_d,) in the direction of the field to the random charge carrier motion. The mobility, μ, is defined as drift velocity per unit of electric field, $\mathcal{E}$, i.e.,

$$\mu = \frac{v_d}{\mathcal{E}} \qquad (1.2)$$

This concept is equally applied to both electrons and holes.

f. Relaxation Time: It is often necessary to know how thermal equilibrium is restored in a semiconductor if it has been disturbed by some effect. When a number of excess carriers is introduced, the charges will recombine with charges of opposite sign to give an exponential decay toward the equilibrium numbers and thus electrical neutrality also occurs exponentially with a time constant, τ_o, called dielectric relaxation time, i.e.,

$$\tau_o = RC = \rho\frac{d}{A} \cdot \frac{\chi A}{4\pi d} = \frac{\rho\chi}{4\pi} \qquad (1.3)$$

where R and C are equivalent resistance and capacitance of a parallel plate crystal of thickness d, area A, resistivity ρ, and dielectric constant of χ.

g. Collection or Transit Time: If a charge carrier of drift velocity, v_d, after traveling a distance, d, is collected at an electrode in a time known as the collection time, τ_c, then

this time is given by the equation,

$$\tau_c = \frac{d}{v_d} \quad .$$

But according to the equation (1.2) $v_d = \mu \mathcal{E}$ and also $\mathcal{E} = \frac{V_a}{d}$, where V_a is the applied voltage across the distance, d. Thus,

$$\tau_c = \frac{d^2}{\mu V_a} \qquad (1.4)$$

It appears reasonable that 99% of the carriers should be collected, i.e.,

$$e^{-\frac{\tau_c}{\tau}} = 0.99$$

where τ is the carrier lifetime. This gives

$$\tau = 10^2 \tau_c \qquad (1.5)$$

which indicates that in order to have 99% charge collection efficiency, the carrier life time must be 10^2 times longer than the collection time. However, due to difficulties in preparation of a perfect crystal, the practical limits appear to be

$$\tau = 10 \tau_c \quad .$$

1.2 Electron-Hole Production:

When a charged particle or a gamma ray passes through a semiconductor, it produces electron-hole pairs. The total

number of pairs produced within the medium is E/ϵ, where E is the energy of incoming particle and ϵ is the average energy required to produce an electron-hole pair. For a nonrelativistic particle the maximum energy transfer is given by

$$E_{max} = [4mM/(m + M)^2] E \qquad (1.6)$$

where M and E are mass and the energy of incident particle and m is the electron mass. For an alpha-particle of 4-Mev energy, E_{max} = 2 Kev. Thus it is seen that the energy transfer to the electrons of the medium is rather large compared with the value of ϵ for germanium (2.84 ev) and for silicon (3.23 ev). These values are almost three times higher than their corresponding energy gap "E_g". The difference between E_g and ϵ is considered to be caused by the fact that the extra energy has been dissipated through strong coupling of electrons to the lattice vibration of the solids.

1.3 Motion and collection of charge carriers:

When a charged particle produces electron-hole pairs in a semiconductor crystal, the electric field across the medium causes these carriers to move toward the appropriate electrodes and induces a negative charge in the external circuit thus producing a voltage $v(t)$ at the output of the medium. If $q_p(t)$ and $q_n(t)$ are the charges induced on the collecting

electrodes by positive and the negative charges respectively, the output voltage is given by

$$v(t) = [q_p(t) + q_n(t)] / C \qquad (1.7)$$

where C is the capacitance of the medium. If N-ion pairs have been produced, the total charge induced will be given as

$$\int_0^\infty q(t)dt = Ne = \int_0^\infty [q_p(t) + q_n(t)]dt \qquad (1.8)$$

Suppose these N-ion pairs are produced at a level x_o in the crystal and after a collection time τ_c, these charges are collected at positive and negative electrodes indicated as x_+ and x_- respectively and are shown in Fig. (1.1a). The values of the q_p and q_n in terms of Green's reciprocal theorem (6) is given as

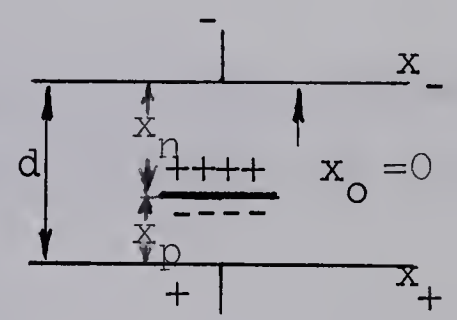

(a)

$$q_p(t) = \frac{d-x_p}{d} q(t) \quad \text{and}$$

$$q_n(t) = -\frac{d-x_n}{d} q(t).$$ The equations (1.7) and (1.8) together lead to the equation

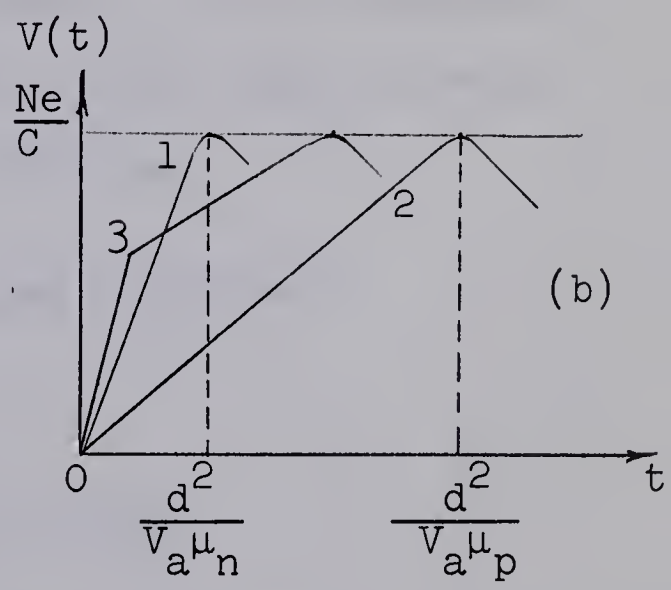

Fig. (1.1). Time dependen of induced voltage for thr different positions of the electron-hole production. Reference (7).

$$V = \frac{Ne}{C} \left[\frac{d-x_p}{d} - \frac{d-x_n}{d} \right] \qquad (1.9)$$

This equation indicates that

a - if the ion pairs are produced next to the negative electrode, i.e., $x_p = d \quad x_n = 0$, the entire signal is due to the motion of the electrons. The voltage $V(t)$ builds up linearly to a value of $\frac{Ne}{C}$, reaching this value when the electrons are collected.

b - If the electron-hole pairs are produced next to the positive electrode, the entire signal will be due to the motion of the holes.

c - In this case which the charge carriers have been produced in the region away from the electrode, both electrons and holes contribute to the output signal.

These three cases are shown in Fig. (1.1b) from which it is clear that the time constant of the circuit must be much longer than the collection time of the carriers.

Recalling equation (1.9), one can substitute $x_p = v_{dp}\tau_{cp}$ and $x_n = -v_{dn}\tau_{cn}$ to get

$$|V| = \frac{Ne}{C} \quad \frac{Va}{d^2} \quad (\mu_p\tau_{cp} + \mu_n\tau_{cn})$$

However, efficient charge collection can be limited by several factors:

1. The existence of the trapping and recombination centers;
2. A polarization effect, in which the charge accumulated in the interior of the detector medium sets up an internal

field opposed to that produced by the applied collecting voltage. This field reduces the electric field and therefore the efficiency of charge collection.

3. Secondary current associated with the dielectric relaxation time τ_o. If $\tau_o < \tau_c$, secondary current flows until the charge centers causing it are either neutralized or collected.

1.4 P-N junction detectors:

Experimental evidence has shown that a lower concentration of charge carriers exists at the interface of a P-type and an N-type semiconductor material when they are brought to contact than in anyone of them individually. In such a case, the two conduction bands are in electrical contact, one containing electrons and the other nearly empty. As there is always a tendency for diffusion of electrons and holes toward lower density regions, electrons flow from N-type to P-type. The P-type thus acquires a negative charge. The N-type correspondingly acquires a positive charge because now it contains a number of ionized donors whose charges are not balanced by an equal number of free electrons. In the valence band exactly the same process occurs. Some of the holes move from the P-side into the N-side and leave behind a negative charge due to ionized acceptors. Therefore, there will be a transit flow

of majority carriers which establishes a positive charge on the N-side and an equal negative charge on the P-side, thus creating a potential barrier at the junction whose magnitude at equilibrium is such that the net flow of carrier across the junction due to diffusion is zero. At equilibrium the majority carriers on both sides of the junction are separated by this potential barrier and if the carriers acquire sufficient kinetic energy they can cross this barrier. Equilibrium is reached when the fermi level is at the same height on both sides of the junction. The region in the vicinity of the junction which is depleted of charge carriers, is called space charge region or depletion region.

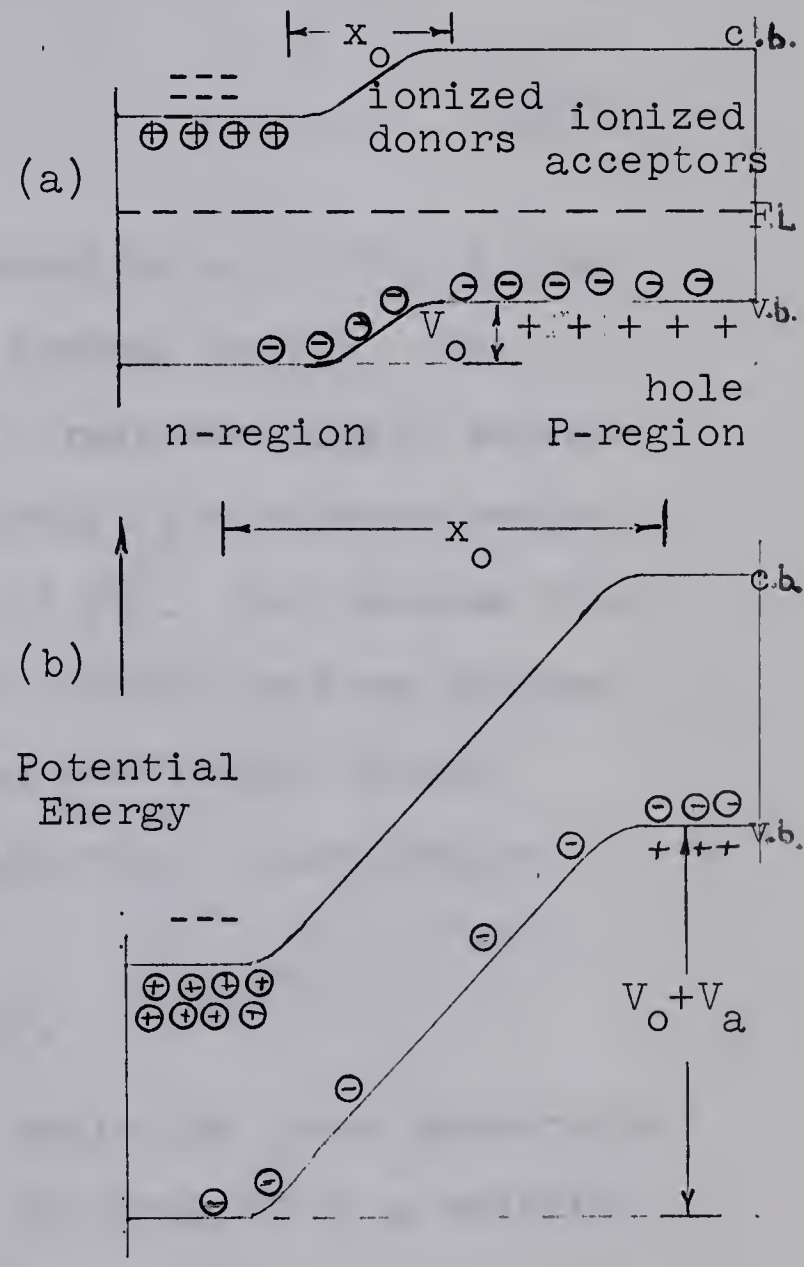

Fig. (1.2). Diffused n-P junction and formation of the depletion region.
(a) with no bias.
(b) with reverse bias.

Reference (7).

Since the density of acceptors in the P-type material is much lower relative to that of donors in the N-type, (this is the case when N-type has been doped by a donor rich impurity material) the space charge region extends further into the P-region

than into the N-region. The result of the above discussion is shown in Fig. (1.2a) where x_o is the thickness of the depletion layer.

The height of potential barrier V_o, can be obtained from the relationship

$$V_o = \frac{kT}{e} \ell n \frac{P_p}{P_n} \qquad (1.11)$$

where P_p and P_n are the hole concentration in the P-type and N-type material and kT is the thermal energy. The application of an external potential (reversed bias), extends the space charge region and consequently, the barrier height rises to $(V_o + V_a)$ as shown in Fig. (1.2b). The reverse bias assists the built-in voltage, V_o, to remove the free charges from the depletion region and reduces the charge carrier concentration below the thermal equilibrium concentration.

1.5 Thickness of the depletion layer.

The distance to which the depletion layer penetrates into each region of the crystal can be obtained by a solution to the Poisson's equation for P-type material

$$\frac{\partial^2 V(x)}{\partial x^2} = - \frac{4\pi}{\chi} (N_A + n - P) \qquad (1.12)$$

where N_A is the acceptor impurity concentration, n and P, are the local electron and hole concentration and χ, the

dielectric constant of the P-type material.

In order to simplify equation (1.12), it is necessary to make some assumptions.

1. Depletion region contains no carrier at all, i.e. $n = 0$, $P = 0$.
2. The junction is abrupt.
3. Acceptor concentration N_A is much less than donor concentration.
4. Excess charge in N-type is equal and opposite to that in P-type material.

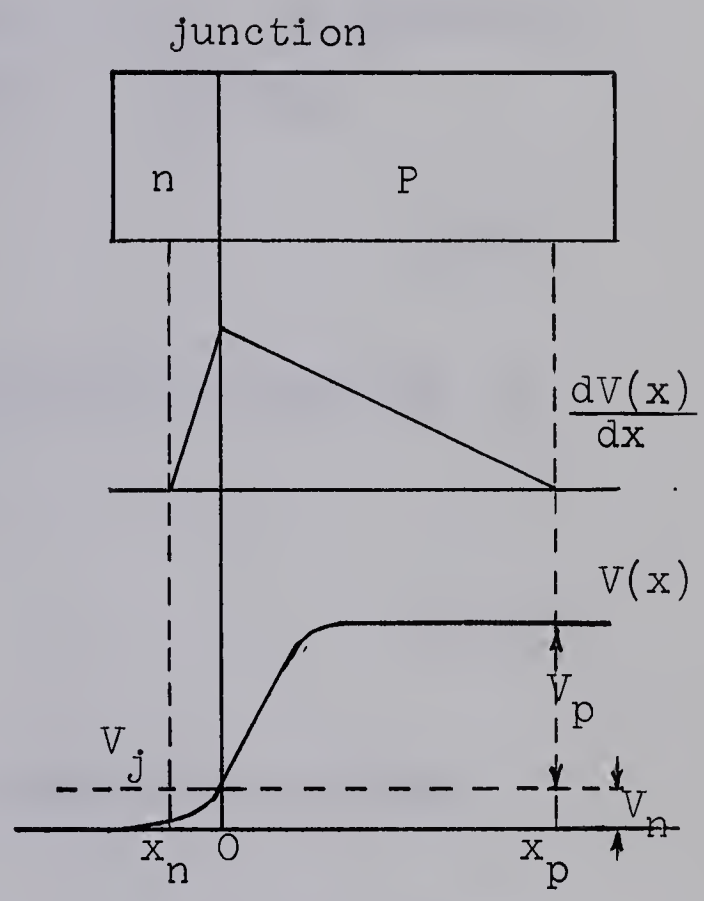

Fig. (1.3). The potential and field distribution in the depletion region. Reference (7).

Under the first assumption and by the help of Fig. (1.3), equation (1.12) becomes

$$\frac{\partial^2 V(x)}{\partial x^2} = -\frac{4\pi e}{\chi} N_A \qquad (1.13)$$

Successive integration results

$$V(x) = -\frac{2\pi e N_A}{\chi}(x^2 - 2x x_p) + V_j \qquad (1.14)$$

where V_j is the potential at junction. The application of the

boundary conditions (2), results,

$$x_p^2 = \frac{V_p \chi}{2\pi e N_A} \quad , \qquad x_n^2 = \frac{V_n \chi}{2\pi e N_D} \quad . \tag{1.15}$$

But according to the assumptions (3) and (4), x_n is negligible in comparison with x_p, and one can write in general,

$$x^2 = \frac{V\chi}{2\pi e N_A} \tag{1.16}$$

Since $V = V_o + V_a$, where V_a is the applied voltage and V_o is given by equation (1.11), we obtain,

$$x^2 = \frac{(V_o + V_a)\ \chi}{2\pi e N_A} \quad . \tag{1.17}$$

If all acceptors are notionized then the resistivity is given by

$$\rho = \frac{1}{N_A e \mu_p + N_D e \mu_n} \tag{1.18}$$

but with the consideration of assumption that all acceptors are normally ionized (1.18) becomes

$$\rho = \frac{1}{N_A e \mu_p} \tag{1.19}$$

and by neglecting the value of V_o, (which is of the order of 0.5 ev) in comparison with V_a, the equation (1.17) may be written in the form of

$$x = \left[\frac{\chi \mu_p}{2\pi}\ \rho\ V_a\ \right]^{\frac{1}{2}} \quad . \tag{1.20}$$

The capacity of the reverse bias junction will be that of a parallel plate condenser of thickness x, junction area A, and with a dielectric constant of χ, i.e.,

$$C = \frac{\chi A}{4\pi x} \qquad \text{(e.s.u.)} \qquad (1.21)$$

or

$$C = A\left[\frac{\chi}{8\pi\mu_p \rho V_a}\right]^{\frac{1}{2}} \qquad \text{(e.s.u.)} \qquad (1.22)$$

Fig. (1.3) also indicates that the electric field across the crystal contributes only to the depletion layer. Its maximum value occurs at the junction and beyond the depletion region its value drops to zero.

1.6 Reverse current:

The steady current passed by the detector in absence of radiation is termed reverse current. This current in junction detectors is very small but is an important factor in operation of detectors as it can be the main source of noise in the system and may limit resolution. An explanation for this current can be given by study of impurity levels and imperfection centers in the crystal. Fig. (1.4) indicates an impurity center in the forbidden energy gap and four possible electronic transitions which control the free carrier population.

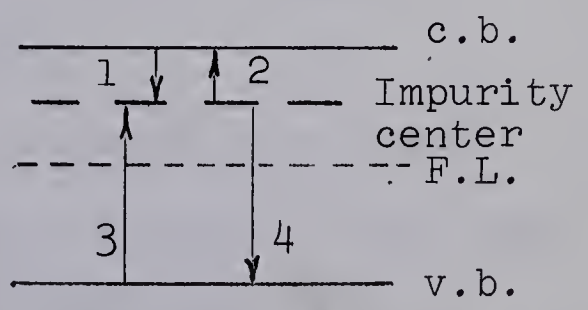

Fig. (1.4). Impurity centers and the four possible electronic transitions. Reference (7).

1. Electron may be captured from conduction band, or,
2. Electron may be released into conduction band.
3. Electron may be captured from the valence band (i.e., hole generation), or,
4. Electron may be generated into the valence band (i.e., trapping process).

It should be noted that not all these processes are possible at the same time. An electron has to be captured before it can be released.

One of the functions of such an impurity center is the restoration of equilibrium after excess carriers have been generated. A center can capture an electron first, then a hole which is the restoration of an electron to the valence band in two steps. However, these centers are responsible for the current through the bulk material. There is also another current called surface leakage current, which is described in section 1.6 b.

a. Bulk current.

This current has two components; first the drift current and second, the generation current.

1. Drift current: This current is due to the diffusion of minority carriers into the depletion region because of the fact that there are always a few holes in the N-side which are

subject to diffusion into the depletion region as a result of attraction by the negative charges on the P-side. As soon as they come under the influence of electric field they accelerate and cross the depletion layer. This current is shown by symbol I_{dn}, indicating the drift current from N-side to P-side. There is also a small continuous flow of electrons from the P-side to the N-side indicated as I_{dp}. This dual flow causes a drift current flowing from the N-side to the P-side which is proportional to the area of the junction

$$I_d = I_{dn} + I_{dp} \quad . \tag{1.23}$$

2. Generation current, I_g, which is due to the carrier generation in the depletion region by means of trapping. These carriers are swept out by the electric field as soon as they are formed. This current depends on generation rate, g, and is proportional to the volume of depletion region.

$$I_g = 2gxe \quad . \tag{1.24}$$

At equilibrium the flow of minority carriers is balanced by an equal flow of majority carriers (i.e., the diffusion current I_D) in the opposite direction. Therefore,

$$| I_D | = I_d + I_g \quad . \tag{1.25}$$

At ordinary temperature I_D is very small (of the order of 10^{-9} Amp/cm^3). If the depletion region is small, I_g, the

generation current is very small compared with I_d and thus,

$$|I_D| = I_d \qquad (1.26)$$

Application of an external potential increases the height of the barrier and extends the depletion region. This potential has no effect on I_d but it raises I_g to I'_g and meanwhile, the diffusion current will reduce to I'_D and the equality of (1.25) is no longer valid, i.e., $I'_D \neq I_d + I'_g$, but rather

$$I_d + I'_g - |I'_D| = I_r \qquad (1.27)$$

where I_r is the reverse current. The maximum value of diffusion current is I_D, thus

$$I'_D = I_D \exp(-eV_o/kT) \quad . \qquad (1.28)$$

At zero bias $I_D = I_d$, hence,

$$I'_D = I_d \exp(-eV_o/kT) \quad . \qquad (1.29)$$

Combination of (1.27) and (1.29) gives the reverse current at zero bias,

$$I_r = I_d \left(1 - e^{-\frac{eV_o}{kT}}\right) + I'_g \qquad (1.30)$$

and at bias, V_a,

$$I_r = I_d \left[1 - e^{-\frac{e(V_o+V_a)}{kT}}\right] + I'_g \quad . \qquad (1.31)$$

It is clear that in equation (1.31) when bias V_a increases the reverse current increases as well. The value of I_d and I'_g is evaluated in the reference [9] and the results of these evaluations are as follows:

$$I_d = e\, n_i^{\frac{3}{2}} \sqrt{\mu_p \mu_n\, kT}\, \left(\frac{\mu_p^{\frac{1}{2}}\, \rho_p}{\tau_n^{\frac{1}{2}}} + \frac{\mu_n^{\frac{1}{2}}\, \rho_n}{\tau_p^{\frac{1}{2}}} \right) \qquad (1.32)$$

$$I'_g = e\, n_i \sqrt{\left(\frac{\chi \mu_p}{2\pi}\right)}\, \left(\frac{\rho V_a}{\tau_n}\right)^{\frac{1}{2}} \qquad (1.33)$$

In the above equation τ_n, τ_p are minority carriers life time ρ_p, ρ_n are the resistivities of P-type and N-type materials respectively, ρ is the resistivity of depletion region and n_i is the intrinsic electron concentration. It must be noted that the value of I_d is independent of applied voltage up to the break down point.

b. Surface leakage current.

The third component of reverse current is surface leakage current. For ordinary detector geometries at a bias of about 100 volts it appears even with a good surface condition, the leakage current is much higher than generation current and will contribute to both shot noise and flicker noise which will be considered later. Atmospheric contamination occurs very easily leading to a catastrophic increase in surface leakage.

This results in break down even at very low bias. The theory of surface effects is very extensive and is beyond the scope of this work, but a simple understanding of this effect is possible. At the surface there are additional localized energy levels which arise from non-uniform distribution of nuclei. There are even further localized energy levels arising from oxidation and contamination. The surface layer, therefore, contains a space charge which alters the whole energy band system and moves the energy gap relative to its position in the bulk material. With or without this layer it is very usual for the conductivity to be greater at the surface than in the bulk material. A moist atmosphere is a common cause of high surface conductivity. The higher concentration of local energy levels at the surface leads to increased trapping and recombination. Sometimes the number of surface trapping centers are so high that the majority of the carriers begin and end their lives at the surface. Surface trapping can be kept at a minimum only by very careful control of contamination and the condition of the surface.

The surface leakage current is one cause for the electrical noise which limits energy resolution. Surface trapping reduces the life time of carriers and gives rise to collection problems which also contribute to electrical noise.

1.7 Pulse height.

The charge released in a detector is closely proportional to the energy absorbed in the depletion region and is independent of the nature of the incoming particle. By considering an equivalent circuit of a detector such as in Fig. (1.5), assuming full carrier collection, the pulse height is defined as

$$P = \frac{Q}{C_d + C_p} \qquad (1.37)$$

where,

C_d = detector capacitance given by equation (1.25).

C_p = input capacitance of pre-amplifier plus stray capacity, C_s.

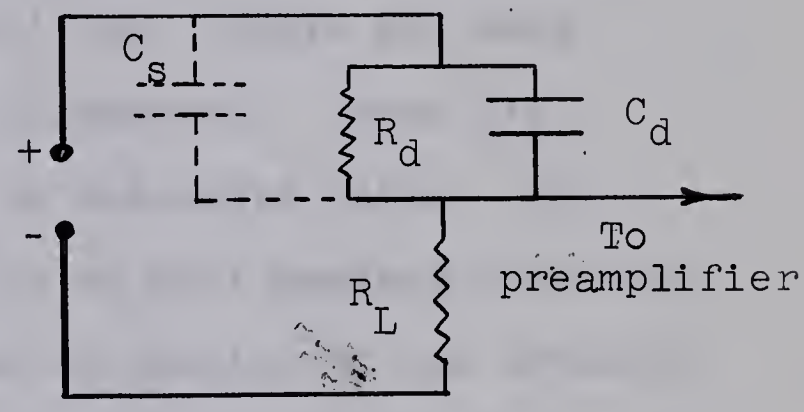

Fig. (1.5). Equivalent circuit of a detector. Reference (8).

If the bias is constant C_d is also constant. Thus, the main contribution to the pulse height is C_p which must be as small as possible.

The rise time can be affected by two factors. First, the collection time must be small and secondly, the effective time constant of detectors plus preamplifier must be larger than the collection time.

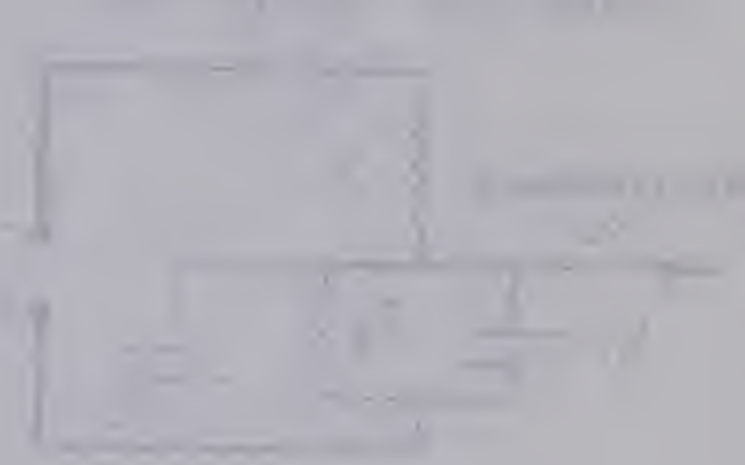

1.8 Energy resolution.

An important application of semiconductor detectors is in particle spectrometry where the signal amplitude is a measure of the incident particle energy. An ideal counter for this purpose would be one in which particles of a given energy always produce signals of a given amplitude. However, in practice this never happens, basically, because the process of ion pair formation is a statistical one. There are many ways by which the intrinsic width is broadened. These are also statistical in nature and will be discussed later. The width of the pulse height distribution at half maximum intensity (FWHF) is a measure of the resolution or quality of the detector and its associated electronics. If the shape of the pulse height distribution is Gaussian, then the standard deviation gives directly the resolution. The Gaussian distribution has a form given in general by

$$f(x) = \frac{(2\pi)^{-\frac{1}{2}}}{\sigma} \exp\left[\frac{-(x - x_{\frac{1}{2}})^2}{2\sigma^2}\right] \qquad (1.34)$$

where σ is the standard deviation and the width, $w = [2(x - x_{\frac{1}{2}})]$, is defined as (FWHM). By application of proper boundary conditions, equation (1.34) reduces to

$$w = 2.35\ \sigma_E \qquad (1.35)$$

where σ_E is the standard deviation in energy.

In general, the resolution due to all the effects can be written in the form of

$$W = \left(\sum_{i=1}^{n} w_i^2 \right)^{\frac{1}{2}} \tag{1.36}$$

where w_i represents the contribution of each effect. The greatest contribution to the standard deviation is that due to fluctuation in N, the number of ion pairs produced by the incident particle, i.e.,

$$\sigma = \sqrt{N} \tag{1.37}$$

where σ is the standard deviation corresponding to the uncertainty of number of electron-hole pairs produced. If ϵ is the energy to produce an electron-hole pair, then the standard deviation in energy, σ_E, can be written as

$$\sigma_E = \epsilon\sigma = \epsilon\sqrt{N} \tag{1.38}$$

but $N = \frac{E}{\epsilon}$, therefore we obtain,

$$\sigma_E = (\epsilon E)^{\frac{1}{2}} \tag{1.39}$$

which is the standard deviation of energy dissipated in the detector by a single particle. Hence,

$$w_i = 2.35\ (\epsilon E)^{\frac{1}{2}} \quad . \tag{1.40}$$

1.9 Noise.

According to the definition, noise is the energy of

an ionizing particle which would produce a signal equal to r.m.s. noise, i.e. $[\overline{(\text{Noise})^2}]^{\frac{1}{2}}$. This definition is exactly the same as the standard deviation of the pulse height described in equation (1.39). On the other hand, any noise in the detector leads to a fluctuation in the distribution of the charge carriers. This shows up as a fluctuating voltage at the output of the detector whose average potential is zero but whose r.m.s. voltage is $[\overline{(V)^2}]^{\frac{1}{2}}$. Therefore one can write equation (1.40) in the following way:

$$w_i = 2.35\,[\overline{(\text{Noise})^2}]^{\frac{1}{2}} \qquad (1.41)$$

or

$$w_i = 2.35\,[\overline{(V)^2}]^{\frac{1}{2}} \quad . \qquad (1.42)$$

In this section the contribution of different sources of noise shall be discussed without mathematical rigour. (For more detailed information the reader may refer to references [8] and [11])

(a) Thermal noise.

This noise occurs in any detector whether or not a current is flowing. It arises because the velocity distribution of the carriers contributes a fluctuating voltage at output whose value is given by

$$\overline{V^2} = \frac{kT}{C} \qquad (1.43)$$

where according to the Fig. (1.5) $C = C_d + C_s$, T is the absolute temperature and k Boltzmann's constant. From the

relationship, $q = Ne = VC$, or $N = \frac{C}{e} V$, one can show that the number of ion pairs necessary to produce a signal equal to $[(\overline{V^2})]^{\frac{1}{2}}$ is given by

$$\Delta N = \frac{C}{e} \left(\frac{kT}{C}\right)^{\frac{1}{2}} \qquad (1.44)$$

and the energy of a particle to give this number of ion pairs is $\epsilon\Delta N$. So that,

$$w = \frac{\epsilon}{e} (kTC)^{\frac{1}{2}} \qquad (1.45)$$

or according to the equation (1.42),

$$w_1 = 2.35 \frac{\epsilon}{e} (kTC)^{\frac{1}{2}} \quad . \qquad (1.46)$$

b. Current noise.

As it has been described in section (1.6), current noise arises when a field is applied to the detector and the resulting current causes a discrete movement of electrons and holes. Any process which interrupts the movement of carriers, destroys the continuity of the current and acts as a source of noise. The processes which are responsible for this noise are trapping, recombination and carrier generation. One can classify the current noise into three groups:

(b_1) Shot Noise: This noise is analogous to a similar source of noise in thermionic valves and it is due to statistical fluctuation in the number of carriers leading to changes in conductivity. This noise has been found to be

$$\overline{V^2} = \frac{N_c t}{2\tau_c} \cdot \frac{e^2}{C^2} \qquad (1.47)$$

where N_c is the carrier concentration in the detector, $t = RC$ where $C = C_d + C_s$ and $R = (R_L R_d)/(R_L + R_d)$ from Fig. (1.5) and τ_c is the collection time in absence of trapping. The number of ion pairs needed to generate a signal equal to the r.m.s. voltage noise is

$$\Delta N = \left(\frac{N_c}{2}\right)^{\frac{1}{2}} \left(\frac{t}{\tau_c}\right)^{\frac{1}{2}} \qquad (1.48)$$

and the resolution due to this cause is

$$w_2 = 2.35\, \epsilon \left(\frac{N_c}{2}\right)^{\frac{1}{2}} \left(\frac{t}{\tau_c}\right)^{\frac{1}{2}} . \qquad (1.49)$$

(b_2) Generation, Recombination and trapping noise: These processes contribute current pulses which are shorter than those due to carriers which traverse the detector without any interruptions, and is given by

$$\overline{V^2} = \frac{N_c}{2} \frac{t\tau}{\tau_c^2} \frac{e^2}{C^2} \qquad (1.50)$$

where τ is the life time of the carriers. The number of ion pairs necessary to produce a signal equal to r.m.s. voltage is

$$\Delta N = \left(\frac{N_c}{2}\right)^{\frac{1}{2}} \left(\frac{t\tau}{\tau_c^2}\right)^{\frac{1}{2}} \qquad (1.51)$$

and the resolution is

$$w_3 = 2.35\, \epsilon \left(\frac{N_c}{2}\right)^{\frac{1}{2}} \left(\frac{t\tau}{\tau_c^2}\right)^{\frac{1}{2}} \qquad (1.52)$$

It is clear that when $t = \tau_c$, the effect of this noise is negligible and only shot noise will contribute.

(b_3) Flicker noise: This noise is different from the other two types of current noise. It is rather a low-frequency effect, being proportional to $1/f$ where f is the frequency. This noise resembles flicker noise in vacuum tubes. According to Fonger (10) there are two kinds of flicker noise in semiconductors: 1-surface flicker noise caused by trapping and recombination on surface, and 2-leakage current noise. Fonger has shown that flicker noise is proportional to I_L^2/f where I_L is the surface leakage current. The measurement of this noise is rather difficult but it can be reduced to minimum by surface treatment. Goulding and Hansen (11) have found the energy resolution due to this noise to be approximately

$$w_4 = [0.16t' (i_g + I_L) + 2 \cdot 10^{-4} C^2]^{\frac{1}{2}} \quad (1.53)$$

where t' is the value of integrator and differentiator time constant of the amplifier. $(i_g + I_L)$ is the sum of the detector leakage current and grid current of input tube of the preamplifier expressed in 10^{-9} amperes. C is the total input capacitance of the detector and electronics system in 10^{-12} farad. It is clear that first term contributes to leakage current noise and the second to flicker noise.

1.10 Various types of semiconductor detectors.

(1) Lithium ion drifted detectors.

(1.a) Planar type.

Detectors with depletion layers thicker than one centimeter are made by an ion drift method originally described by Pell (5). This method depends on the finite mobility of the ionized donors or acceptors under an electric field. Most types of impurities have too low a diffusion constant to be suitable for ion drifting. However, lithium, which is a donor impurity with an ionized impurity level of 0.01 ev in germanium and of 0.03 ev in silicon, has a diffusitivity of 10^7 times higher than the other impurities making it a suitable donor for the drifting process. Consider a block of P-type material which originally has a uniform distribution of acceptor centers. When lithium is diffused onto one face the donor-acceptor characteristic will be as it is shown in Fig. (1.6a). The donors and acceptors compensate each other at point, (d), where the impurity concentration is zero. Below point d the number of donors and above point d, the number of acceptors, predominate. Thus junction occurs at point d. When a deep junction has been formed as described above, then the detector is put under drift by applying a reverse bias across the junction. Because the mobility of lithium ion in the crystal is very high at above room temperature the ion drift velocity under the influence of an electric field will also be high. As is shown in Fig. (1.6b), Pell described that after drifting the

lithium ion concentration has a long plateau at a level which just compensates the acceptor centers.

The process of ion drift results in the production of a layer in the crystal which has become intrinsic by compensation. The depth of this layer can be controlled by controlling the drift time, the temperature and the applied bias during the drifting process. The drifting equation can be obtained from consideration of the following equation,

$$1/t_d = \frac{\mu_{\ell g} V_a}{x^2} \qquad (1.54)$$

where $\mu_{\ell g}$* is the mobility of lithium, (ℓ) in germanium, (g). V_a is the applied voltage and x is the thickness of the depletion region. According to the Einstein relation

$$\frac{1}{2}kT\mu_{\ell g} = eD_{g_\ell} \qquad (1.55)$$

where e is the electronic charge and D_{g_ℓ} is the diffusion constant of germanium (g), for lithium, (ℓ). Equations (1.54) and (1.55) give

$$x = \left[\frac{2eD_{g_\ell} V_a t_d}{kT}\right]^{\frac{1}{2}} \qquad (1.56)$$

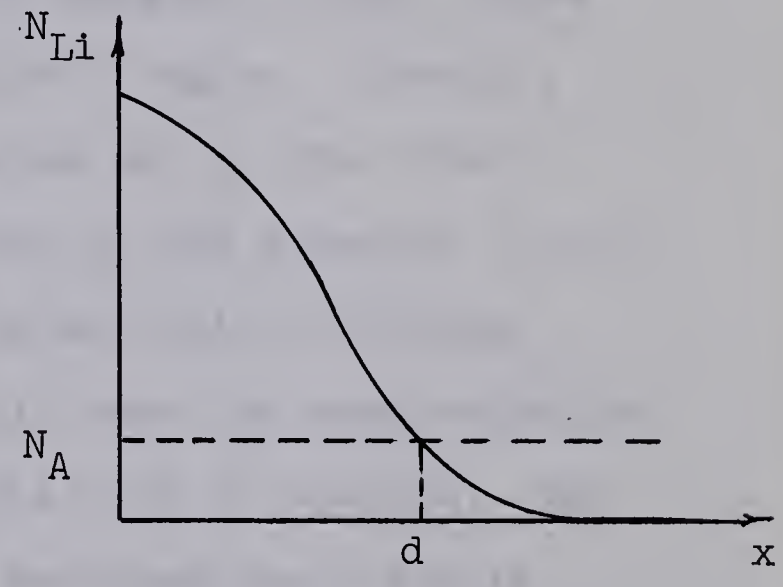

Fig. (1.6 a). Diffusion of Lithium in Germanium. Reference (9).

---

* A nomograph for lithium mobility in germanium is given in a paper by J. Takacs, Nuclear Instruments and Methods, 33, (1965), 171-172.

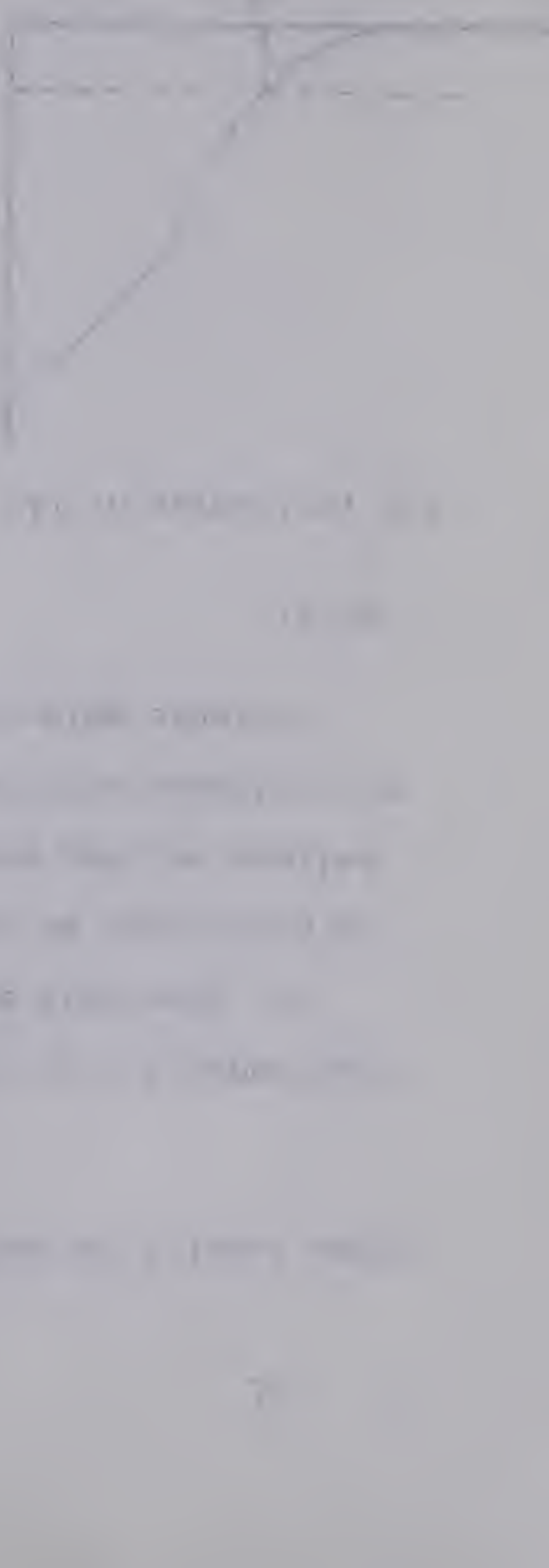

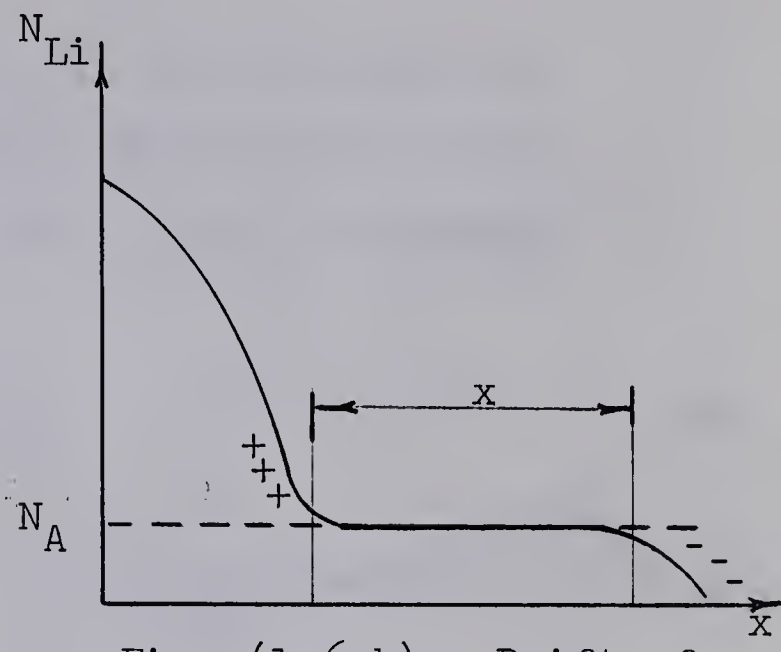

Fig. (1.6 b). Drift of Lithium in Germanium. Reference (9).

This equation indicates that as temperature decreases the depletion depth increases. Although higher temperatures give a higher diffusitivity of lithium ions, there is a practical upper limit which must be imposed on this temperature. This is because for temperatures above the critical value, $(65^{o}C)^{*}$, the drift time of carriers decreases and the carrier concentration increases, both of which results in an increase in the leakage or reverse current. It would appear also that in equation (1.55) there is no limit to the width of the intrinsic region. However, there is a limit to the drifting process set by the effect of carrier generation current described by the equation (1.24). This can be explained in the following way which the ions moving in the intrinsic region must all have the same velocity distribution otherwise the drifting will not be uniform. The ions distribute themselves in such a way that the field is kept constant in the depletion region. While carriers move through this region, they contribute a space charge of linear form shown in Fig. (1.7a), but lithium ions must compensate this space charge to give a uniform distribution and therefore

---

* A discussion of this critical temperature is given in a paper by Hanson and Jarrett, UCRL-11589, August 7, 1964, Lawrence Radiation Laboratory, Berkeley, California, U.S.A.

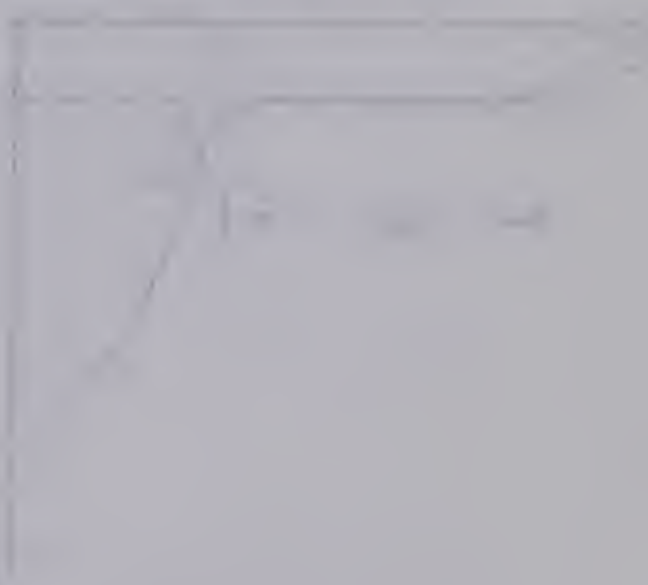

Fig. (1.6b) takes the form of Fig. (1.7b). As the depth of space charge region increases, the compensation becomes less complete, and the slope of plateau in Fig. (1.7b) increases. Hence, no further ion drift will occur when the value of space charge concentration approaches to the acceptor concentration, N_A. In fact, the practical limit arises before this stage is reached due to the precipitation of the lithium ions in the crystal.

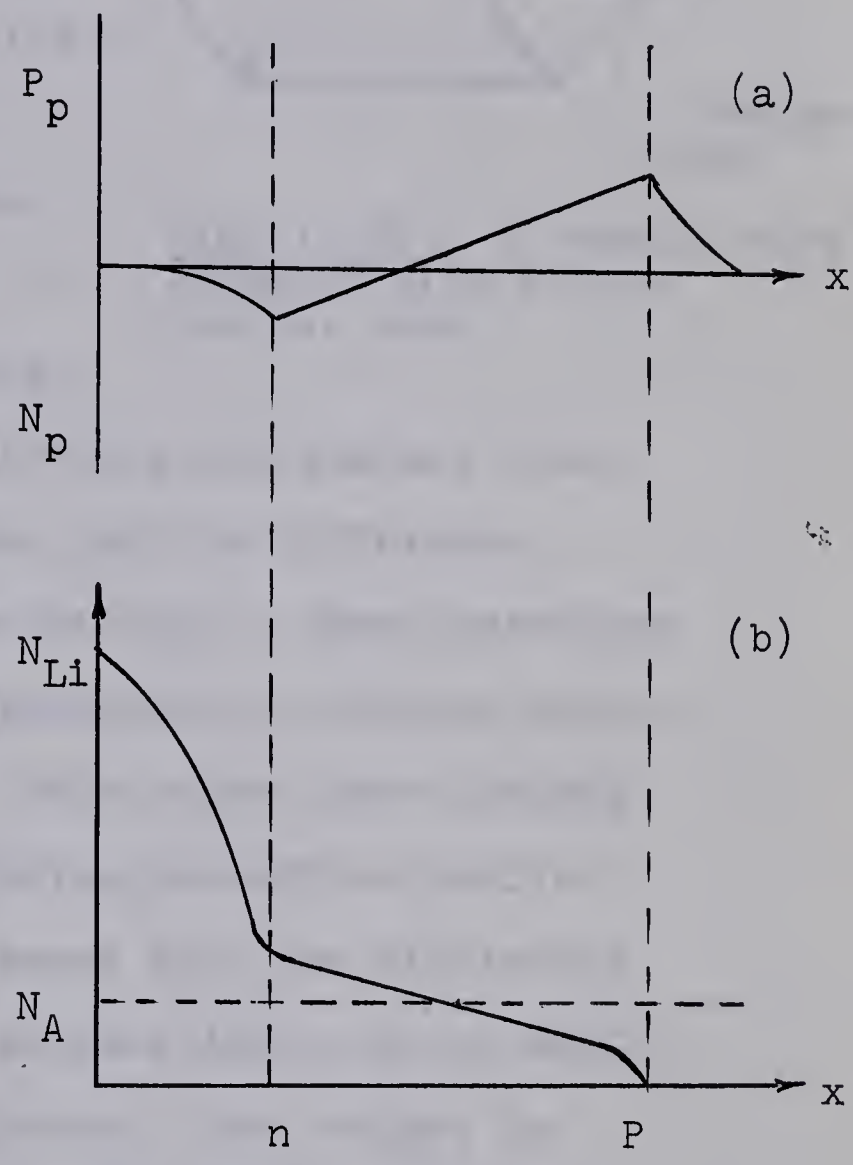

Fig. (1.7). (a) Space charge distribution due to the generation current. (b) Precipitation of Lithium in Germanium. Reference (9).

(1.b) Coaxial type.

The principle of this type of detector is the same as planar type with the only difference being the method of drifting. In this case, lithium is drifted into the crystal from all surfaces except one face as first described by Tavendale (12). Coaxial drifting provides a much larger sensitive volume for a given drift time and from the same area of crystal than with planar type drifting. Detectors with large sensitive volumes have high efficiencies and can be used in coincidence experiments as well

as in gamma ray spectrometry. Their leakage current is much less than it is for planar type as the most part of junction area is inside the material and cannot be contaminated. Fig. (1.8) shows a schematic diagram of these detectors with a P-type central core.

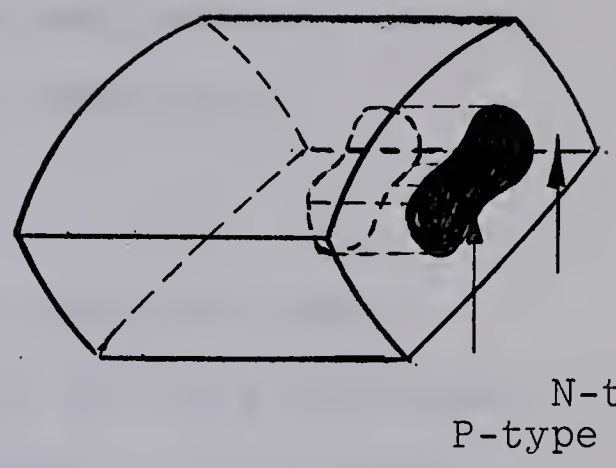

Fig. (1.8). A coaxial-type detector with P-type central core.

2. Surface barrier or $(\frac{dE}{dx})$ detectors.

These detectors are similar in principle and their properties to the junction detectors, but the difference lies in the method of obtaining the junction. These detectors are made of N-type crystals where spontaneous oxidation gives an inversion layer on the surface. This oxide layer induces a state of high density of holes, having properties similar to a diffused P-type layer. There seems only one difficulty with this type of detector in that surface layer is not sufficiently conducting to provide electrodes. The contact to this layer is made by the evaporation of a thin gold layer. These detectors will respond linearly to the energy lost $(\frac{dE}{dx})$ in the sensitive region by an incident charged particle. The thinner a sensitive layer the less will be the energy spread of the transmitted particles. The advantage of the surface barrier detectors over junction detectors is that the process of making the former does not involve heat treatment and carrier lifetime, is therefore not decreased. The carrier with

higher life time in turn results in lower bulk reverse current, reduces the noise and improves the energy resolution.

3. Totally depleted or (E) detectors.

Totally depleted detectors are detectors whose compensated or intrinsic region extends to the back electrode. The advantages of totally depleted detectors are the existence of two windows through which particles may enter the sensitive region. Second, is the absence of the series resistance between the sensitive region and the electrodes which always limits the pulse rise time of the detector and third, since capacitance of the detector is constant the applied voltage has no effect on this capacitance. In totally depleted detectors the incident particle may lose all its energy in the depletion region and thus the output signal gives an indication of the energy of incoming particles.

4. $(\frac{dE}{dx}, E)$ detectors.

In non-relativistic limits the energy lost by a particle in traversing a given distance Δx in matter is proportional to (mZ^2/E) where Z is the atomic number of a particle of mass m and energy E, i.e.

$$\frac{dE}{dx} \propto \frac{mZ^2}{E} \qquad (1.57)$$

If a particle first traversed a thin or a $(\frac{dE}{dx})$ detector and it afterward stopped in a thick or E detector, the product of

the two signalsis a measure of quantity (mZ^2). A ($\frac{dE}{dx}$, E) detector is an assembly of two detectors in line. To accomplish this double detection, pulse height multiplication must be done electronically.

1.11. Irradiation effects.

Extensive irradiation of semiconductor detectors causes deterioration of their properties. The irradiation produces lattice defects and other imperfections in the crystal which serve as trapping centers. These centers lower the carrier life time. Consequently, the rise time increases, the collection efficiency lowers and altogether leads to very poor energy resolution. It has also been reported (13) that detectors can be seriously damaged if they are subjected to the bombardment of low energy heavy ions such as glow discharges caused by applied voltage between the surface of the detector and the other regions such as the accelerator target which serves as the source of radiation. This effect may also arise by the glow discharges of ionization gauge in vacuo.

CHAPTER 2

PREPARATION OF THE GERMANIUM LITHIUM-ION-DRIFTED DETECTORS

2.1 Material.

From the discussion in Chapter-1 it was pointed out that the major factors which contribute to the collection of charge carriers are the impurities and imperfection in the crystal. Therefore it is of great importance to know the properties of a suitable material used in fabrication of crystal detectors. The material should have the following characteristics:

(a) High resistivity: high resistivity material is required in order to make the application of high electric fields possible and thus to minimize the carrier loss by trapping process. If the resistivity is not sufficiently high a very large current flows through the detector and produces a source of noise. This noise, in turn, limits the maximum electric field that can be applied. The higher the resistivity, the lower the charge carrier concentration and the more intrinsic the material will be. In practice it is not possible to produce materials of intrinsic resistivities, rather they are near intrinsic. As an example, at room remperature the values of near intrinsic resistivity for germanium is about 50 ohm-cm and that of silicon is 230 kilo ohm-cm.

(b) High carrier mobility: high carrier mobility is needed to give rapid carrier collection time. This is also evident from equation (1.4). The values of carrier mobilities for near intrinsic materials of germanium and silicon are given in Table (2.1). It may be noticed that (a) is inconsistent with (b) but one should consider the overall effect.

(c) Long carrier life time: carrier life time must be long for both electrons and holes so that complete collection can occur before trapping effect becomes important. Carrier life time is directly related to the carrier concentration or resistivity of material. As an example, for a germanium material of resistivity of 5 to 10 ohm-cm the minority carrier life time is about 100 μ sec, and that of a resistivity 30 to 40 ohm-cm the life time will be about 400 μ sec.

(d) Low trapping rate: low trapping rate is desired in order to increase the efficiency of charge collection. Space charge trapping also reduces the efficiency of collection and leads to an increase in conductivity. The above properties must be retained and remain constant under long application of the electric field. Investigations have shown that to a limited extent, only two materials, germanium and silicon fulfill the above conditions. The physical properties of near intrinsic of these two materials is given in Table (2.1). Both materials, however, have low energy gaps and hence their resistivities

TABLE 2-1

The Physical Properties of Near Intrinsic Silicon and Germanium at Room Temperature (8)

Property	Silicon	Germanium
Periodic table	Group IV b	Group IV b
Atomic number	14	32
Atomic weight	28.09	72.60
Stable isotope mass number	28, 29, 30	70, 72, 73, 74, 76
Crystal structure	Face-centered cubic	Face-centered cubic
Lattice constant	5.42 Å	5.657 Å
Number of atoms per cm^2	4.96×10^{22}	4.41×10^{22}
Density	2.33 gm/cm^3	5.33 gm/cm^3
Melting point	1420°C	936°C
Boiling point	2600°C	2825°C
Coefficient of thermal expansion (linear)	4.2×10^{-6}/°C	6.1×10^{-6}/°C
Thermal conductivity	0.20 cal/cm/sec/°C	0.14 cal/cm/sec/°C
Specific heat (0° - 100°C)	0.181 cal/gm/°C	0.074 cal/gm/°C
Dielectric constant	12	16
Energy per electron-hole pair (ϵ)	3.34 ev	2.85 ev
Energy gap	1.106 ev	0.66 ev 0.75 ev at 77°K
Intrinsic resistivity	230 kΩ cm	47 Ω cm
Intrinsic carrier concentration	$1.5 \times 10^{10}/cm^3$	$2.35 \times 10^{10}/cm^3$
Electron drift mobility	1350 cm^2/volt-sec	3800 cm^2/volt-sec
Hole drift mobility	480 cm^2/volt-sec	1800 cm^2/volt-sec
Electron diffusion constant	35 cm^2/sec	92 cm^2/sec
Hole diffusion constant	12.4 cm^2/sec	44 cm^2/sec

are not high enough to be used directly as a detector. They need to be given different treatments which we shall discuss in the later sections. Of these two materials, germanium seems to offer greater number advantages than silicon.

Germanium, has higher atomic number, which stops a particle about twice the energy that would be stopped in silicon and has better efficiency for detecting the photo-peaks in gamma spectrometry. It has a higher coulomb barrier which lowers the energy required to release an electron-hole pair and gives better statistics.

The disadvantages of germanium for the purpose of detector fabrication are, 1-low resistivity, and 2-necessity of cooling to liquid air temperature.

2.2 Method of preparation.

It has been noted that the higher the purity of the crystal the better it will be. All efforts in the preparation of a detector are directed toward producing a material as nearly intrinsic as possible. The material used in preparation of these detectors was 8 to 10 ohm-cm, P-type, gallium doped, single crystal of germanium grown in (111) plane. Its dislocation density were 2000 to 2200 pits/cm^2 and the minority carrier life time was about 100 μ sec. It had a trapezoidal shaped cross section of 8.5 cm^2 and was manufactured by Sylvania

Electric Company* . The principle of the method of detector preparation in all laboratories is almost the same but some minor differences arise from the fact that each laboratory may make some modifications in the fabrication method either for its own convenience or for preparing a better detector or both. Of course, it should be noted that the key to success lies in these apparently minor differences.

The main steps that have been followed in the fabrication of the detectors are as follows:

(1) It is necessary to provide a supply of deionized distilled water of resistivity more than 2 x 10^6 ohm-cm for the purpose of the whole washing processes of crystals. It has been found out that the waters of resistivities less than 2 x 10^6 Ω-cm contain sufficient impurities to contaminate the surface of the crystal. The deionizer used was a Bantam** demineralizer with a mixed bed resin cartridge. This bed removes the ionized impurities mainly the silica and CO_2 impurities by chemical ion exchange process.

(2) The crystal is cut to the desired thickness with a crystal cutter*** .

(3) Both faces of the crystal as well as its edges are lapped using wet carborundum paper, starting from 400 grit or less, depending on the roughness of the crystal surface and working

---

* Sylvania Electric Products Inc., Towanda, Pennsylvania, U.S.A.

** Model BD-5,5-25 G.P.H., Barnstead Still and Sterilizing Co., Boston 31, Mass., U.S.A.

*** Model 716, South Bay Technology Group, Sherman Oaks, Calif.

up to 600 grit. The crystal should be rotated frequently to ensure a scratch-free surface and should be washed with cool tap water frequently in order to protect the crystal from the heat generated during the lapping process. Finally, the crystal is polished with a slurry of Al_2O_3 0.1 to 0.3 microns particle size or with a 600 mesh or higher silicon carbide slurry. The polishing process stops when a surface with no visible scratch is obtained.

(4) After once being washed with tap water, the crystal is cleaned for about 10 minutes using an ultrasonic agitator* in an Alconox solution, contained in a plastic or, preferably, Teflon beaker. If this agitator is not available, the crystal should be agitated in the beaker itself. It is then washed with distilled water. Note that after this step all the washing processes should be done with distilled water. It is important that the crystal not come into contact with metal during washing procedures. Thus, they must be handled with plastic-covered or Teflon tweezers.

(5) The crystal is dried with filter paper and transferred to another plastic beaker containing very clean ether or

---

* Di SON Tegnator System 40, Ultrasonic Industries Inc., Engineers Hill, Long Island, N.Y., U.S.A.

chloroform. Then it is placed in the agitator for about two minutes. It should be noted that all chemicals used must be reagent grade and each chemical should have its own beaker that is not used for other purposes, and solvents should never be used more than once.

(6) The crystal is washed with methyl alcohol and then with distilled water. The excess water is blotted from the crystal with filter paper.

(7) Etching: At this stage the crystal is ready to be given a chemical polish or etch. The etching mechanism is based on the fact that nitric acid oxidizes the surface while hydrofluoric acid deoxidizes. Thus, a mixture of both acids causes the removal of a surface layer from the crystal. A solution containing two parts nitric acid to one part hydrofluoric acid (48%) is prepared and then the crystal etched for about two minutes. During this time the crystal should be agitated in the beaker at a rather fast rate. The yellowish smoke due to nitrogen monoxide released from the reaction can be seen after about one minute. At the end of two minutes the smoke turns to a very dark brown color. The reaction also creates a large amount of heat. However, the temperature of solution should not be allowed to exceed $45^{\circ}C$. This can be prevented by immersing almost half part of the beaker in a cool water bath. It should also be noted that the etchant

should cover the whole crystal. This can be done by using 50 cc of solution in a beaker of 100 cc in volume. Sometimes it appears that this solution produces a number of pits on the surface. In this case, one can make a weaker solution such as 3 to 5 parts nitric acid and one part hydrofluoric acid. Such etchant requires an etching time of three to five minutes respectively. All the etching processes should be performed under a fume hood or a mask should be worn in order to avoid inhalation of the nitrogen oxide.

(8) The crystal is then removed from the etchant by diluting the solution with water in time intervals of 30 seconds for a time of two minutes and then washed with at least one liter of water. This way of diluting the solution provides a slow and uniform weakening of the etchant and also it protects the crystal against a sudden decrease in the temperature of the etchant. At this stage, the crystal is ready for diffusion of lithium onto one face.

(9) Lithium evaporation: prior to the evaporation of the lithium onto the crystal, a strip of 1 to 2 millimetersin diameter is cut from a piece of lithium which is stored in the mineral oil. After cutting, the lithium is dipped in benzene to remove the oil and is wrapped around a tungsten wire filament and heated in vacuo (about 5×10^{-5} cm Hg) until the lithium oxide and the other contaminants (black color) evaporate and

the cleaned (silver color) lithium remain on the wire. The volume of the lithium which is wrapped around the wire should not be larger than 1/2 cm^3 and current is raised very slowly, otherwise the melted lithium will fall off the filament. After this step the evaporator is not vented unless the crystal is ready for evaporation. In order to protect the edges of the crystal from the diffusion of lithium, the perimeter of the slice should be painted by "Aquo Dag", a colloidal suspension of carbon in alcohol or water. The edges are then covered by a strip of aluminum foil to prevent the Dag from peeling off. The crystal is transferred to the evaporator system which is immediately pumped down to prevent the lithium from further oxidation. The crystal is separated from the heater block by a block of hard carbon* of thickness of 1/8"to 1/4" in order to protect the crystal from any thermal shock caused by the heater. There is also a shadow plate, position controlled from the outside, which prevents the crystal from seeing the lithium prior to the evaporation time. All the devices under the bell-jar must be cleaned.

ii. The crystal is preheated to about 425°C and kept at this temperature for about half an hour. Three minutes before evaporation time, lithium is heated again and then the shadow plate is removed. Lithium is evaporated for about 3 to 5 minutes

---

* Do ALL Canada Ltd., 10 Meridian Road, Rexdale, Ontario.

onto the crystal surface. (Although heating the crystal for half an hour may reduce the minority carrier life time, the effect of this change is negligible compared with the magnitude of surface leakage current caused by other effects).

The entire arrangement for the evaporation of lithium is shown in Fig. (2.1). Preheating the crystal for half an hour provides a diffusion depth of up to 500 microns. Three minutes after evaporation helium (chilled in liquid air) is bled into the bell-jar to assist cooling. The cooling time which depends on the size of crystal and the heater, should be as short as possible in order to obtain a uniform diffused layer. The rate of cooling is rapid at first but total cooling time to about 60°C is done in one hour. The cooling time could be reduced to about 15 minutes if one provides a system which can remove the carbon block together with the crystal from the heater right after evaporation.

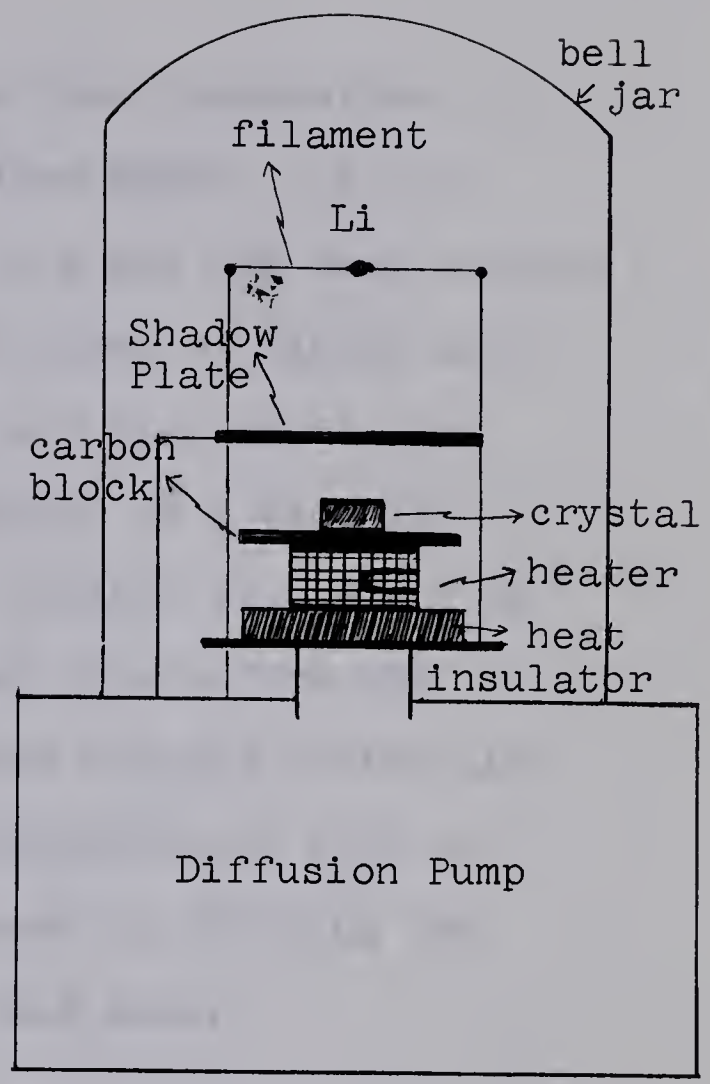

Fig. (2.1). The system used for evaporation of Li onto surface of the germanium crystal.

(10) After cooling down the crystal to room temperature, it is washed in alcohol and then in distilled water. If the excess lithium on the surface and aquo dag has not been removed by this wash, then a weak solution of 5 parts of nitric acid to 1 part of hydrofluoric acid is made and the crystal is etched for about 10 to 30 seconds, followed by a wash in distilled water. After this wash, the crystal should not be exposed to air for an extended period of time before the plating process. However, if it has been exposed to the air the crystal should be given a wash in hydrofluoric acid for about 10 to 15 seconds and rinsed in water by diluting the solution then washing thoroughly with pure water.

(11) Nickel plating: After step (10) the crystal should not be removed from the water unless the nickel plating solution is ready. The method of electroless nickel plating as described by Brunner (14) is applied. The plating reaction is catalytically controlled and since the product of reaction, namely, the nickel catalyzes the reaction, the nickel plating continues to build up indefinitely as long as the temperature and the supply of solution is maintained. The composition of the plating bath is as follows:

Nickel chloride ($NiCl_2$, 6 H_2O)	30 g/l
Sodium hypophosphite (NaH_2PO_2,H_2O)	10 g/l
Ammonium chloride (NH_4Cl)	50 g/l
Ammonium citrate [$(NH_4)_2HC_6H_5O_7$]	65 g/l

Ammonium hydroxide (NH_4OH) was added until the solution turned from green to blue (pH 8 to 10) and during the whole process of plating the pH of the solution is kept at a value between 8 to 10. A solution of 100 cc is raised to a temperature of 90° to 100° C. Although a higher plating rate could be achieved by increasing the temperature, this range of temperature has proven adequate. The crystal should then be handled by tweezers and held in the steam above the solution for about one to two minutes. This avoids a rapid change in the temperature of the crystal. The crystal is then placed in the solution very slowly. After about two minutes plating should start. Once plating has started, a plating time of three minutes provides a sufficient layer of nickel over the whole crystal. A sign which accompanies plating is the appearance of numerous hydrogen bubbles around the crystal. Sometimes the plating process takes a long time to start. Under such circumstances bringing a more electronegative material such as aluminum in contact with the crystal will accelerate the process. A strip of aluminum foil dipped in solution catalyzes the plating process and plating on the aluminum foil starts

immediately which helps the nickel to plate the crystal as well. Sometimes it is necessary to leave the aluminum foil in the solution during the plating period. The solution is allowed to cool down to room temperature and is then transferred to another beaker and washed with water, alcohol and water again. The nickel solution is returned to its container as it can be reused. A used plating solution plates better than a fresh solution.

(12) Etching the nickel off the edges: recalling step (9), if the edges have been covered by Dag during diffusion of lithium, etching the edges will be sufficient. If not, about one millimeter of the crystal should be cut off the edges after step (11). However, it seems better to lap between 50 to 100 microns off the edges even if Dag had been used. At this stage and after following steps (4) and (5) one can check the diffusion depth of lithium in the crystal by copper plating.

(13) Copper plating: copper which is more electropositive than germanium can be deposited by an electrochemical displacement method which induces a potential difference across the junction and application of reverse bias increases this potential and makes more disposition of copper on the crystal available. The composition of the copper plating solution is as follows:

10% copper sulphate ($CuSO_4$) or copper nitrate [$Cu(NO_3)_2$]
10% hydrofluoric acid (HF).

The crystal is dipped into the solution and a reverse bias of 12 to 15 volts is applied. Copper deposits more on the P-side and the junction appears clearly on the edges of the crystal. Copper can be removed by washing the crystal in a diluted nitric acid solution (one part nitric acid to ten parts water) for about 10 to 15 seconds followed by rinsing with water. Alternatively one can repeat steps (3) to (6).

(14) Diode characteristic measurements: by application of a 5-volt reverse bias on the diffused lithium crystal the diode characteristic is measured. If the reverse current is less than the forward current, the crystal is readied for the drifting process.

(15) Masking procedure: after step (13) both faces of the crystal are covered with Apiezon wax dissolved in trichloro-ethylene and then dried and etched as described in step (7). During this process sections of the wax come off sometimes. This indicates that the wax solution is too thin. Sometimes the wax peels back from the edges, indicating that it has been "painted on" instead of "flowed on" from a puddle of wax pushed around by the brush. Usually, a large volume of the etchant solution must be used to keep the temperature from rising and thus prevents softening of the wax.

(16) The crystal is transferred to a plastic beaker of trichloroethylene or xylene and the wax removed completely. The crystal is then washed with alcohol and water and dried by blotting the excess water with filter paper. At this stage the crystal is ready for the drifting process.

2.3 Drifting procedure.

Two types of drifting techniques have been used. The operation principle of these drifting devices are described in Chapter 3.

(1) Automatic drifting (15) at constant current has been used for crystals of total thickness less than one centimeter. The crystal was mounted in the drifting device and reverse bias was increased very slowly to 100 volts. The current at the beginning is very low (about 5 mA) but increases rapidly (depending on the characteristic of the crystal) to about 50 to 80 mA when the temperature reaches 45°C. After half an hour at this bias, the voltage may be raised further. If breakdown occurs, the breakdown voltage noted, the crystal removed from the drifting device and the edges etched. It is then put back under drift. This time the voltage is raised to just below the previously noted breakdown voltage. After a certain length of time the expected depletion depth can be determined from equations (1.56) or (1.22), and experimentally by copper plating or by the method of hot probe described in

section 2.8. Sometimes drifting stops for the reason explained in section 1.10a. In this case the crystal should be removed from drifting device, and the edges should be etched with two to one etchant solution. Then the crystal is put back under drift if the etching procedure did not improve the drifting conditions. The crystal should be heated to 400°C under vacuo and cooled down rapidly. However, if this procedure also was not effective in improvement of drifting conditions, the lithium should be evaporated again onto the N-side of the crystal after removing of the nickel contacts by the etchant solution and then, following steps (9) to (16). Depletion depths of 3 to 5 millimeters have been obtained under a bias of 100 to 200 volts during a drifting time of one week. It has been suggested by Palms, et al (16) that if the drifting process is carried out under a very dry nitrogen atmosphere, then a diode which has been prepared from a near intrinsic material, can be drifted under 500 volts at a current of 30 mA and a temperature of 55°C.

(2) The boiling liquid drifting apparatus (17).

Crystals of more than 8 mm in thickness, specifically the coaxial-type crystals cannot be drifted with the drifting device described previously due to the fact that their large volumes draw more current. Consequently, the electric field across the crystal drops to a small value (less than 30 volts at 100 mA and 40°C) and thus drifting rate reduces largely.

The liquid boiling device which operates at a constant temperature (namely the boiling point of the used liquid), will provide a maximum drifting current of 4 Amp. A bias of 250 volts is possible depending on the breakdown voltage of the crystal. Typically, crystals were drifted at a bias of 100 volts with a current of 2.5 Amps at 61.3°C, the boiling point of the chloroform used. For a given current the voltage drops as the drifting rate decreases. Start up and reconditioning procedures are similar to those described for the constant current device. With this apparatus, a depletion region of 4 mm in thickness was achieved for a planar-type crystal of total thickness of 12 mm in five days, and a sensitive region 7 to 8 mm deep was obtained for a coaxial-type in two weeks. It has been also suggested by Camp (18) that a drift temperature lower than 40°C has several advantages. It reduces the problem of lithium precipitation, i.e., the lithium ions precipitate in the sensitive region near the P-side and make no further drifting possible as is described in section 1.10a. It decreases the leakage or drifting current and allows the application of higher voltages. The high temperature drifting also produces non-uniform drifting rate, i.e., in the central part of the crystal where the temperature is higher and the electric field is stronger, the drift rate is more than the neighboring regions and thus lithium distribution is not uniform.

For this reason if the drifting temperature is more than 30°C the crystal requires a clean up drift (as is described in the next section) immediately after high temperature drifting.

2.4 Clean-up drift.

Prior to mounting the crystal in the test chamber or in a cryostat, it is necessary to flatten and smoothen the distribution of the lithium in the crystal. This process which is called "clean-up" is carried out in the following way. If the crystal has already been drifted in an automatic drifting device, the temperature is decreased to below room temperature, hence, causing the drifting current to reduce to less than 10 mA at 100 volts. The voltage is then raised until the current reaches 10 mA. Clean-up drift is carried out for 20 to 50 hours. A diode which has been cleaned up properly has a very uniform distribution of lithium or compensated region as indicated when the crystal is copper plated. The best diode obtained required a clean-up condition of 500 volts at 4 mA and a temperature of 20°C for a period of only 24 hours. (The crystals larger than 1 cm in thickness have been cleaned up in the test chamber and the heat dissipated by the crystals has been removed by exposing the test chamber to a flow of air.) After clean up, the edges of the crystal should be etched, washed and mounted in the test chamber as soon as possible, be pumped out and cooled down immediately while etching the edges

require wax masking, drying, and washing, processes which require more than one hour if properly done. On the other hand, Apiezon masking wax often leaves a film on the edges of the crystal if it is not washed properly. This film results in a very high leakage current under vacuum and at liquid air temperature, while this leakage current was negligible compared with the leakage current caused by atmospheric moisture or some other contaminations during the drifting process. However, in order to protect the crystal from the formation of such film, both faces of the crystal were covered by No. 56 electrical tape* or preferably by No. M-407 electrical tape* and its edges etched for two minutes in two to one etchant solution. During etching process the beaker was agitated in cool tap water to minimize the heat produced by the reaction and thus prevent the tape from coming off. In spite of this precaution a peeling around the edges of the tape may still occur. In this case the crystal should be removed from the etchant immediately by diluting the solution by distilled water. If the etching time has not been sufficient, this process can be repeated again, and then is washed thoroughly by distilled water. Then, the tapes were removed and the crystal washed with alcohol water and immediately after with 30% H_2O_2 solution for two to three minutes followed by another wash in alcohol and water. H_2O_2 appears to reduce the number of trapping centers

---

* Minnesota Mining and Manufacturing Co., St. Paul, Minnesota, U. S. A.

created by surface contamination and thus it improves the surface leakage current. After the last wash, the crystal was allowed to dry in the air before being mounted in the cryostat.

2.5 Operation region.

After cooling down the detector to liquid air temperature, a rather good detector shows a leakage current of (1 to 5) x 10^{-9} Amp at 100 volts reverse bias. If a suitable detector has been obtained, then it is necessary to know the region in which a detector has its best characteristic, i.e., the highest bias, lowest leakage current and lowest capacitance. The voltage-leakage current characteristics should be measured as well as the voltage-capacitance characteristics which can be obtained using the simple circuit shown in Fig. 2.2. The operating region is then the region in which a change in detector voltage produces no change in detector leakage current and capacity. Fig. 2.4 shows these characteristics for a detector of area 7 cm^2 and depletion region of 4mm depth.

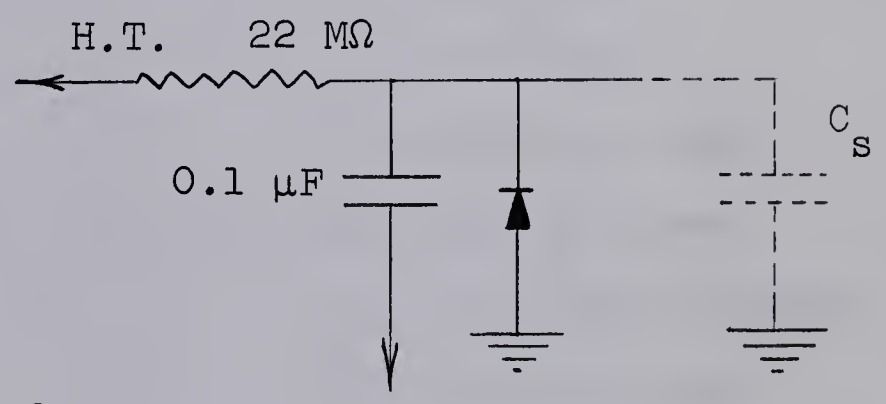

Fig. (2.2). Circuit used for voltage-capacitance characteristic measurement of the detectors.

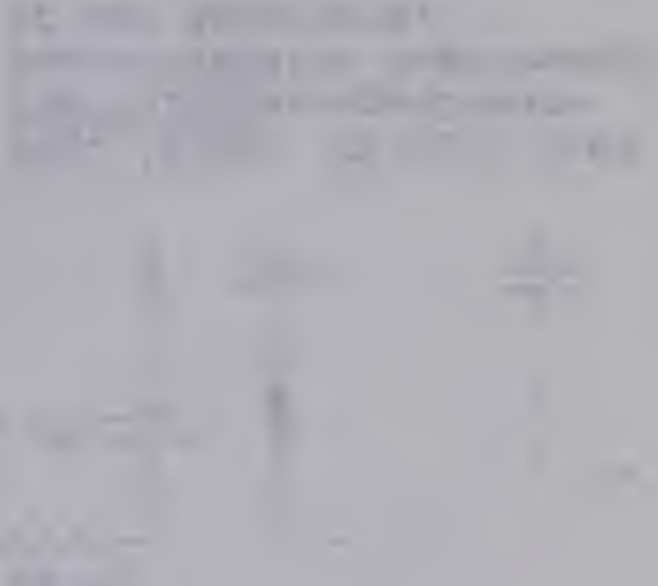

2.6 Calibration results.

The number of detectors have been fabricated are summarized in table 2.2, which indicates their energy resolutions for different sources of gamma-rays. The intrinsic resolution of these detectors are also shown in table 2.2. The experimental arrangement and the electronics system used for these measurements are described in Chapter 3. Figs. 2.5 to 2.8 exhibit the energy spectrum of the sources Co^{57}, Na^{22}, Cs^{137}, Co^{60}, and RdTh for a detector with 3 cm^3 sensitive volume.

2.7 Photo-peak efficiency measurement.

When a detector is used as a high-resolution gamma-ray spectrometer it is important to know the absolute photo-peak efficiency. In order to make efficiency measurements, it is necessary to have accurately calibrated sources, but such calibrated sources were not available at the time of measurement. Since the characteristics of the germanium used in the fabrication of these detectors were the same as those of the material used by Tavendale (19) at the Chalk River Nuclear Laboratories, the absolute efficiences for the detectors made at this laboratory were normalized to those of Tavendale's by considering the effects of solid angle and the depth of the depletion region. This normalization gave an approximation to the absolute efficiences of the detectors as is shown in Fig. 2.9.

Table 2.2

Energy resolution of the detectors for various sources of γ-rays and their intrinsic resolution in KeV.

Crystal No.	Co^{57} E_γ		Na^{22} E_γ		Cs^{137} E_γ	Co^{60} E_γ		RdTh E_γ			Pulser	Intrinsic resolution at 661 KeV
	122	136	511	1276	661	1173	1333	1600	2110	2620		
1	-	-	20	-	25	-	-	-	-	-	11	16.7
2	-	-	9.4	-	-	-	-	-	-	-	7	-
3	-	-	8	-	7.5	-	-	-	-	-	7	4.0
4	-	-	12	-	13	15	20	-	-	-	8	10.0
5	3.7	4.1	6.8	-	8.5	9.6	12	-	-	-	3.5	7.7
6	3.2	3.4	4.2	5.7	4.6	5.2	6	6	6.5	7.7	3	3.4

2.8 Hot probe method for the measurement of depletion depth.

This method has been used in the measurement of window thickness of the detectors but it can also be used for depletion depth measurement as well. The system consists of a pencil-shaped soldering iron, a galvanometer and the detector, all of which are connected in series as is shown in Fig. 2.3. The principle of operation is based upon the fact that when heat is applied to the P-side or N-side holes are generated and generated current can be indicated by a galvanometer. By bringing the soldering iron to a temperature of approximately 50°C and applying the iron to the N-side the galvanometer indicates the maximum generated current. When the iron is moved on the edge of the crystal toward the junction the current decreases. When the iron is crossing the depletion region very small current flows but when the iron reaches the P-side, a sudden and rather high current indication appears in the galvanometer in a direction opposite to that which was indicated for the N-side. With this method one may measure the window thickness and thus decrease this thickness to the desired length.

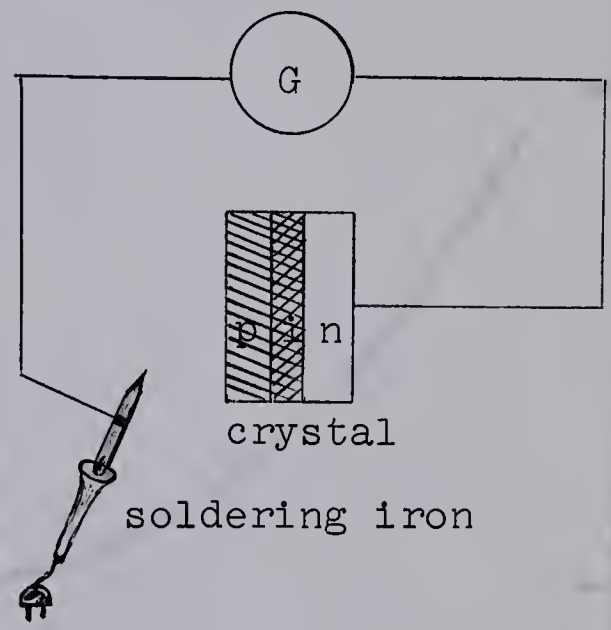

Fig. (2.3). Hot probe device for measurement of depletion depth and the window thickness.

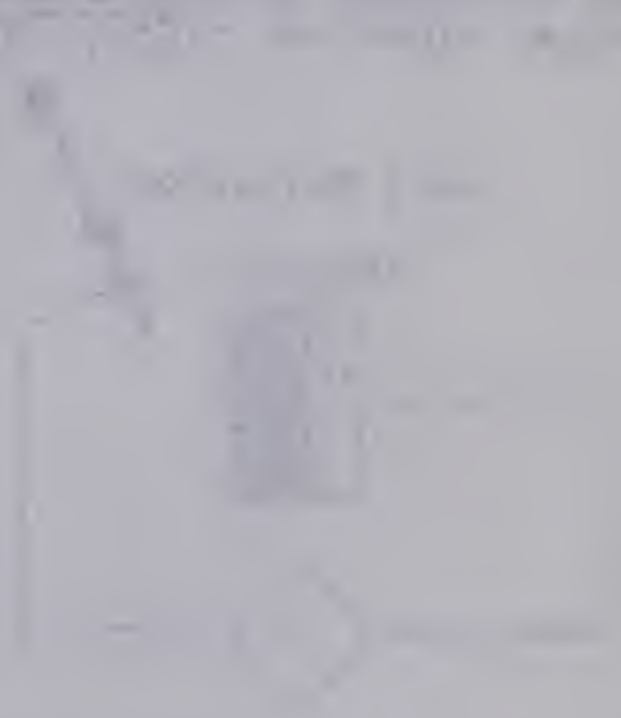

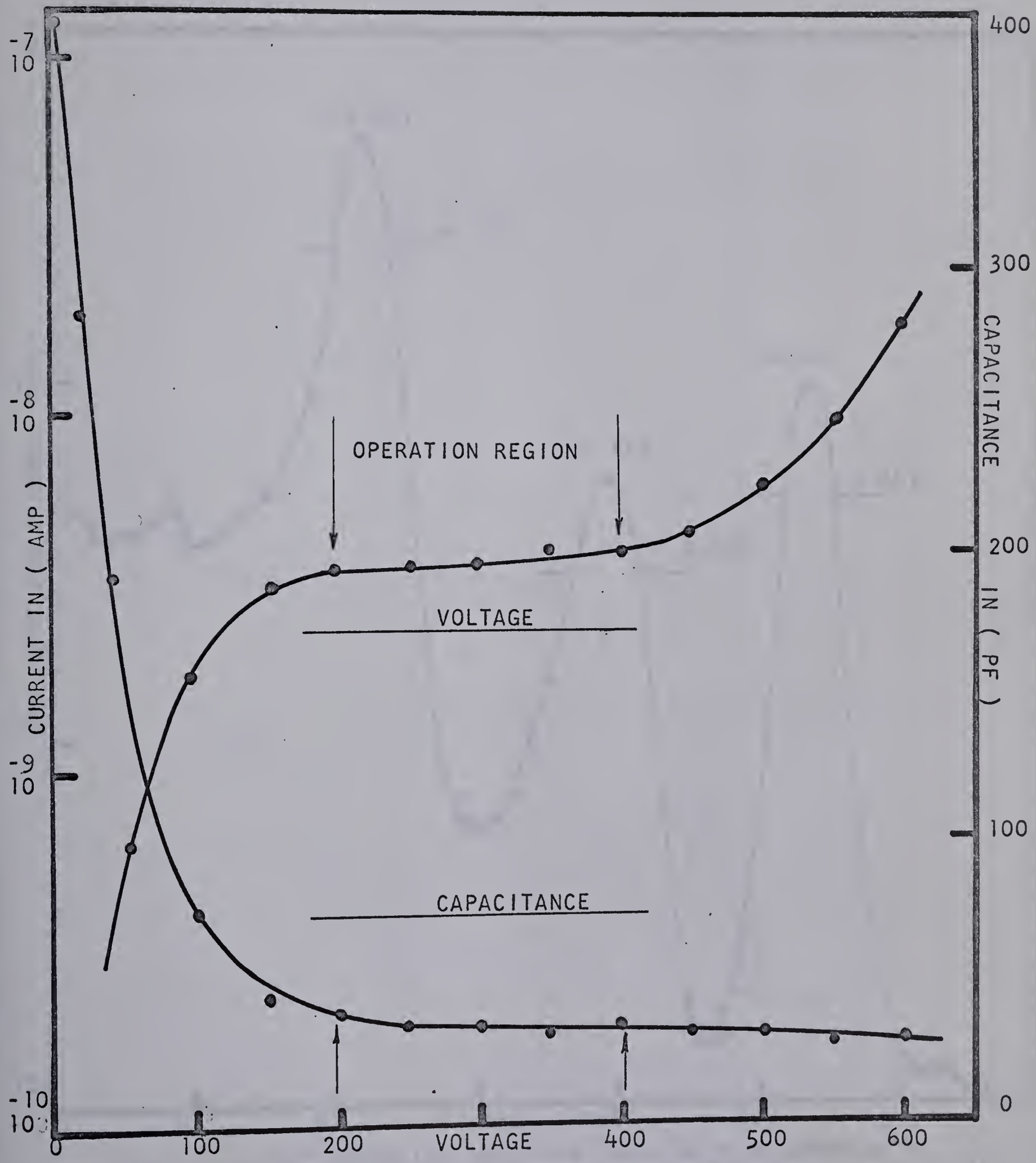

Fig 2-4. Voltage-leakage current and voltage-capacitance charactristics of a detector of area 7cm^2, and intrinsic depth 4mm.

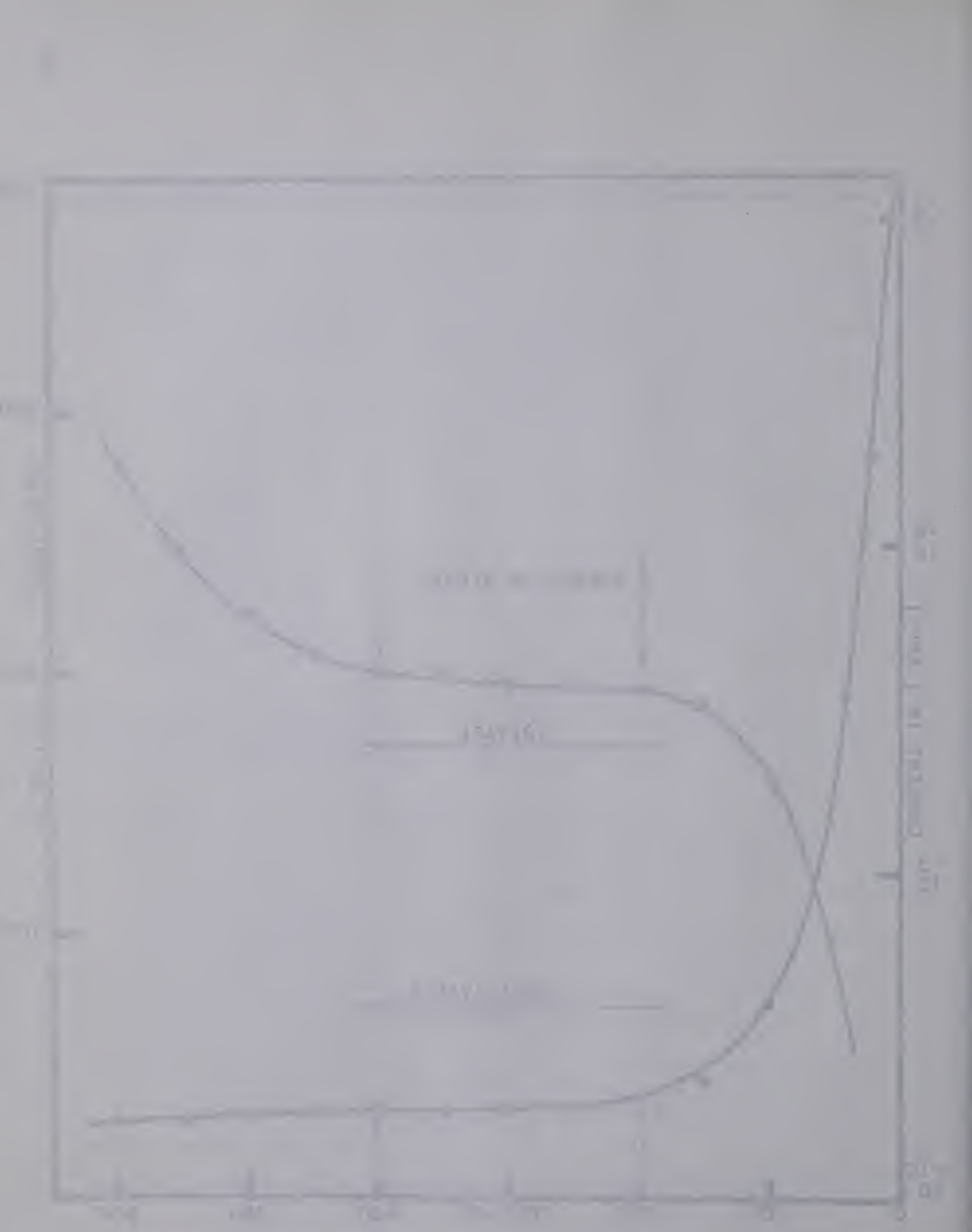

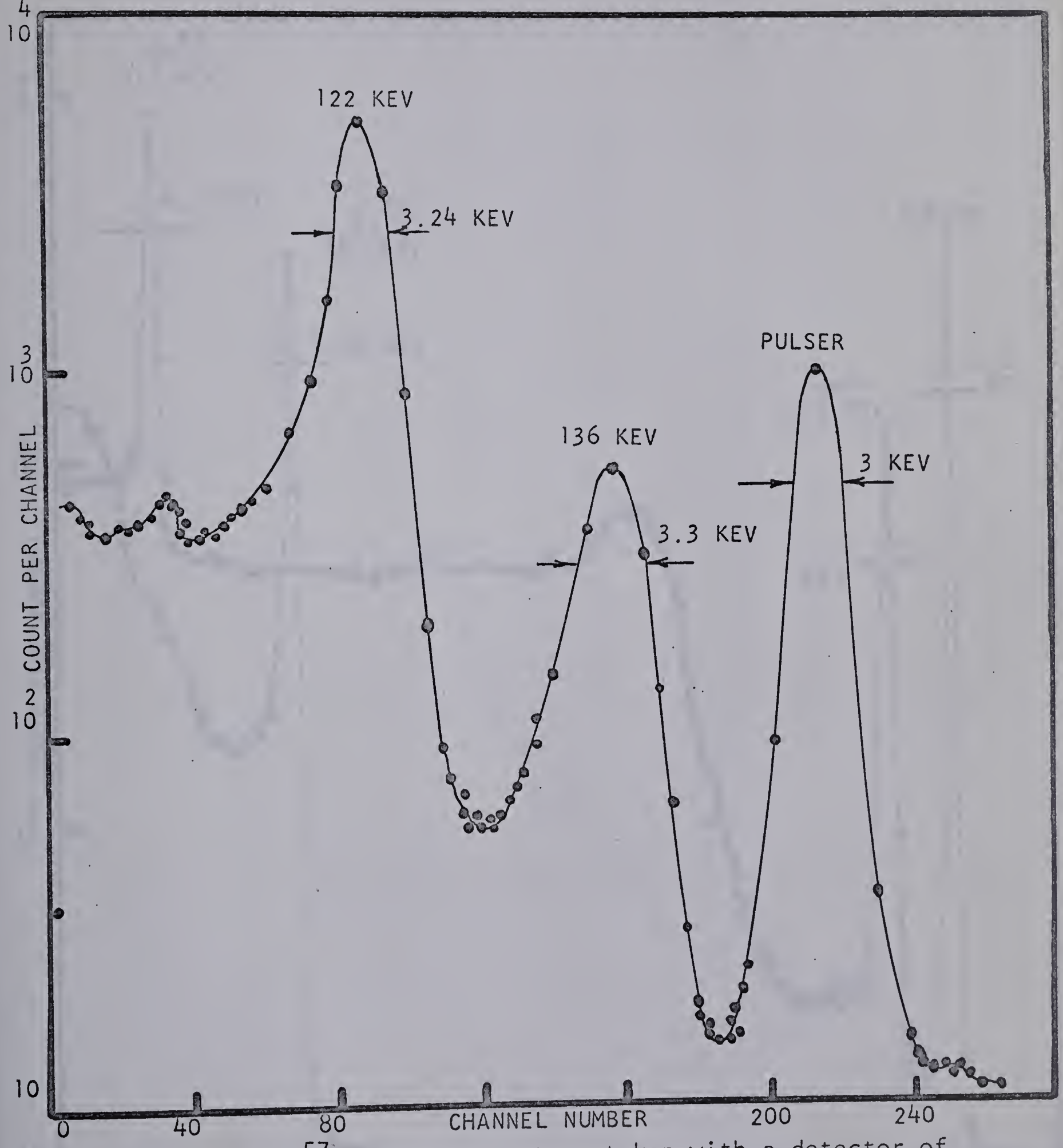

Fig 2-5. A Co^{57} gamma-ray spectrum taken with a detector of area $7cm^2$, intrinsic depth 4mm and at a bias of 400 volts.

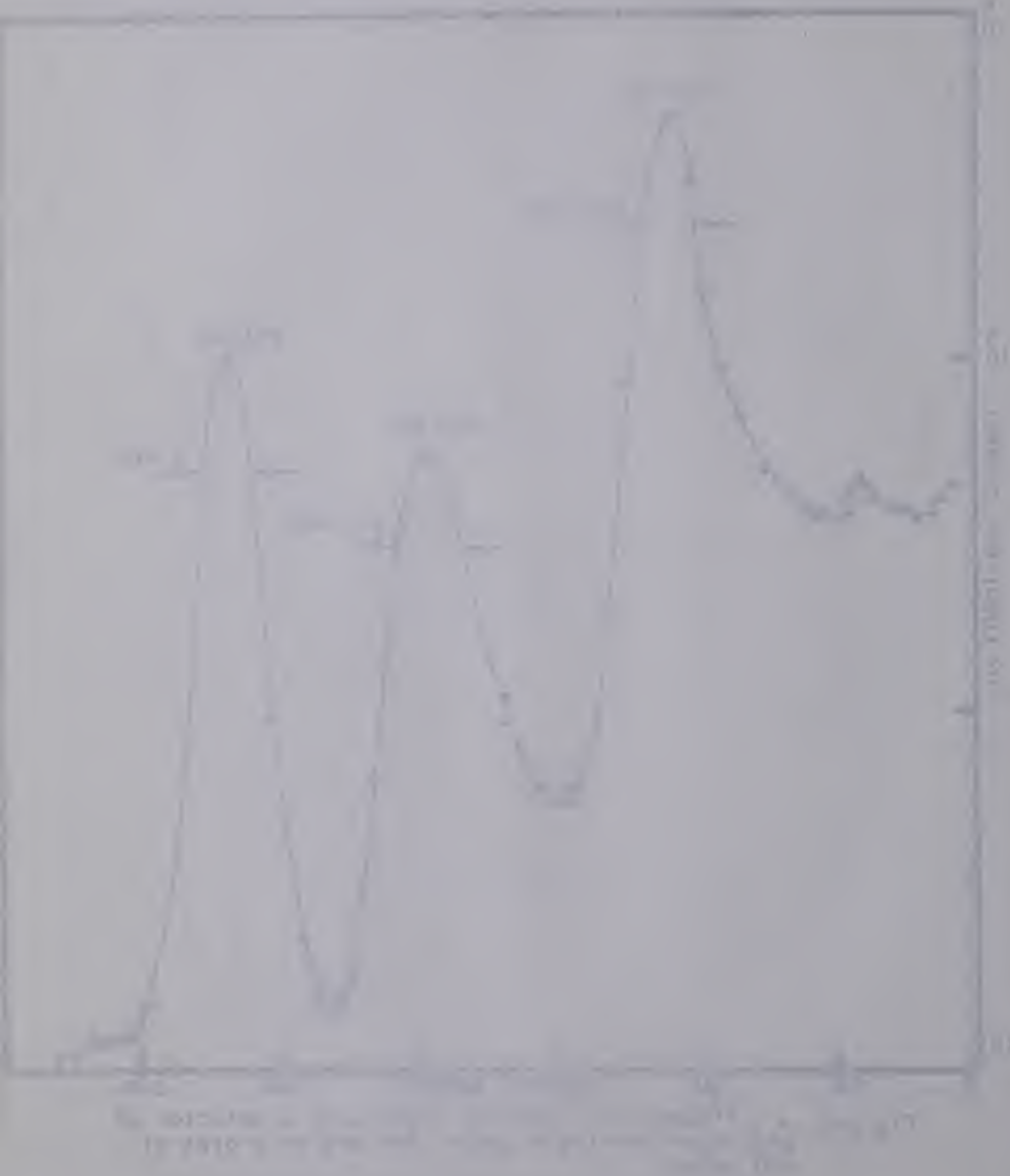

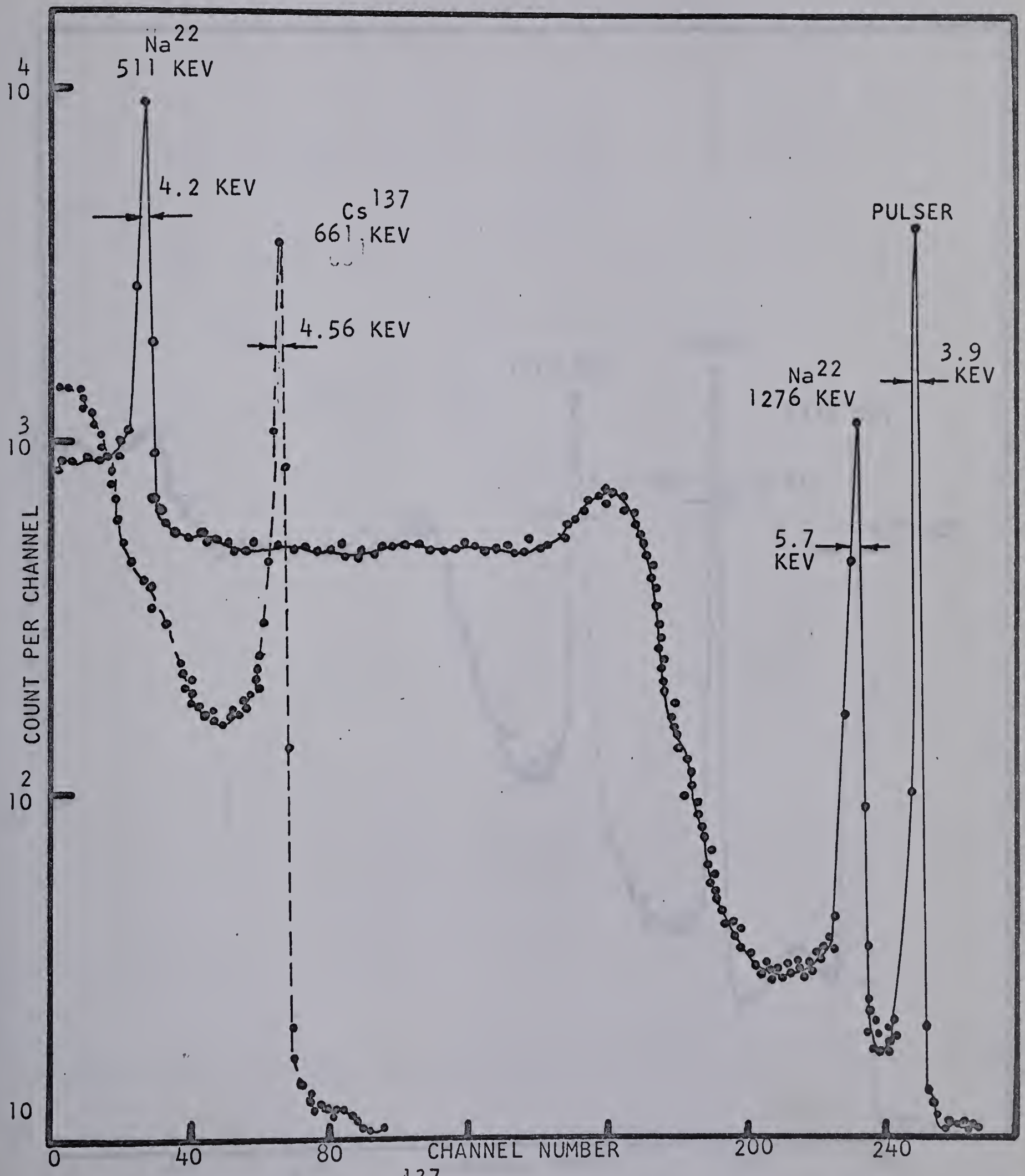

Fig 2-6. Na^{22} and Cs^{137} gamma-ray spectrum taken with a detector of area $7cm^2$, intrinsic depth 4mm and at a bias of 400 volts.

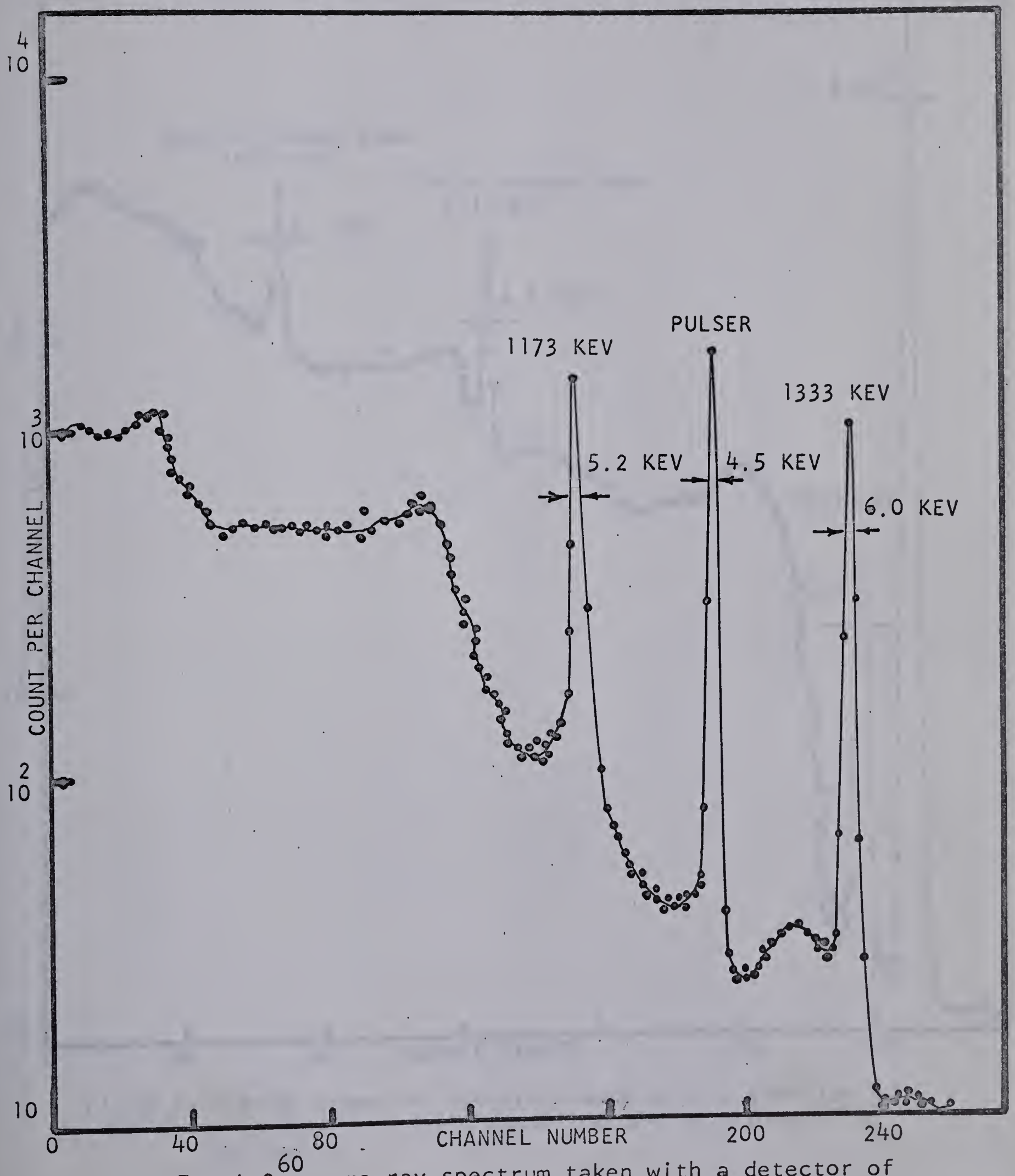

Fig 2-7 . A Co gamma-ray spectrum taken with a detector of area 7cm^2, intrinsic depth 4mm and at a bias of 400 volts.

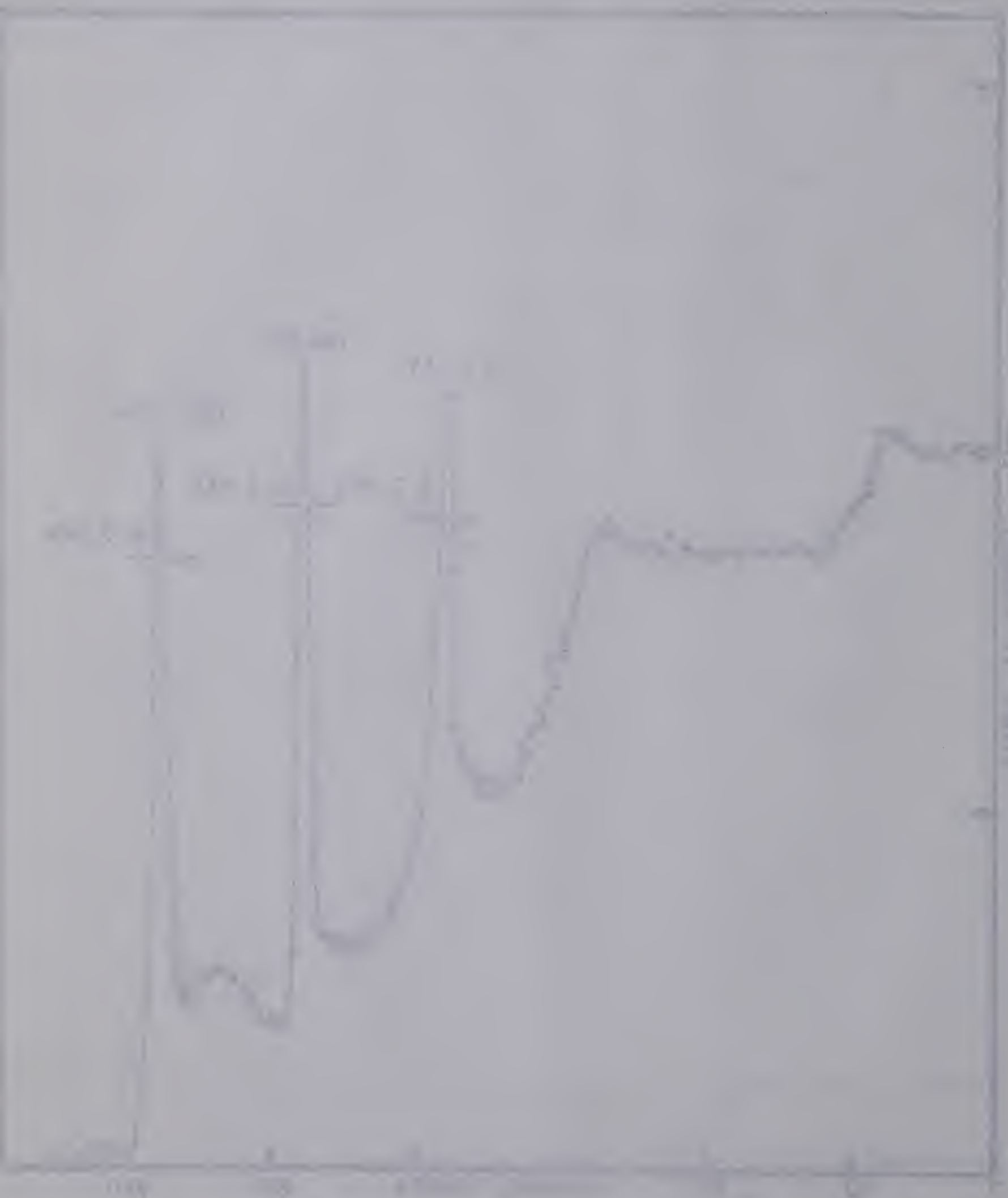

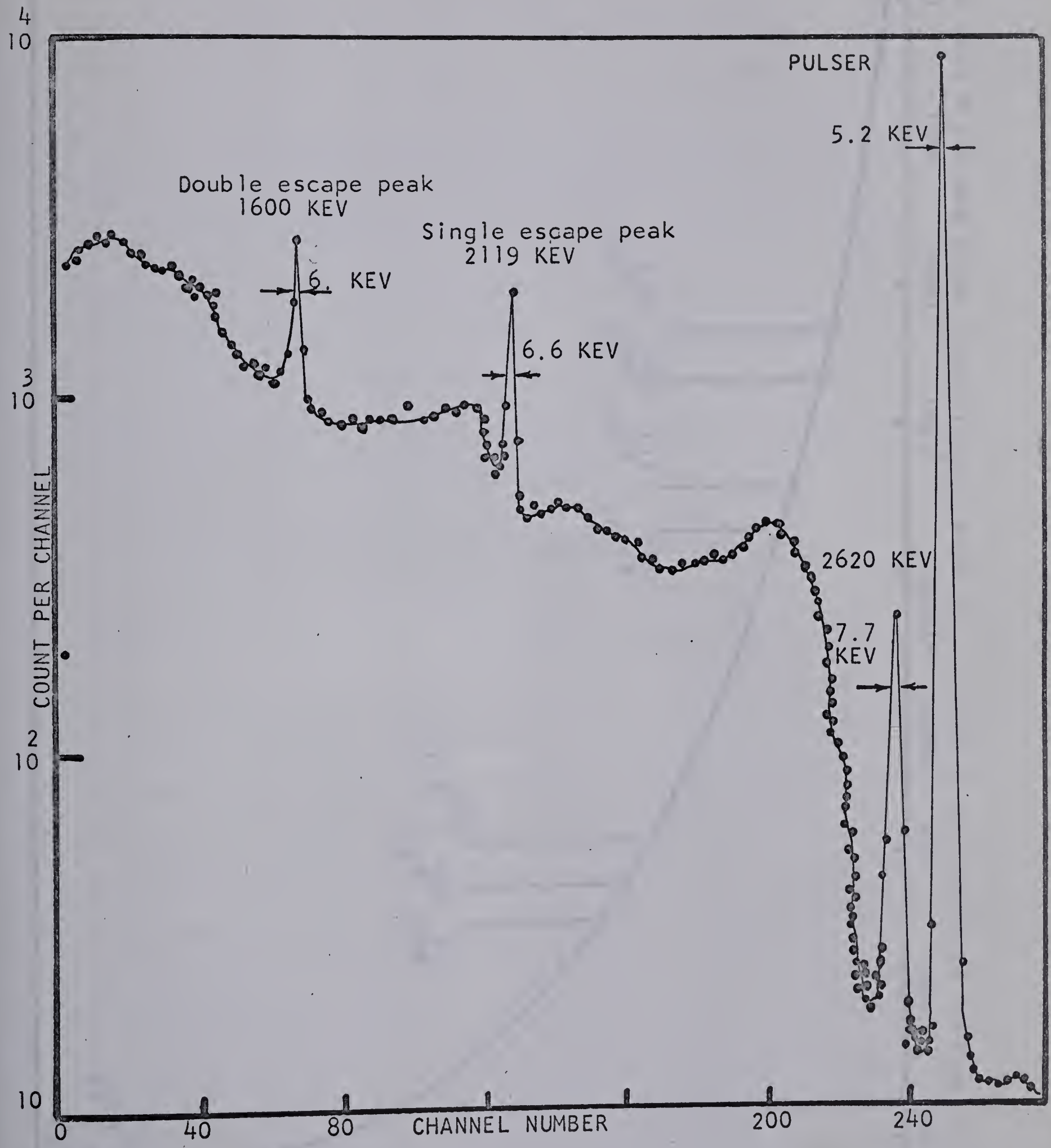

Fig 2-8 A RdTh gamma-ray spectrum taken with a detector of area 7cm^2, intrinsic depth 4mm and at a bias of 400 volts.

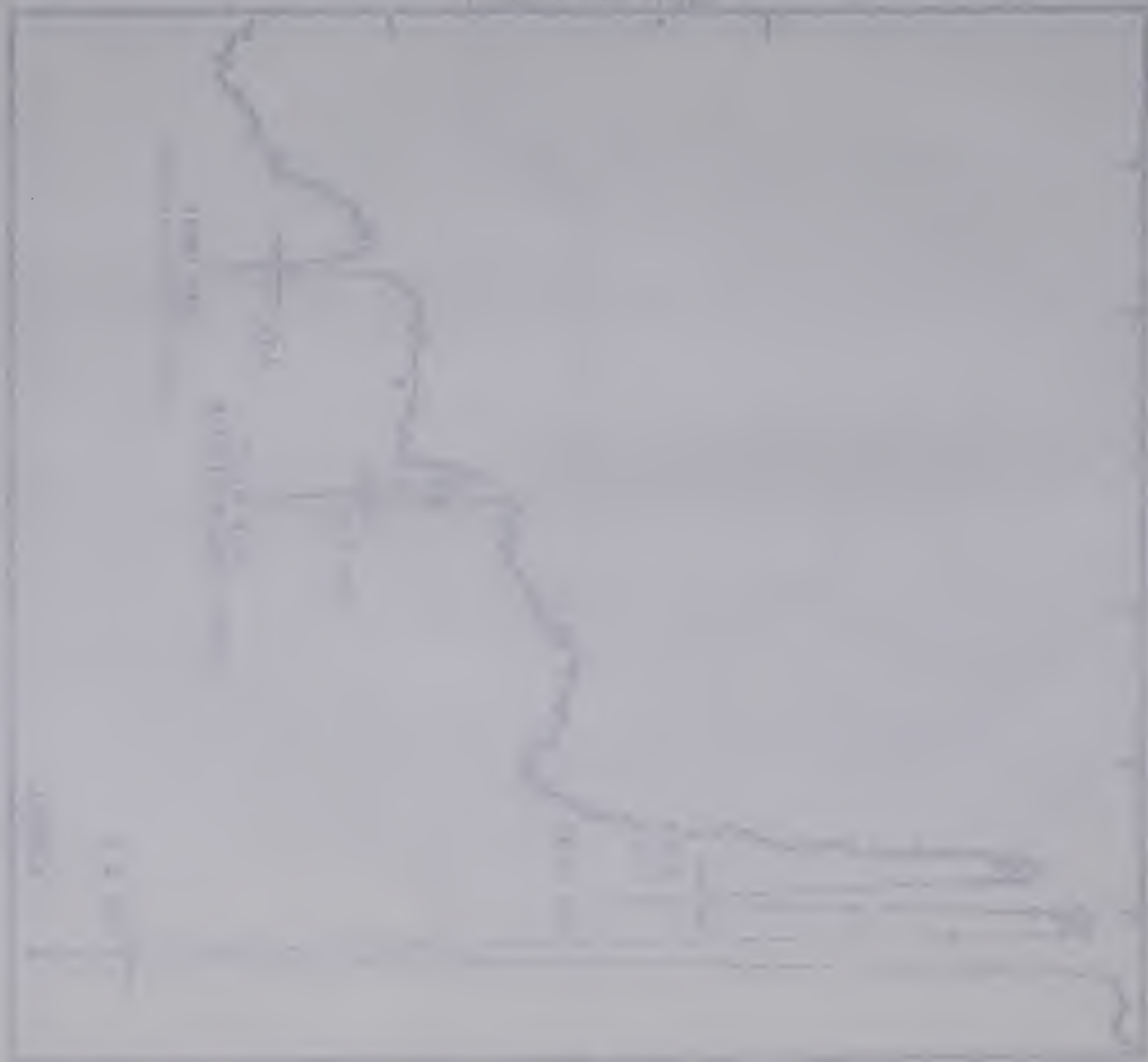

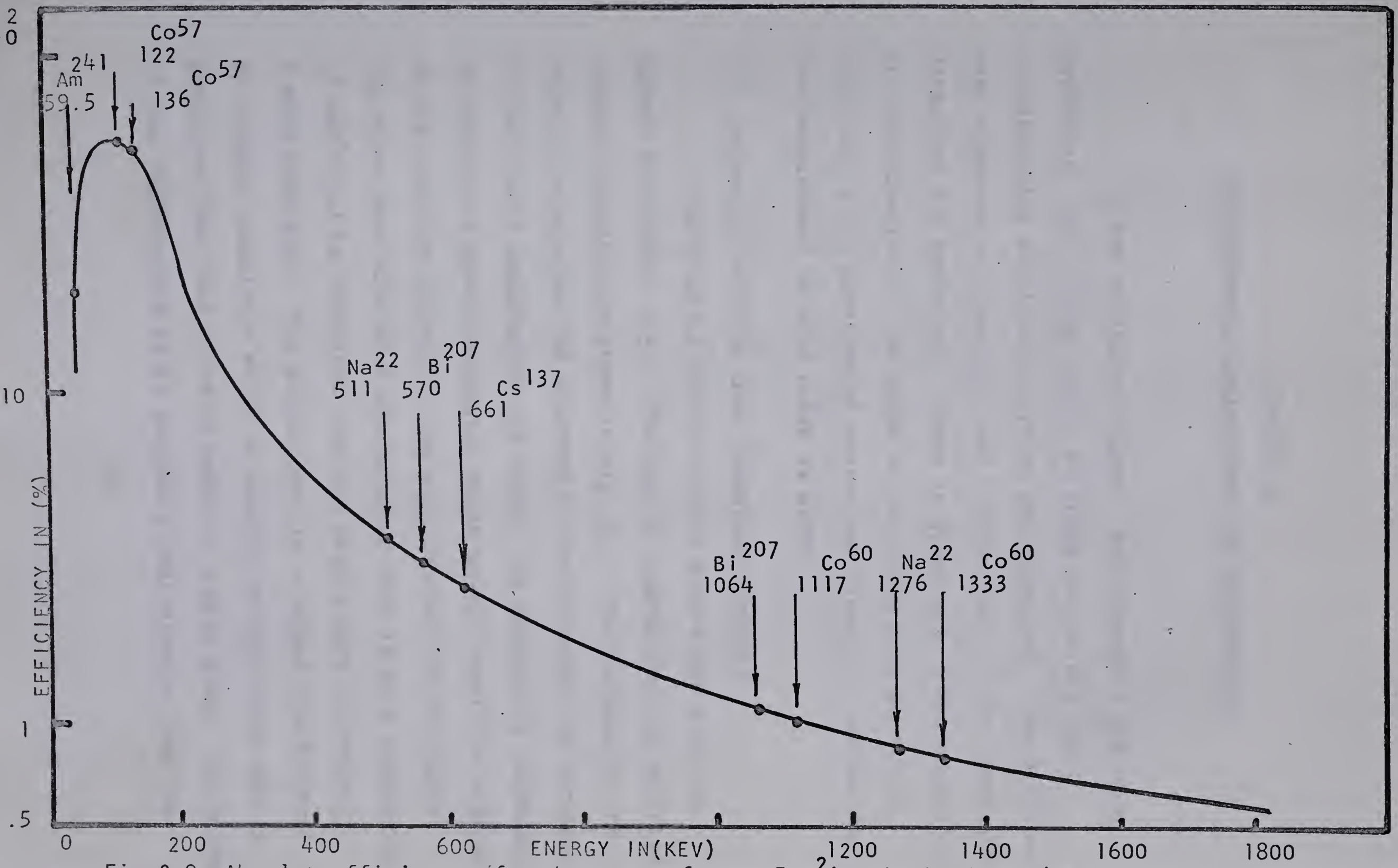

Fig 2-9. Absolut efficiency of a detector of area 7cm^2, intrinsic depth 4mm and a bias of 400 volts.

CHAPTER 3

EXPERIMENTAL ARRANGEMENT AND ELECTRONICS

In the following chapter, the automatic drifting apparatus, the boiling liquid drifting device and their corresponding electronics system are discussed. The different test chambers or cryostats used for the test of the fabricated detectors are described. There is given also a discussion for the contribution of the noise to the width of a gamma-ray line due to the electronics system and finally, a method for the measurement of this noise is given.

3.1 Automatic drifting oven (constant current)

The original design of this device was given by Hansen and Jarrett (15). The oven's diagram and its modified control circuits are shown in Fig. 3.1. The purpose of the oven is to maintain the drifting current constant by regulation of the oven's temperature and hence, the detector's temperature by means of a power transistor whose on-off condition depends on the detector current. The oven consists of two parts. The first part sits on a cooled plate that is at a temperature of $-20^{o}C$ and is separated from the second part by means of a mica insulator. The second part is a copper plate heated by a power transistor which is mounted on the bottom and is insulated from this plate by means of a mica sheet. The purpose of the cooled plate is to provide a heat sink so that the

temperature of the copper plate can be controlled. In order to describe the operation of the circuit, we assume that the power transistor T_4 is ON and the oven is heating up. As the detector temperature increases, its current increases. As a result the potential across the in line current demand resistor R_1 increases and thus the potential at the base of transistor T_1 decreases. The potential at the emitter of T_1 decreases by the same amount. When the potential of the emitter reaches that of the base of T_2, transistor T_2 begins to conduct. The emitter is thus clamped by the emitter-base junction T_2 at a potential of about -6.2 volts. As the base of transistor T_1 drops further in potential, T_1 cuts off. Before T_1 cuts off it was drawing about 1.3 mA from the base of T_3 and this base current was sufficient to keep T_3 in saturation, i.e., T_3 was able to supply enough current to the base of the power transistor T_4 and to the resistor R_{21} to keep the potential at the same value as the potential at the emitter of T_3. When T_1 cuts off, it stops drawing current from the base of T_3 and because of the reverse bias that is applied to its emitter-base by potential developed across the diode D_4, T_3 cuts off. The current fed to the base of T_4 is shut off and hence the power transistor T_4 shuts off. The OFF condition of T_4 causes a sudden decrease in detector temperature resulting from cooling of the copper plate by the refrigerated plate underneath. This reduced temperature

causes a decrease in detector current passing through the current demand resistor and an increase in the base voltage of T_1. Thus T_1 turns ON, T_2 cuts off and as a result the power transistor T_4 turns ON again. The silicon diode D_2 is used to prevent a reverse bias of more than two volts from developing at the emitter base junction of T_1. Hence, when the copper plate potential drops to a large negative value, the base of T_1 clamps and all the voltage is developed across diode D_2. Such a large negative voltage may result by momentarily disconnecting a demand current resistor or by detector breakdown. Diode D_1 protects the demand current resistors as well as T_1. With this system it is possible to set a desired drift current by choosing an appropriate demand current resistor. The temperature of the oven and hence of the detector can be adjusted in such a way so as to supply this current. However, the maximum current is restricted to 92 mA because of the value of current demand resistor R_{11} and the detector voltage is restricted accordingly. The drifting temperature is usually the variable that is fixed and voltage and current adjusted to be compatible with this temperature. Switch positions 1 to 5 correspond to the five different drifting ovens, each operated with its own control circuit.

3.2 Boiling liquid drifting apparatus (constant temperature).

Drifting at a constant temperature by immersion in boiling liquid to remove the heat from the crystal was suggested

by Miller et al (19) in 1963 and was used by Tavendale (20) at Chalk River Nuclear Laboratories. The boiling liquid apparatus used was similar to that of Tavendale's to which a simple modification was made in its condensing system. As it is seen in Fig. 3.2, the device is a pyrex glass vessel made from two separate parts. The female part is only a liquid container but the male part contains the conical-helix condensation coils and the crystal holder as well. The crystal holder is made from Teflon and the leads, which also act as supports, are of nickel. The contacts are clamped against the nickel plated surface of the crystal by Teflon or nickel screws. The liquid used was chloroform whose boiling point is 61.3°C, is non-flammable, and in this application is chemically inactive. It is also possible to use methyl-dichloride (B.P. 40°C), Freon, T.F. (B.P. 47.6°C) which is a cleaning agent, Pentene (B.P. 36°C) and Fluorocarbon F.C—75 (B.P. 53°C) or a mixture of the aforementioned liquids to obtain desired boiling temperature. The vessel has an external heater which helps to bring the liquid to its boiling point. The condensation coils, cooled by cold tap water, condense the liquid vapour and carry off the heat dissipated during operation. In order to control the current, 300-watt light bulbs were used in series with the crystal as variable resistors which also protect the circuit in case a thermal runaway condition develops, i.e., in case a crystal breakdown occurs. At the beginning of

the drift, the voltage is kept at approximately 100 volts in order to avoid damage to the thin junction. The current is usually below 10 mA at this voltage but it increases rapidly with increasing temperature of the liquid. During this period no further increase in voltage should be made. When the liquid reaches its boiling point the voltage can be raised just below the breakdown voltage of the crystal. At this stage the drift current is between one to three amperes at a voltage between 80 to 150 volts, depending on the characteristics of the crystal. After drifting about 2 to 4 mm, loss of lithium by precipitation becomes apparent resulting in a decrease in the drifting voltage, i.e., the voltage across the detector drops to approximately 30 volts. This condition can be overcome by reheating the crystal briefly at about 400°C in vacuo or by reevaporating lithium as was described in Chapter 2. Since the center of the crystal is hotter than the edges and because electric field in the center is greater, the average drift rate will therefore be greater in the center as was also mentioned in Chapter 2. This must be taken into account if "drift through" is to be avoided. The drift through is to be avoided in order that the sensitive region is not extended to the opposite electrode.

3.3 Cryostats.

(1) RCA* cryostat: This cryostat which was designed by RCA Victor Company for their encapsulated detectors, has been used in this laboratory for detectors whose total thicknesses were less than one centimeter. In order to make leakage current measurements possible, the crystal mount was modified by insulating it from the cold finger with a mica sheet and by adding another BNC connector to the end cap as is shown in Fig. 3.3.

(2) Brookhaven National Laboratory** cryostat: This device can be used for larger detectors, specifically, the coaxial-type, and has much faster cooling speed than the RCA cryostat. The diagram for this cryostat is given in Fig. 3.4.

3.4 Electronics.

As is shown in Fig. 3.3, the electronics system consists of a low noise charge sensitive preamplifier***, a linear RC amplifier**** and a pulse height analyzer*****. A pulser# is used as an indication of the intrinsic resolution

---

*Model HP-6108, RCA Victor Co. Ltd., Montreal, Canada.

**Brookhaven National Laboratory, Upton, N.Y., U.S.A.

***CRGP-1182 by A.J. Tavendale, Chalk River, Ontario, September 1964, AECL-2071.

****No. EB-5336, General Purpose Pulse Amplifier, Chalk River, Ontario, Canada.

*****Model CN-110, Technical Measurement Corporation, North Haven, Connecticut, U.S.A.

#Precision Sliding Pulser, Model 413, S-22, Radiation Instrument Co., Silver Spring, Maryland, U.S.A.

of the electronic system. The preamplifier was designed by Tavendale[18] and its circuit diagram is given in Fig. 3.5. It is based on two 7788 tubes in cascade followed by a 7308 tube used as a long-tailed pair and then a white cathode follower stage. With zero input capacity, the electronic noise is 2 kev (FWHM). Its rise time is approximately 25 n sec. In order to obtain the optimum signal-to-noise ratio, the pulse is shaped in an amplifier with adjustable differentiation and integration time-constants. In general the optimum performance of a preamplifier-amplifier system is obtained with equal time-constants of 1 or 2 μ sec. These values depend upon the spectral distributions of the preamplifier noise and the detector leakage current noise. To be able to record a reasonably large gamma energy range and to have a reasonable number of channels defining each peak, a pulse height analyzer of about 1000 channels is required. The pulse-height analyzer used for detector testing was only a 256 channel analyzer.

3.5 Electronic Noise Measurement.

In order to determine the intrinsic resolution of a detector, it is necessary to know the magnitude of the noise contributed to the width of a gamma-ray line due to the amplifying system alone. For convenience, consider the equivalent circuit of a charge sensitive preamplifier as is shown in Fig. 3.6. The sensitivity of such a preamplifier is

$$S = \frac{V_o}{Q_{in}} \qquad (3.1)$$

The V_o and Q_{in} are defined in this way that if one applies a peak-to-peak voltage V_T (test voltage) to the input of the preamplifier through a small capacity C_{in} (input capacity), by neglecting the value of C_s (stray capacities), the charge fed in is approximately

$$Q_{in} = C_{in} V_T \qquad (3.2)$$

and thus an output voltage V_o appears at the output. In this case, for a measured r.m.s. voltage V_n, at the output of preamplifier, "with pulse generator disconnected," there is an equivalent input charge Q_n given by

$$Q_n = \frac{V_n}{S} = Ne \qquad (3.3)$$

where N is the number of electron-hole pairs required to produce the charge Q_n at the input, and e is the electronic

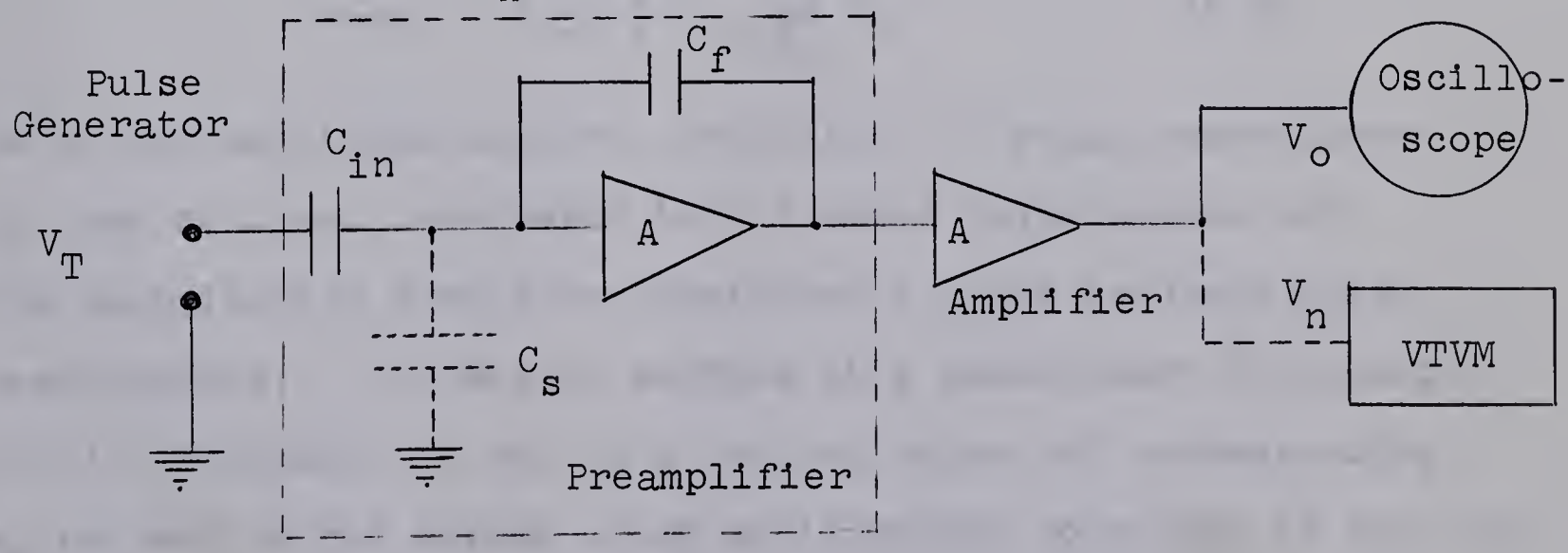

Fig. (3.6). Equivalent circuit of a charge sensitive amplifier and the system used for the electronics noise measurement.

charge. Hence Ne is considered as the effective amount of charge being produced at the input of the ideal preamplifier. Substituting equation (3.1) in (3.3) for the value of S, gives

$$N = \frac{V_n}{V_o} \frac{Q_{in}}{e} \quad . \qquad (3.4)$$

Now if ϵ is defined as the energy in electron volts required to produce one electron-hole pair in the crystal, this effective r.m.s. noise at the input of the preamplifier is given by

$$N(ev) = N\epsilon = \frac{\epsilon}{e} \cdot \frac{V_n}{V_o} Q_{in} \quad . \qquad (3.5)$$

Recalling equation (3.2), equation (3.5) becomes

$$N(ev)_{r.m.s.} = \frac{\epsilon}{e} \frac{V_n}{V_o} C_{in} V_T \quad . \qquad (3.6)$$

Therefore, using equation (1.41) the contribution of the electronics noise to the width of gamma-line is given by

$$W(ev) = 2.35 \frac{\epsilon}{e} C_{in} \frac{V_n}{V_o} V_T \quad . \qquad (3.7)$$

As it was mentioned earlier, the effect of stray capacitance, C_s, has not been considered in the above calculations but its contribution should be considered in more accurate noise measurements. In order to perform this measurement by equation (3.7), the pulser is set to a desired value and corresponding V_o is read on the screen of an oscilloscope connected to the out-

put of the amplifier. In this way the contribution of amplifier noise has also been accounted for as well as that of the preamplifier. Next, the pulser is turned off and the output of the amplifier is connected to a vacuum tube voltmeter in order to obtain the value of V_n. The value of ϵ is given in Table 2.1 and that of C_{in} is 0.5 pf according to Fig. 3.5.

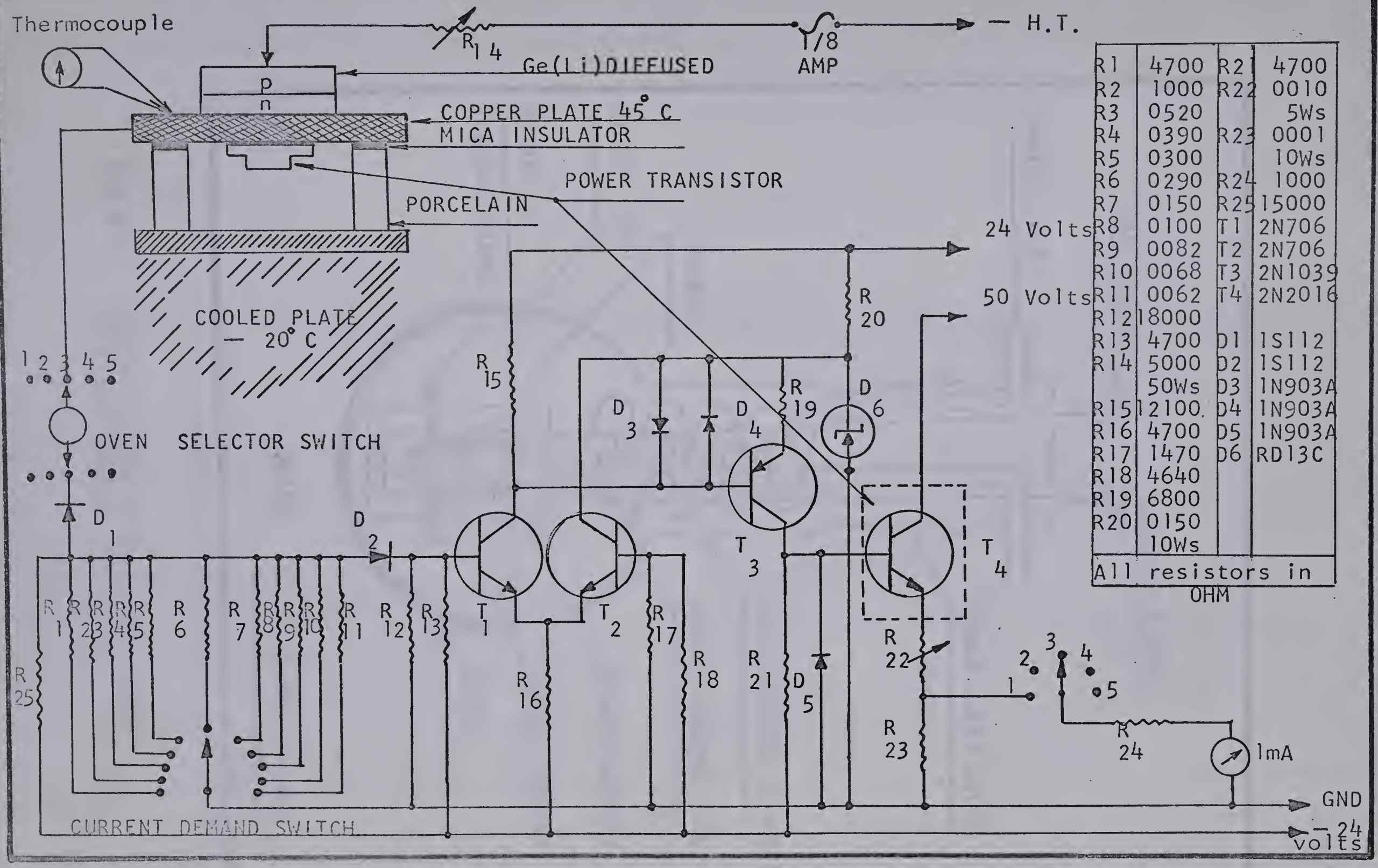

R1	4700	R21	4700
R2	1000	R22	0010
R3	0520		5Ws
R4	0390	R23	0001
R5	0300		10Ws
R6	0290	R24	1000
R7	0150	R25	15000
R8	0100	T1	2N706
R9	0082	T2	2N706
R10	0068	T3	2N1039
R11	0062	T4	2N2016
R12	18000		
R13	4700	D1	1S112
R14	5000	D2	1S112
	50Ws	D3	1N903A
R15	12100.	D4	1N903A
R16	4700	D5	1N903A
R17	1470	D6	RD13C
R18	4640		
R19	6800		
R20	0150		
	10Ws		

All resistors in OHM

Fig 3-1. Automatic drifting oven and its control circuit.

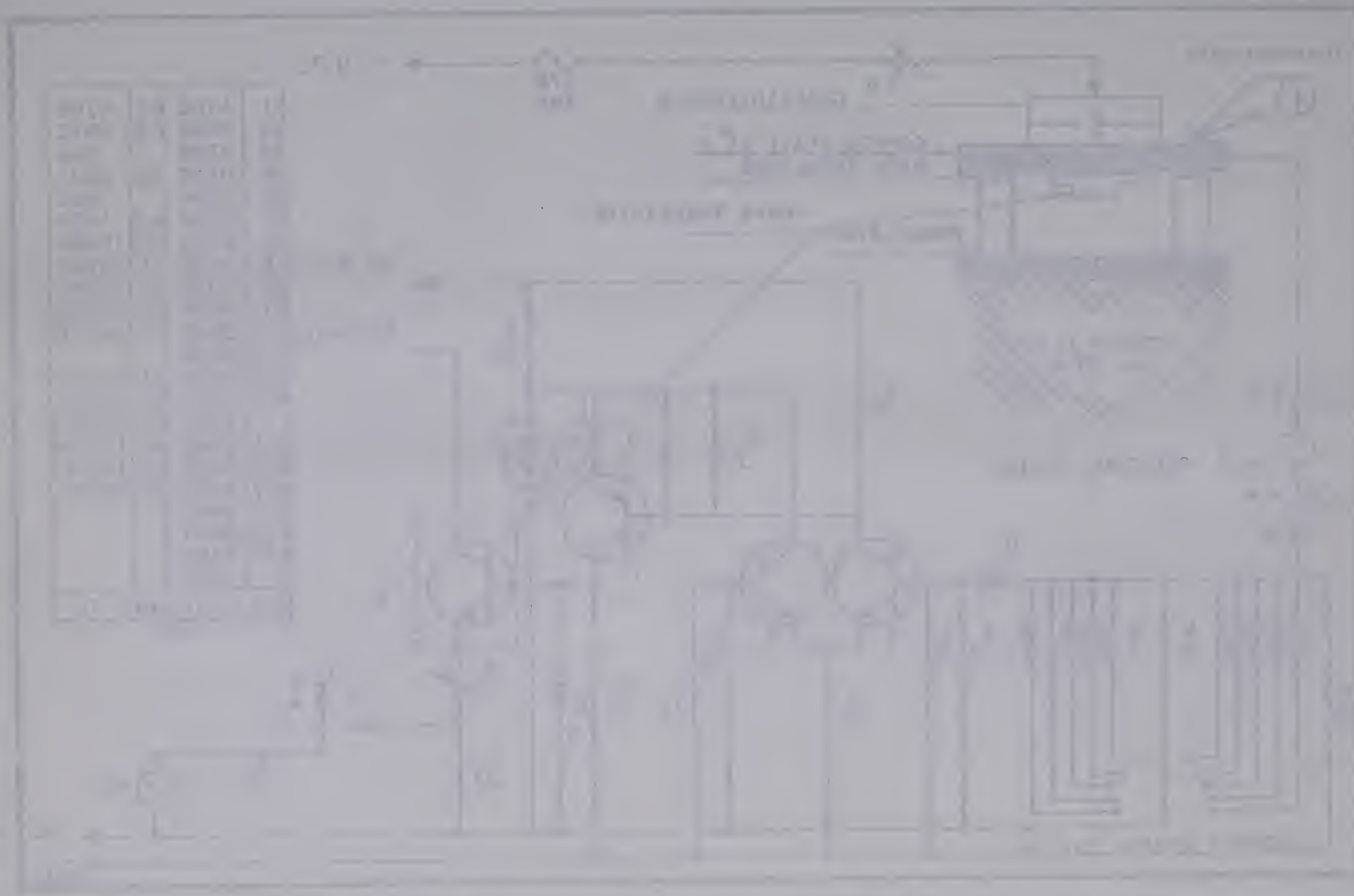

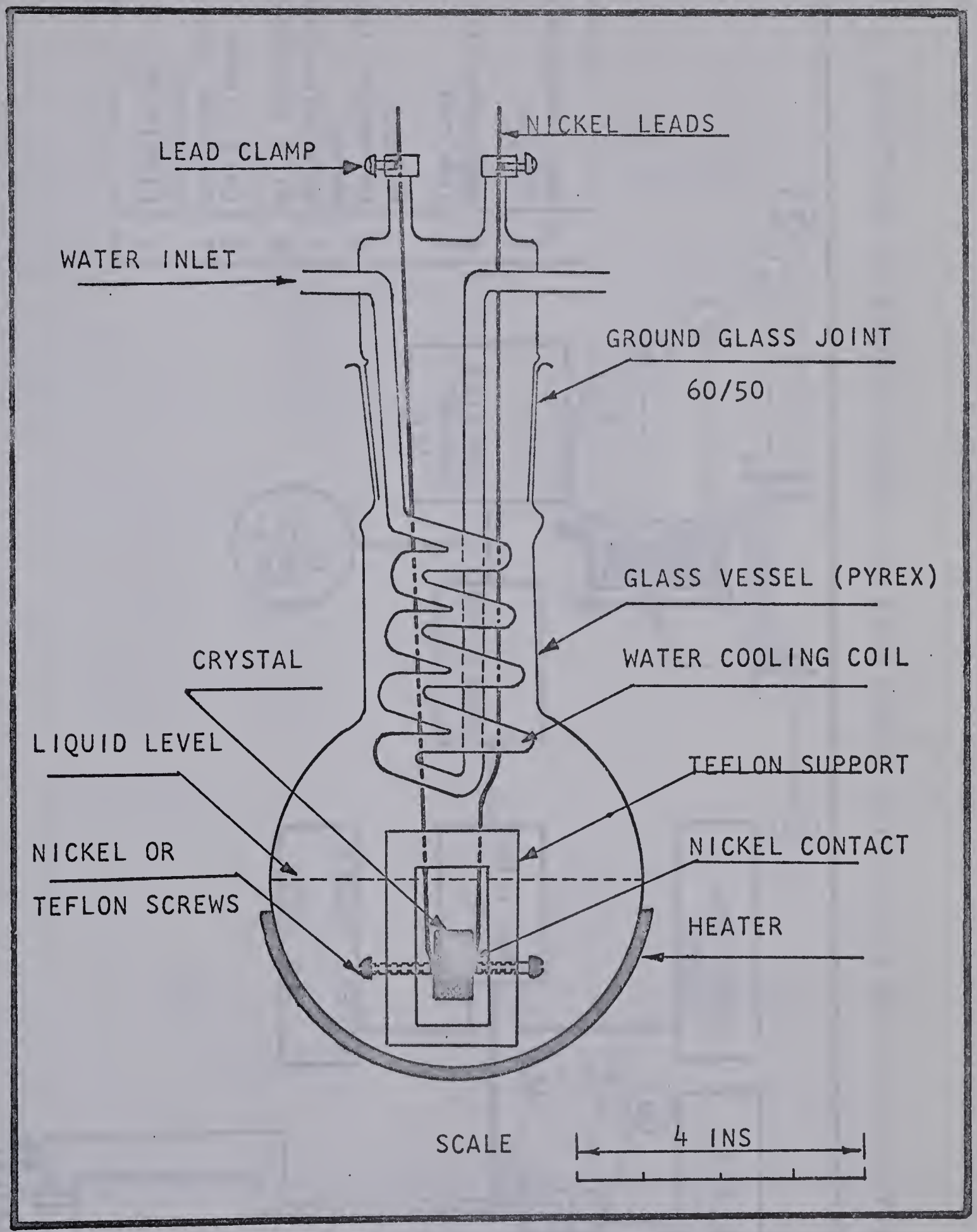

Fig 3-2. CROSS-SECTION OF BOILING LIQUID DRIFTING VESSEL.

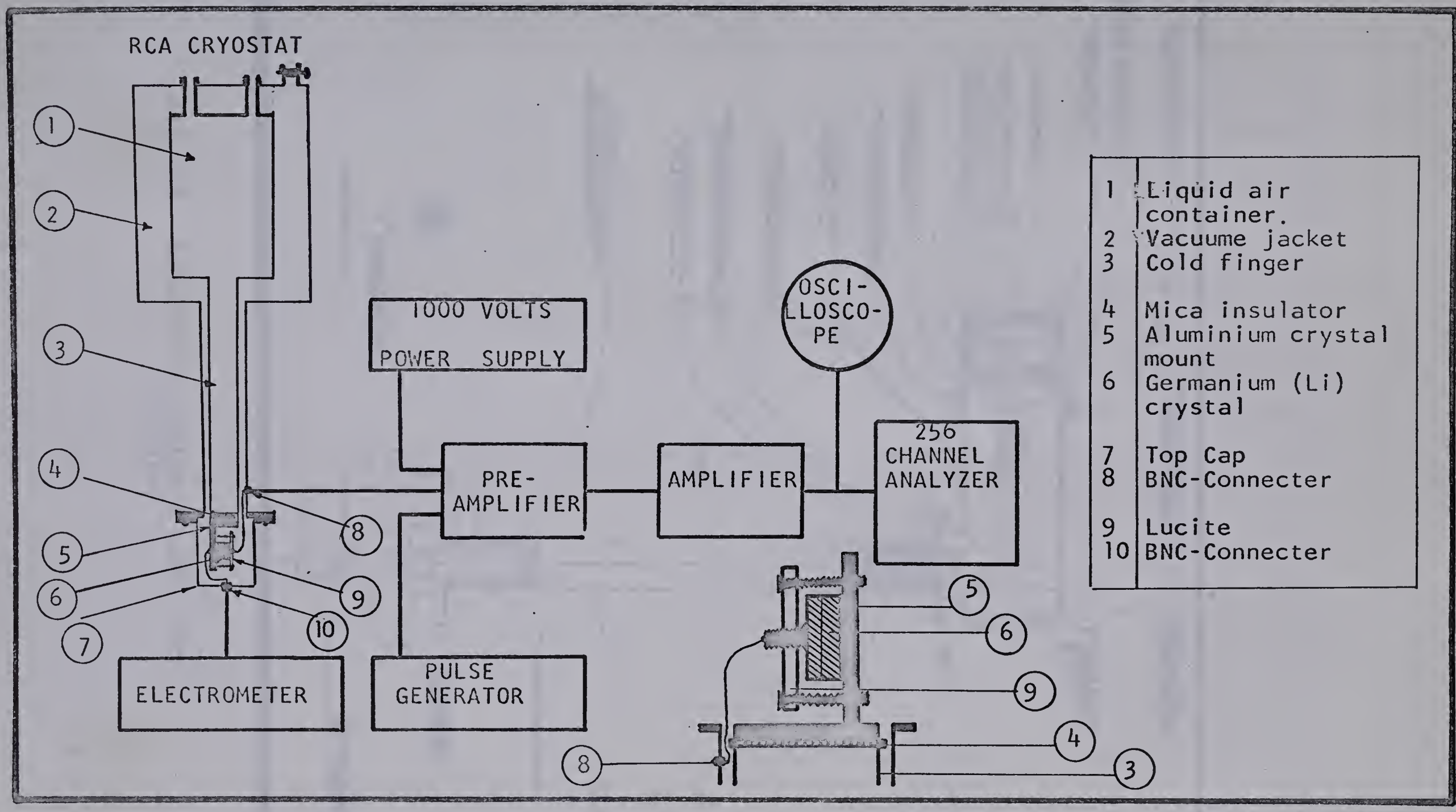

Fig 3-3. RCA-Cryostat and electronics system used for the chractristics measurment of detectors.

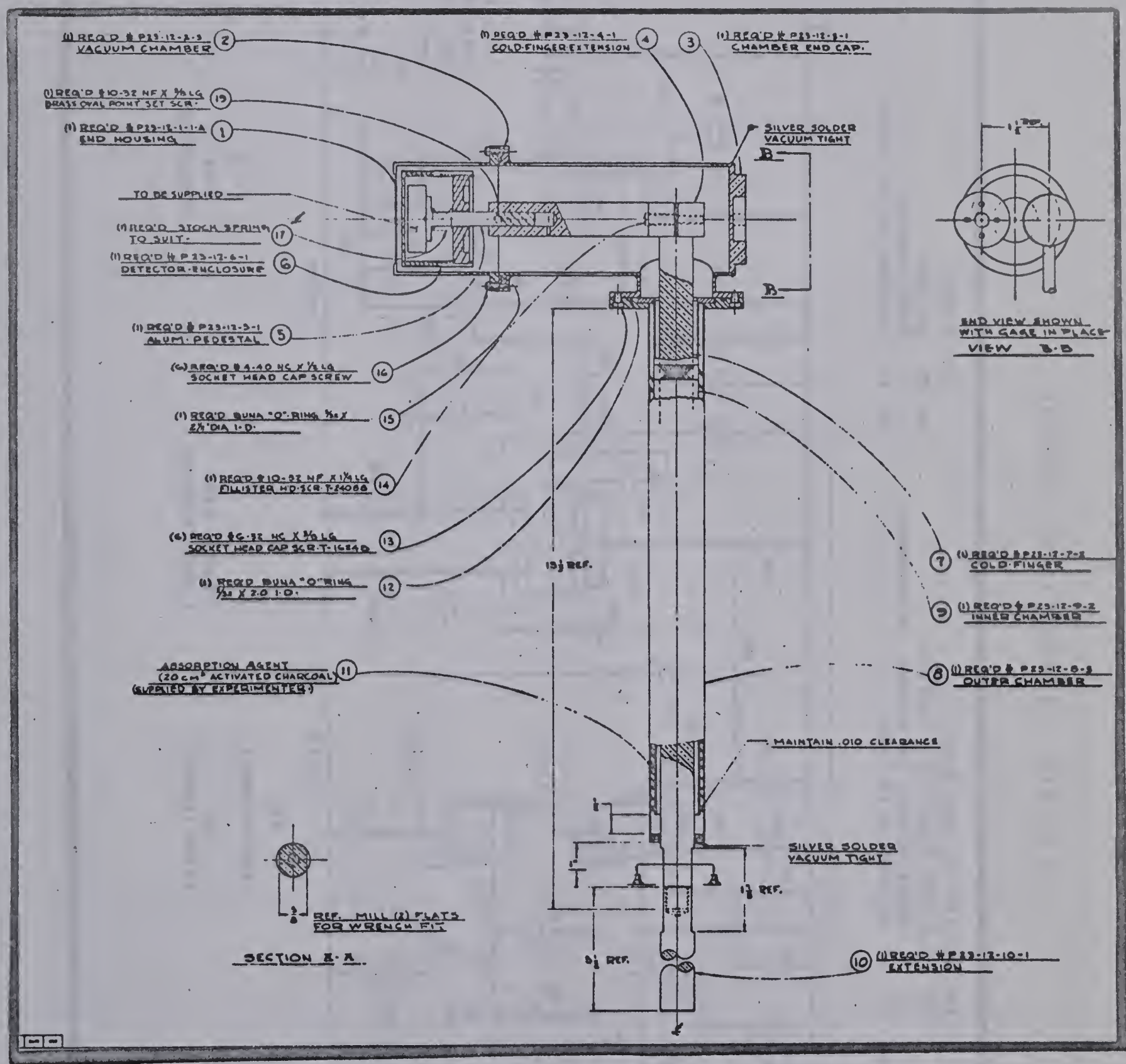

Fig 3-4. Brookhaven National Laboratory CRYOSTAT.

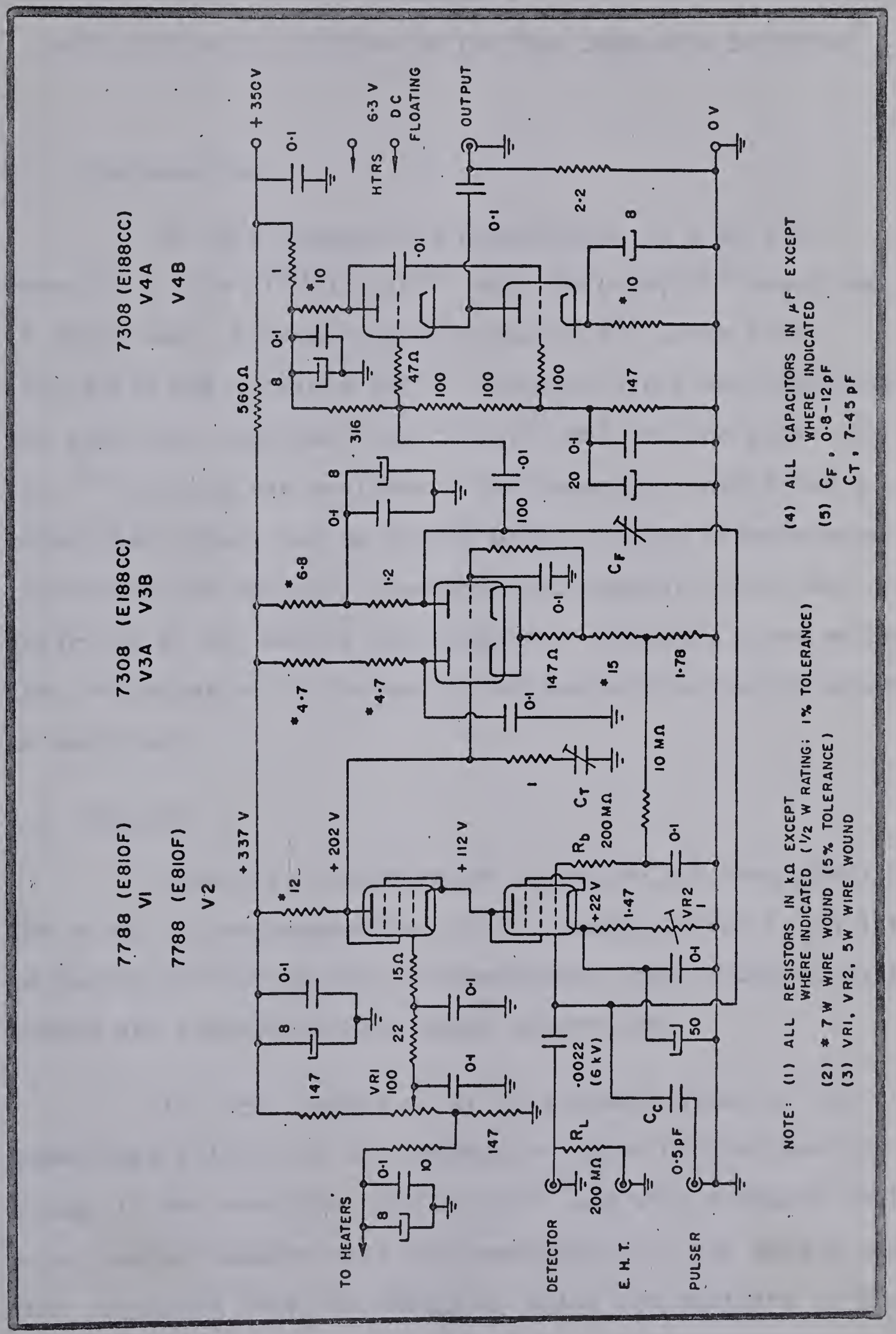

Fig 3-5. Preamplifier circuit.

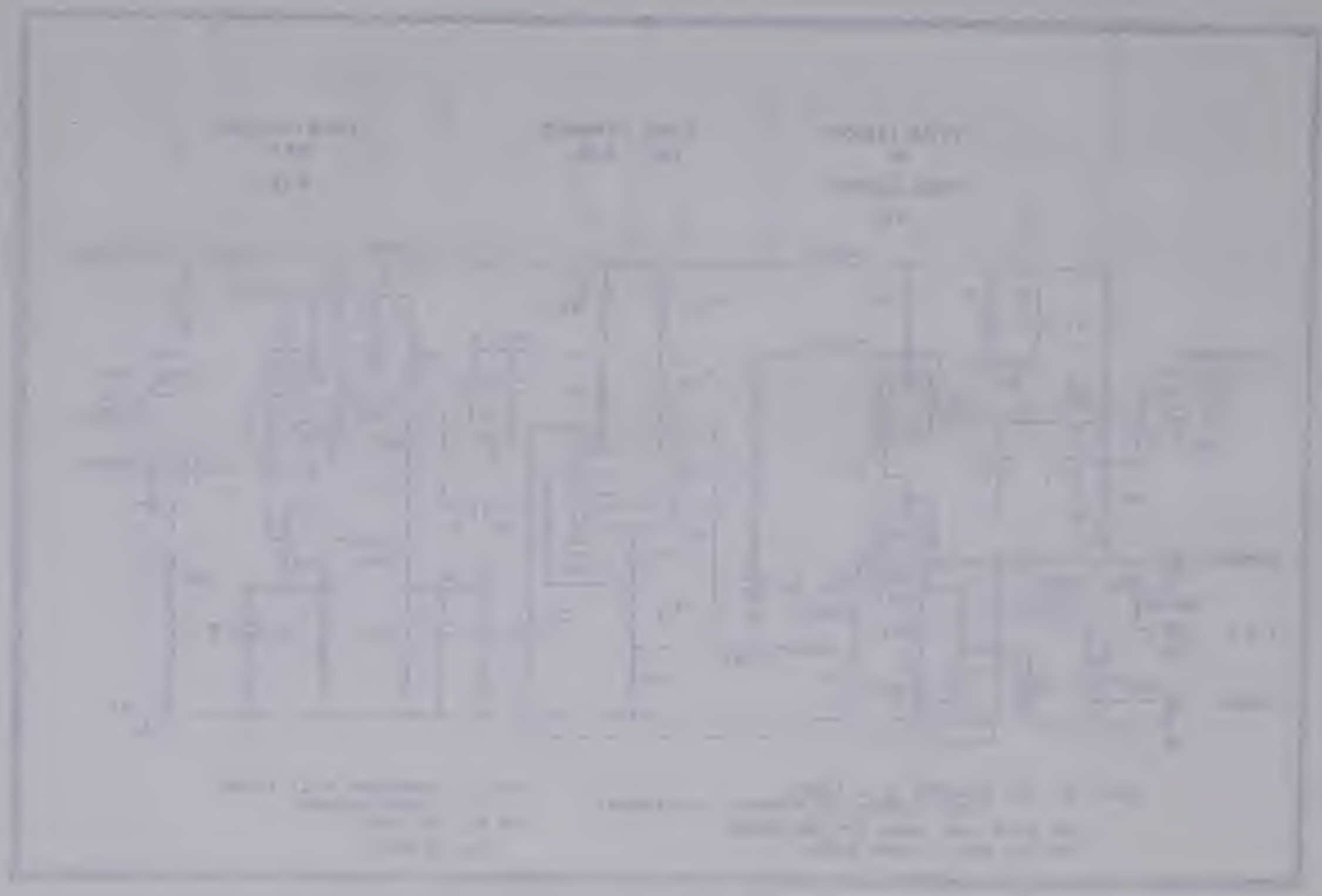

CHAPTER 4

APPLICATION OF LITHIUM-ION DRIFTED GERMANIUM DETECTOR

4.1 Introduction.

In this chapter the application of a Ge (Li) detector to the $Si^{30}(d,n\gamma)P^{31}$ and $Be^{9}(\alpha,n\gamma)C^{12}$ reactions is described. A gamma-ray spectrum of P^{31} up to 8 Mev excitation was obtained and 12 transion lines were identified. The gamma-ray spectrum from the 4.43 MeV excited state of the C^{12} nucleus was analyzed. The gamma-rays exhibited a broadening effect and an energy shift. These effects were interpreted as Doppler broadening and Doppler shift, which are described at the end of this chapter. Finally, a new method for the determination of nuclear lifetimes using a Ge(Li) detector is described.

4.2 History.

Recently, considerable attention has been given to the study of the preparation of P^{31} energy levels in an attempt to decide whether or not the theoretical prediction of various models are compatible with these properties.

In 1958, Broude et al (21) made a study of the gamma-rays emitted at ten resonances below one MeV proton energy in the reaction $Si^{30}(P,\gamma)P^{31}$ and they compared their experimental results with the predictions of the Nilson model. They concluded that the energies, spins and parities of the

lower levels are in agreement with the model but their decay properties however are not. In 1962, Harris and Seagondollar (22) studied the gamma-ray decay scheme of P^{31} in the same reaction, $Si^{30}(P,\gamma)P^{31}$, from eight resonances between one and two MeV. They found that the 3.51 MeV level decays to either the 1.27 or the 2.23 MeV level (or both) in addition to the well known decay to the ground state. They also reported that the 4.26 MeV level decays to the ground state and to the first excited state with the branching ratios of 84 and 16 percent respectively. They found a relatively strong and well isolated transition to the 3.41 MeV level at 1509 KeV resonance which determined the previously unknown spin and parity of the 3.41 MeV level. In 1966 Davies (23) identified eleven previously unreported excited states in the region of excitation from 5 to 8 MeV and found the spins and parities of P^{31} levels at 5.01, 5.25, 6.38, 6.48, 6.60, and 7.11 MeV. He also reported (23) that the levels at 6.38 and 7.14 MeV have isotopic spin of T = 3/2, corresponding to the ground and first excited states of Si^{31}. However, it is clear that more information on the properties of the excited states of P^{31} is necessary for a complete understanding of this nucleus and the purpose of the present experiment was to obtain branching ratios for the P^{31} gamma-rays by means of the $Si^{30}(d,n\gamma)P^{31}$ reaction and a germanium-lithium ion drifted detector whose theory and fabrication method have been described in the previous chapters.

4.3 Experimental arrangement.

The reaction under study was initiated by a beam of deutrons from the 6 MeV Van de Graaff accelerator of the University of Alberta. The beam emerging from the accelerator was stabilized by means of slits which are located at the focus of a 90° analyzing magnet. The signals from these slits are fed to a corona stabilizer which in turn controls the terminal voltage of the accelerator. The analyzed beam passes through the switching magnet, a quadrupole lens, a set of collimating slits and a liquid nitrogen carbon trap before it enters the target chamber. A side view illustration of the target chamber and beam path is given in Fig. 4.1. The Si^{30} target was 210 $\mu g/cm^2$ thick, enriched to approximately 90% in Si^{30} in the form of SiO_2 deposited on gold*. The liquid nitrogen carbon trap which was located 3 feet from the target chamber serves to minimize the carbon build-up on the target during bombardment. The gamma-ray detector was located at a distance of five inches from the target spot. The amplification system was the same system which was described in Chapter two and the electronic noise of the system, with zero input capacity, was 2.8 KeV. The data was fed to an on line computer (SDS-920) by means of a 1024 channel TMC** analog-to-digital converter.

---

* Supplied by A.E.R.E., Harwell, United Kingdom.

** Model CN-1024, Technical Measurement Corporation, North Haven, Connecticut, U.S.A.

4.4 Experimental results.

Prior to the performance of $Si^{30}(d,n\gamma)P^{31}$ reaction an energy calibration of the detection system was made by means of the gamma-ray sources indicated in Chapter two. The higher range energy calibration was accomplished by means of $Be^{9}(\alpha,n\gamma)C^{12}$ reaction. The 4.43 Mev gamma-ray from the first excited state of C^{12} along with its single and double escape peaks at 3.92 and 3.41 MeV respectively served as calibration points. These with the standard source lines, provided an accurate calibration up to 5 MeV as is shown in Fig. 4.3.

By reference to the decay scheme of P^{31} given by Endt and Van der Leun (24) shown in Fig. 4.2, one may notice that the expected gamma-ray spectrum from $Si^{30}(d,n\gamma)P^{31}$ reaction will be very complex. In addition, there are a large number of contaminant reactions as is given in table 4.1, whose transition lines strongly contribute to the recorded gamma-ray spectrum.

Table 4.1

Contaminant reactions accompanied with the reaction $Si^{30}(d,n\gamma)P^{31}$.

$Si^{29}(d,n\gamma)P^{30}$	$Si^{30}(d,P\gamma)Si^{31}$
$Si^{28}(d,n\gamma)P^{29}$	$Si^{29}(d,P\gamma)Si^{30}$
$O^{16}(d,n\gamma)F^{17}$	$Si^{28}(d,P\gamma)Si^{29}$
$N^{14}(d,n\gamma)O^{15}$	$O^{16}(d,P\gamma)O^{17}$
$C^{12}(d,n\gamma)N^{13}$	$N^{14}(d,P\gamma)N^{15}$
	$C^{12}(d,P\gamma)C^{13}$

Among the above reactions, the most prolific competing reaction is $Si^{30}(d,P\gamma)Si^{31}$. Consequently, a detector of very good resolution and reasonable efficiency would be able to distinguish between the transition lines resulting from all the mentioned reactions.

The deuteron bombarding energy for the $Si^{30}(d,n\gamma)P^{31}$ experiment was 3.5 MeV. With a Q-value of 5.062 MeV for this reaction, gamma-rays from levels in P^{31} up to 8 MeV would be expected. An attempt was made to obtain the data in coincidence with neutrons, but the counting rate in Ge(Li) detector was too low due to the low efficiency of this counter for energies above 2 MeV as can be observed in Fig. 2.9 of Chapter two. However, due to the lack of time for preparation of a higher efficiency detector a direct gamma-ray spectrum was obtained. This spectrum which is shown in Fig. 4.3 reflects the low efficiency of gamma-detector for gamma energy range above 5 MeV.

A comparison of the energies of lines observed in the spectrum with those which are associated with levels in P^{31} (see Fig. 4.2) indicates that of 30 transition lines observed, only twelve correspond to gamma-rays of P^{31}, and ten with those of Si^{31}. The remainder belong to the other contaminant reactions. In Fig. 4.3 the P^{31} gamma-rays are indicated by feather-shaped arrows. These are also shown by the broken lines in the decay scheme given at the top right-hand corner of the figure. The gamma-rays of Si^{30} are marked

by triangle arrows and by unbroken lines in the decay scheme given at the bottom right-hand corner of Fig. 4.3. However, the resulting spectrum did not provide sufficient information for the measurement of the branching ratios of P^{31} transition lines, due to the fact that accurate measurement of relative intensities of gamma-rays was impossible because of the large background which was present.

The $Be^{9}(\alpha,n\gamma)C^{12}$ reaction was studied using an α-particle energy of 4 MeV. At 4 MeV bombarding energy the reaction is resonant with respect to the neutron emission from the compound nucleus C^{13} to the ground and 4.43 MeV states of C^{12}. The experimental arrangement for this reaction was the same as it was for $Si^{30}(d,n\gamma)P^{31}$ reaction and the resulting gamma spectrum obtained at zero degrees with respect to the direction of the beam is shown in Fig. 4.4. The distortion in the 3.41 MeV double escape peak of the 4.43 MeV gamma-ray from the first excited state of C^{12} nucleus is attributed to Doppler shift of the gamma-rays emitted from the recoiling C^{12*}(4.43 MeV) nucleus. At 90^{o} with respect to the direction of beam, the 3.41 MeV peak exhibited Doppler broadening effect shown in Fig. 4.5 as would be explained.

(a) Doppler shift effect.

It was described that after formation of compound nucleus C^{13}, the C^{13} nucleus decays by neutron emission to the

first excited state of 4.43 MeV of C^{12*} nucleus. The induced nuclear reaction caused by incident ion beams on target, produces recoiling excited nuclei. These nuclei then slow down in the target's backing material of sufficiently high atomic number that no nuclear reactions can take place in it. The gamma-rays emitted by the recoiling excited nucleus at an angle θ with respect to the direction of the recoil will exhibit a Doppler shift whose magnitude is given by

$$E_\gamma(\theta) = E_{\gamma o} \left[1 + \frac{v(t)}{c} \cos \theta\right] \qquad (4.1)$$

where $v(t)$ is the velocity of recoil nucleus at time t, c is the velocity of light, and θ the angle between the direction of emitted gamma-ray and the direction of recoil nucleus. E_γ is the shifted energy and $E_{\gamma o}$ the unshifted energy of the emitted gamma ray. Equation (4.1) indicates that at zero degrees,

$$E_\gamma(0^o) = E_{\gamma o} \left[1 + \frac{v(t)}{c}\right] \qquad (4.2)$$

i.e., at $\theta = 0^o$ the maximum shift occurs. But at $\theta = 90^o$,

$$E_\gamma(90^o) = E_{\gamma o} \quad . \qquad (4.3)$$

An explanation for the shape of shifted gamma-peak of Fig. (4.4) can be given by consideration of Fig. (4.6). The unbroken line indicates the velocity of the recoil nuclei in the stopping

material with respect to time. τ_s is the time at which the velocity of the nuclei decreases to 1/e of its initial velocity, and is called the characteristic slowing down time of the backing material. t_s is the time after which the velocity of the recoil nucleus produces a negligible energy shift in the gamma ray. The unbroken line shows the decay rate of the recoil nuclei at time t. In Fig. (4.6) the region in which $v \simeq 0$ is responsible for the unshifted part of gamma-peak of Fig. (4.4). But the energies of gamma rays emitted during the time $t < t_s$ are Doppler shifted. The value of this observed energy shift obtained for the double escape peak of 4.43 MeV gamma ray from C^{12} nucleus was 20 keV while that calculated from equation (4.1) was 24 keV. These two values indicate a difference of 4 keV between the average energy shift observed, and the maximum energy shift, respectively. In this calculation the energy of recoil nucleus $C^{12*}(4.43)$ was 0.255 MeV at $\theta = 0^{o}$ which was obtained from the kinematics.

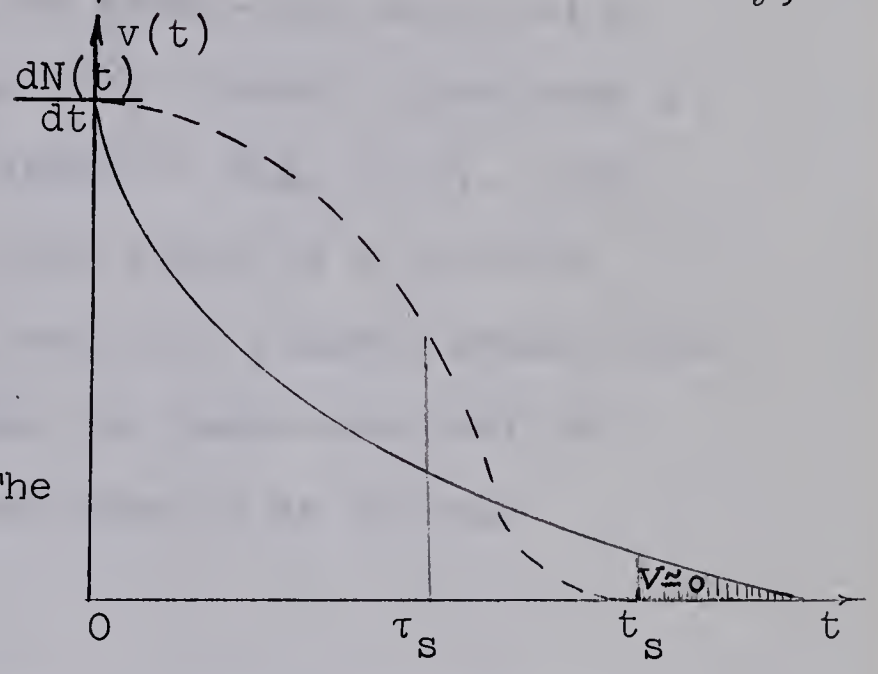

Fig. (4.6). The Velocity distribution and the decay rate of recoil nuclei.

(b) Doppler broadening.

As indicated by equations (4.1) and (4.3) there should not be an energy shift in the gamma-rays detected at $\theta = 90^{\circ}$. The spectrum obtained at 90°, however, does show a large spread or broadening as is shown in Fig. (4.5). The broadening results from the fact that there is a velocity distribution of the recoil nuclei which is roughly symmetrical about an angle of $\theta = 90^{\circ}$, and thus the gamma-peak shifts from both sides of its position and thus in an overall broadening of the gamma line.

The accurate measurement of these Doppler effects is of great importance since it can lead to determination of nuclear lifetimes. This is described in the following section.

4.6 Nuclear life time measurement.

The usual method for nuclear lifetime measurement is Doppler shift attenuation method (DSAM) which employs a NaI(Tl) scintillation counter as is described by Litherland et al (24) and which is applicable for lifetime measurement in the region of 10^{-14} to 10^{-11} second. For lifetimes of greater than 10^{-12} sec the DSAM method does not give accurate results, first, because of the fact that the longer the lifetimes the less the Doppler shift appears. This can be understood from characteristic slowing down time of materials which are about 3×10^{-13} sec. The DSAM method leads to the equation

$$\frac{\overline{\Delta E} \text{ (observed)}}{\Delta E \text{ max}} = \frac{\tau_s}{\tau_s + \tau} \qquad (4.4)$$

in which $\overline{\Delta E}$ (observed) is the mean energy shift observed, ΔE max, the maximum energy shift obtained from equation (4.1), τ_s the slowing down time, and τ the nuclear life time. This equation shows that for lifetimes much greater than τ_s the observed shift is much smaller than maximum shift and thus the result of measurement is less accurate. Second, the resolution of NaI(Tl) counter is not sufficiently good (50 to 150 keV) to resolve the shifted energy from its unshifted part.

For the region 10^{-11} second and greater lifetime measurement can be accomplished by direct electronic timing methods (25). These two methods leave a gap in lifetime measurement from 10^{-11} to 10^{-12} second.

A new recoil method of nuclear lifetime measurement has been developed by Alexander et al (26) in 1965 employing Ge(Li) detectors which span this time region. The high resolution of Ge(Li) detectors allows a direct measurement of both shifted and unshifted gamma-ray which make the lifetime measurement more accurate and more simplified. In this method a thin target with no backing material is used and the residual nucleus can freely recoil into vacuum and finally it stops in a moveable plunger which is located at a distance x from

the target. The distance x can be adjusted so that the recoil nuclei with different energies can be stopped.

Thus one can determine the number of excited nuclei after a time t, by measurement of the intensities of gamma-rays emitted from nuclei slowed down in the plunger at a distance x = vt, where v is the velocity of recoil nuclei and x is the distance between target and plunger.

As described earlier, the nuclei decaying during flight time ($t < t_s$), exhibit a Doppler shift whose intensity is given by

$$I_1 = I_o \left(1 - e^{-\frac{x}{v\tau}}\right) \quad . \qquad (4.5)$$

Those which decay after time t_s, exhibit an unshifted peak of intensity

$$I_2 = I_o e^{-\frac{x}{v\tau}} \quad . \qquad (4.6)$$

Thus the ratio

$$\frac{I_2}{I_2 + I_1} = e^{-\frac{x}{v\tau}} \qquad (4.7)$$

is a measure of lifetime τ, if distance x and the recoil velocity v is known. The Ge(Li) detector of 4 mm thickness used in the $Be^9(\alpha,n\gamma)C^{12*}(4.43)$ reaction was not efficient enough to measure these intensities.

Using this technique, Alexander et al (26) measured the lifetimes of 0.871 MeV state of O^{17} and 6.13 MeV state of O^{16} using a Ge(Li) detector of intrinsic depth of 9 mm and found the lifetimes to be 2.33×10^{-10} sec and 2.5×10^{-11} sec, respectively. A group of investigators (27) in 1966 also reported the measurement of the lifetimes of 0.937 and 1.082 MeV states of F^{18}, using a Ge(Li) detector of 25 cm^3 sensitive volume. The lifetimes of these states are reported to be 6.8×10^{-11} sec and 3×10^{-11} sec respectively.

Thus, it appears from our discussion that the development of Ge(Li) detectors with their excellent resolution has made an important contribution to experimental nuclear physics and promises to play an even more important role in gamma-ray spectrometry and nuclear lifetime measurements as larger sensitive volume and higher efficiency detectors become available.

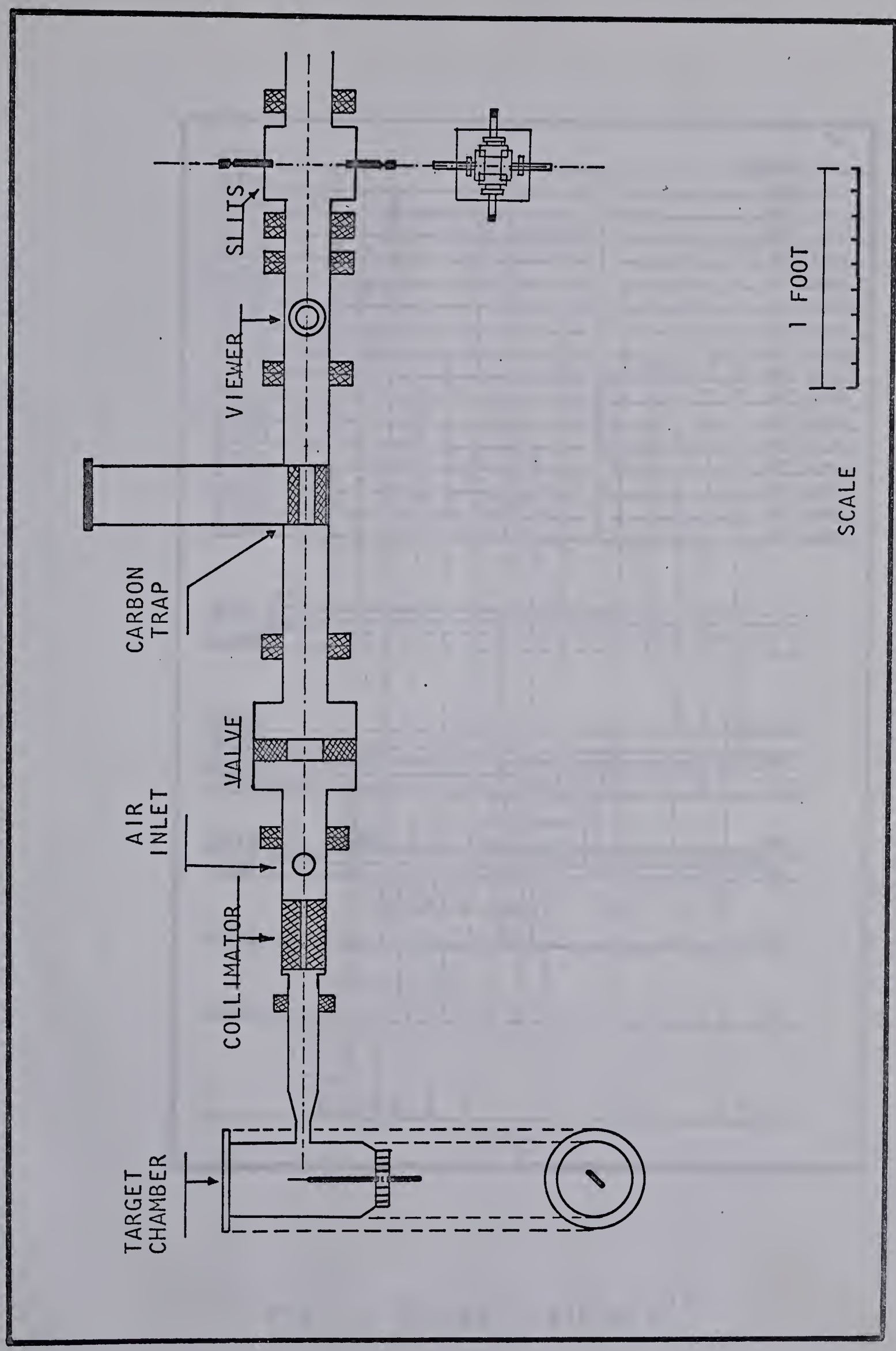

Fig 4-1. Target chember and an illustration of the beam path.
SIDE VIEW

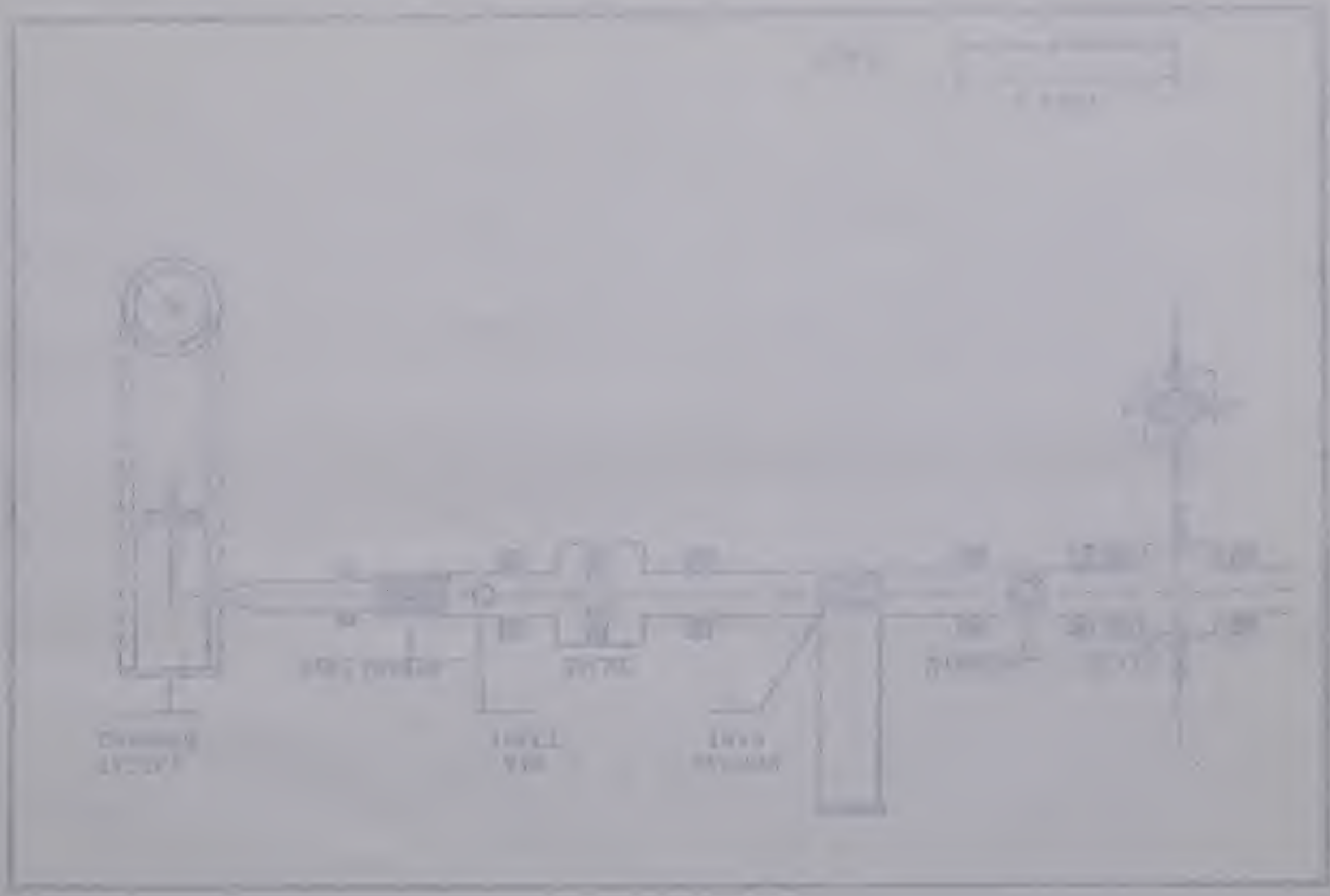

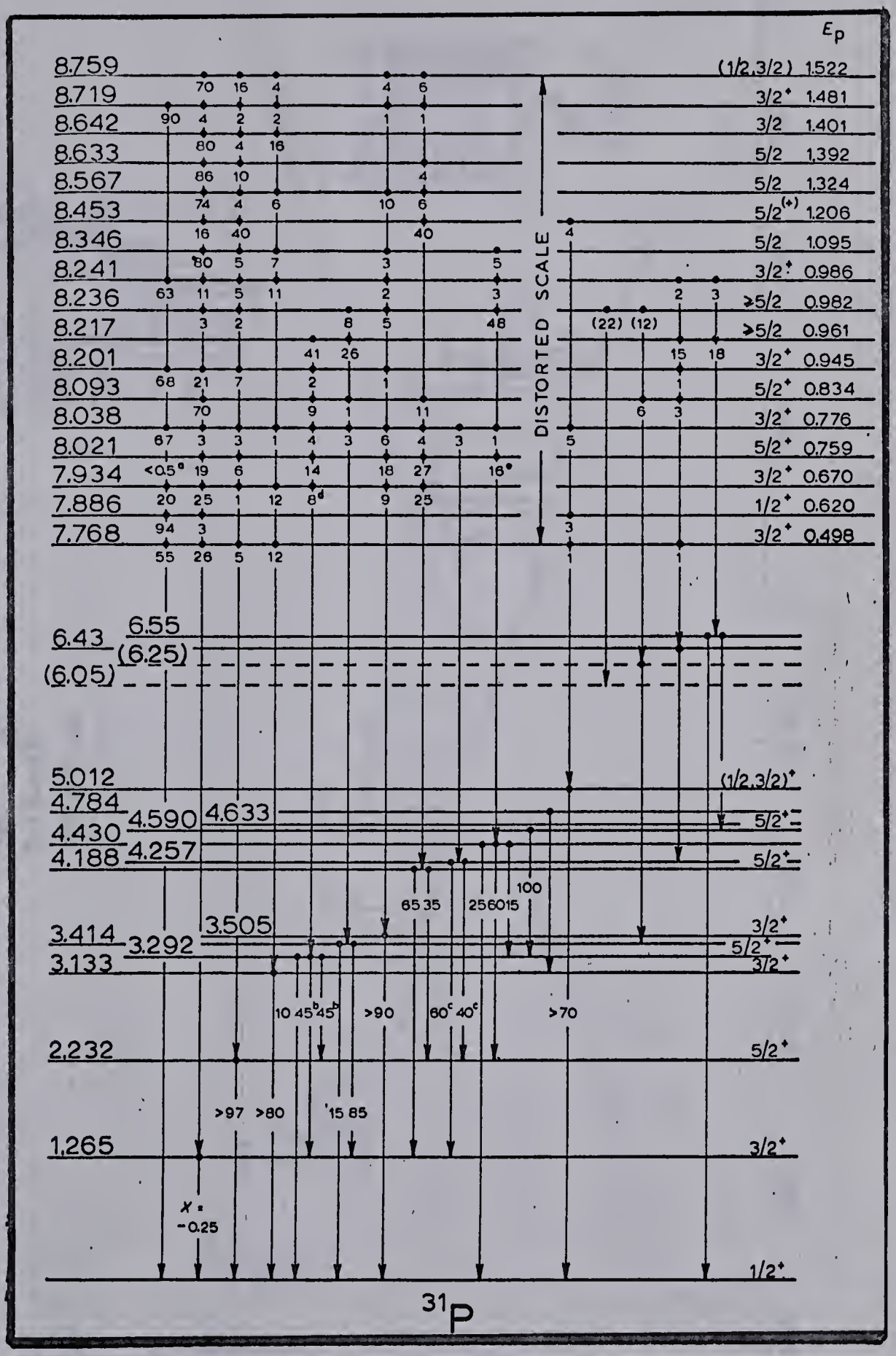

Fig 4-2. Energy levels of P^{31}.

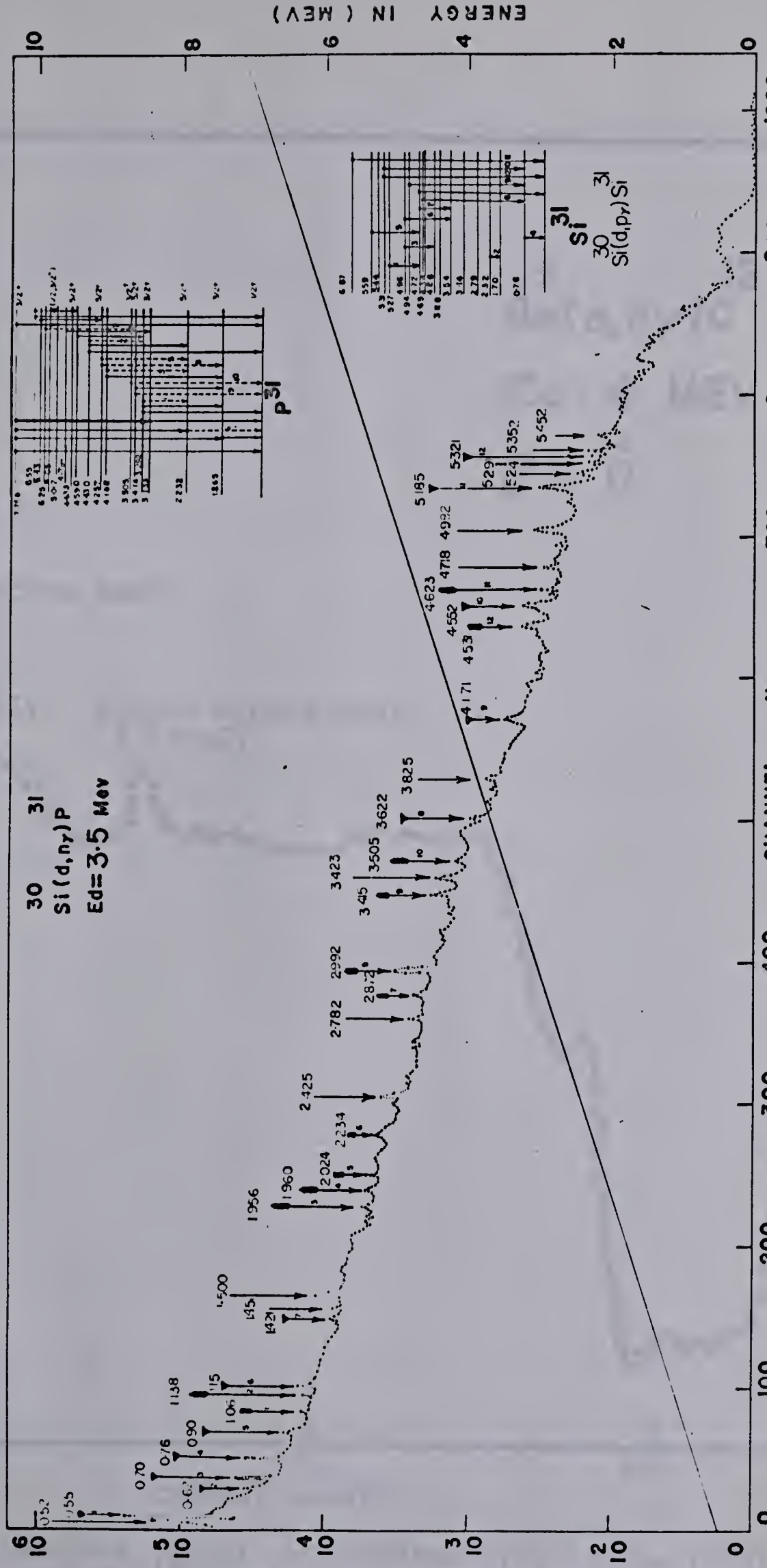

Fig 4-3. Gamma-ray spectrum of p31.

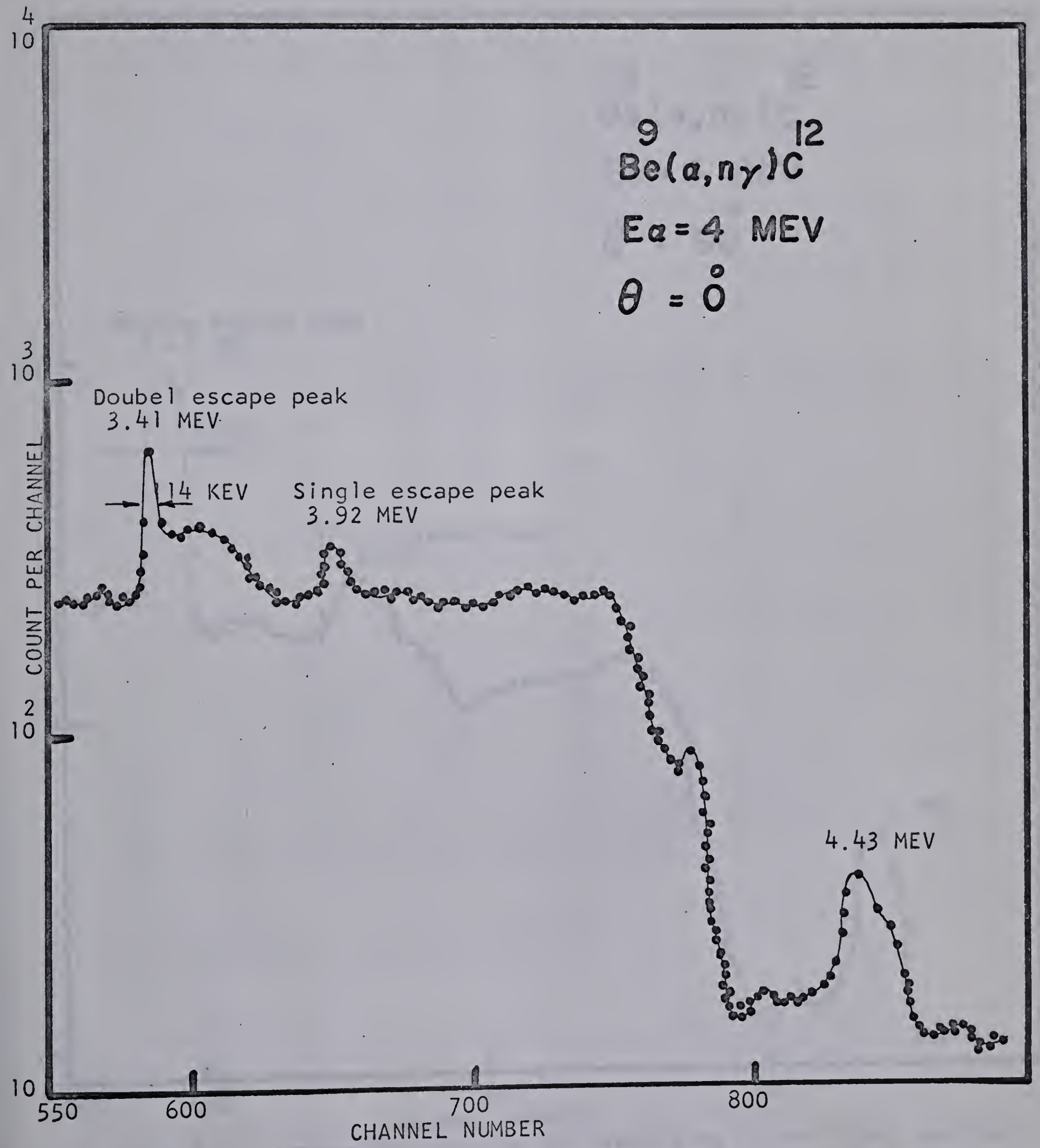

Fig 4-4. Gamma-ray spectrum corresponding to the first excited stat of C^{12}. The gamma-ray detector is located at zero degree with respect to the direction ofincoming beam.

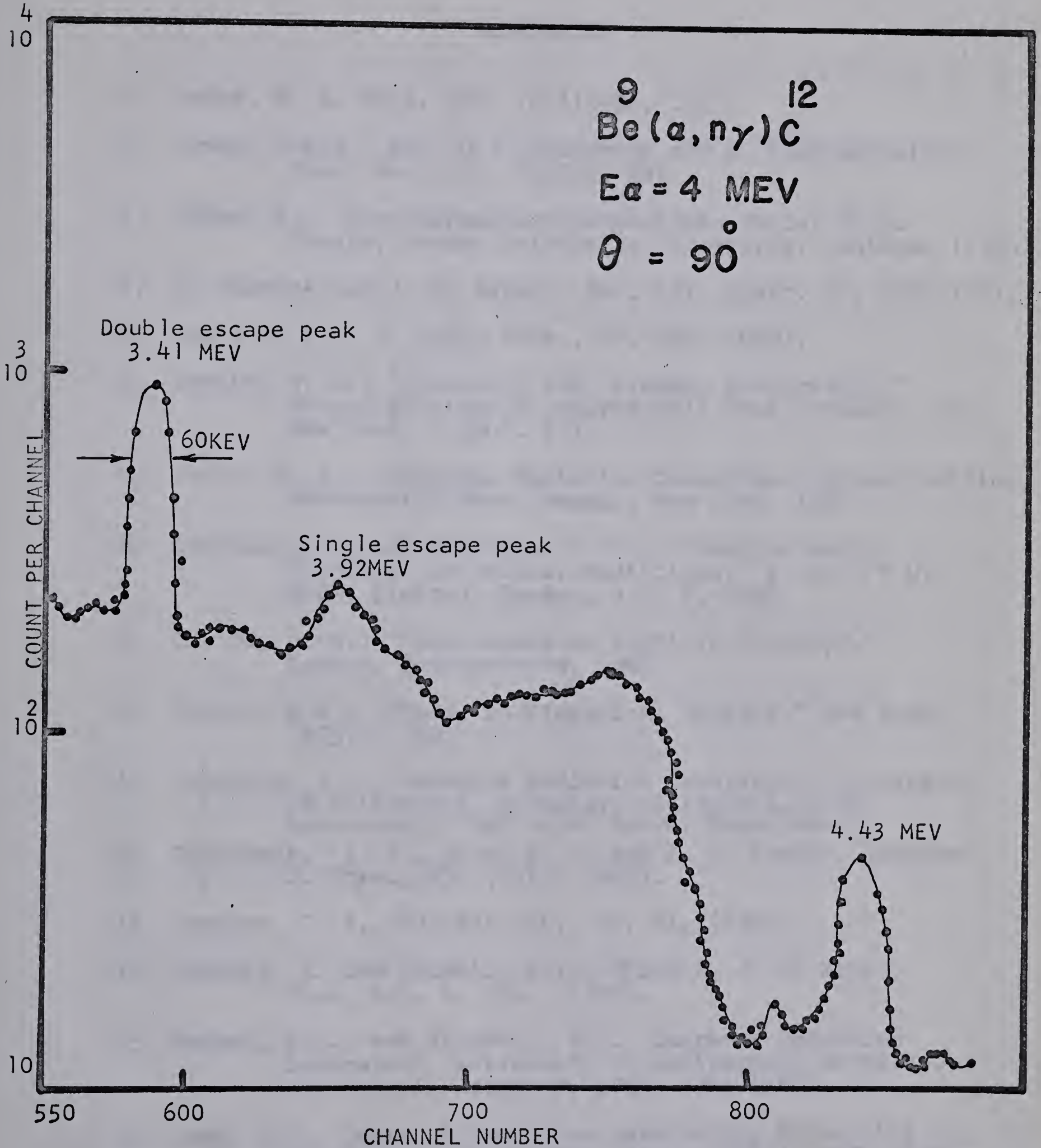

Fig 4-5. Gamma-ray spectrum corresponding to the first excited stat of C^{12}. The gamma detector is located at 90-degree with respect to the direction of incoming beam.

REFERENCES

1. McKay, K. G. Phys. Rev. 76 (1949), 1537.

2. Orman, C.H.Y., Fan, G.F. Goldsmith and E. Lark-Horovitz: Phys. Rev., 78, (1950), 646.

3. Simon, E.: Area Germanium Photovoltaic Cells, Ph.D. Thesis, Purdue University, Lafayette, Indiana, (1955).

4. B. Gossick and J. W. Mayer: Rev. Sci. Instr. 27, 407 (1957).

5. Pell, E. M.: J. Appl. Phys., 31, 291 (1960).

6. Smythe, W. R.: "Statistic and Dynamic Electricity," Second edition-34, McGraw-Hill Book Company, Inc., New York, (1950). (7).

7. Price, W. J.: "Nuclear Radiation Detection," Second edition, McGraw-Hill Book Company, New York, 1964.

8. Dearnaley, G. and Northrop, D. C.: "Semiconductor Counters for Nuclear Radiations," E. and F.N. SPON, Limited, London, W.C. 2, 1963.

9. Taylor, J. M.: "Semiconductor Particle Detector," London, Butterworths, 1963.

10. Fonger, W.H.: "Noise in Electrical Devices," New York, (1957). (9).

11. Goulding, F.S., Lawrence Radiation Laboratory, University of California, Berkeley, California, 1964. Detectors in Radiation Energy Measurement.

12. Tavendale, A. J., Malm, H. L. and I. L. Fowler, Canadian J. Phys., 43, (July, 1965).

13. Bromley, D. A., Nuclear Sci., 32, 61, (1961).

14. Bernner, A. and Riddell, ibid. Miles V. J. of Elec., Chem. Soc. 4, 226, (1957).

15. Hansen, W.L., and Jarrett, B.V., Lawrence Radiation Laboratory, University of California, Berkeley, California, August 7, 1964, UCRL-11589.

16. Camp, D.C., Lawrence Radiation Laboratory, University of California, Livermore, Calif. (1965), URCL-12245, SM-61/33.

17. Palms, J.M. and Greenwood, A.H., Rev. Sci. Inst. 36, 8, 1209 (1965).

18. Tavendale, A.J. and Fowler, I.L., Chalk River Nuclear Laboratory, (1964), GPI-57, AECL-2110.

19. Miller, G.L., Pate, B.D., and Wagner, S., I.E.E.E. Proc. NS-10, 1, 220 (1963).

20. Tavendale, A.J. and Fowler, I.L., "Progress on a fast-drift method for making Li-ion-drift Germanium p-i-n Spectrometer," Chalk River Nuclear Laboratory, Ontario.

21. Broude, C., Green, L.L., and Willmott, J.C., Proc. Phys. Soc. 72, 1097, (1958).

22. Harris, G.I. and Seagondollar, L.W., Phys. Rev. 128-1, 338-581 (1962).

23. Davis, W.G., Ph.D. Thesis, 1966, University of Alberta, Edmonton, Canada.

24. Litherland, A.E., Yates, M.J.L., Hinds, B.M., and Eccleshall, D., Nucl. Phys. 44, 220 (1963).

25. Schwartzchild, A., Proc. Conf. on Electromagnetic Lifetimes and Properties of Nuclear States, Nucl. Sci. 37-974, National Academy of Sciences, Washington, D.C., 1962, page 30.

26. Alexander, T.K., and Allen, K.W., Canadian J. of Phys. 43, 1563, (1965).

27. Alexander, T.K. and Healey, D.C., Phys. Letters, 402, 20, 4, 1966.

24.[1] Endt. P.M. and Van der Leun, C. Energy levels of nuclei Z=11 to Z=20. Nucl. Phys. 34, (1962), 1-324.